



University of Kentucky
UKnowledge

Theses and Dissertations--Chemical and
Materials Engineering

Chemical and Materials Engineering

2012

APPLICATION OF THIN FILM ANALYSIS TECHNIQUES AND CONTROLLED REACTION ENVIRONMENTS TO MODEL AND ENHANCE BIOMASS UTILIZATION BY CELLULOLYTIC BACTERIA

Hsin-Fen Li

University of Kentucky, helenli502@hotmail.com

[Right click to open a feedback form in a new tab to let us know how this document benefits you.](#)

Recommended Citation

Li, Hsin-Fen, "APPLICATION OF THIN FILM ANALYSIS TECHNIQUES AND CONTROLLED REACTION ENVIRONMENTS TO MODEL AND ENHANCE BIOMASS UTILIZATION BY CELLULOLYTIC BACTERIA" (2012). *Theses and Dissertations--Chemical and Materials Engineering*. 13.
https://uknowledge.uky.edu/cme_etds/13

This Doctoral Dissertation is brought to you for free and open access by the Chemical and Materials Engineering at UKnowledge. It has been accepted for inclusion in Theses and Dissertations--Chemical and Materials Engineering by an authorized administrator of UKnowledge. For more information, please contact UKnowledge@lsv.uky.edu.

STUDENT AGREEMENT:

I represent that my thesis or dissertation and abstract are my original work. Proper attribution has been given to all outside sources. I understand that I am solely responsible for obtaining any needed copyright permissions. I have obtained and attached hereto needed written permission statements(s) from the owner(s) of each third-party copyrighted matter to be included in my work, allowing electronic distribution (if such use is not permitted by the fair use doctrine).

I hereby grant to The University of Kentucky and its agents the non-exclusive license to archive and make accessible my work in whole or in part in all forms of media, now or hereafter known. I agree that the document mentioned above may be made available immediately for worldwide access unless a preapproved embargo applies.

I retain all other ownership rights to the copyright of my work. I also retain the right to use in future works (such as articles or books) all or part of my work. I understand that I am free to register the copyright to my work.

REVIEW, APPROVAL AND ACCEPTANCE

The document mentioned above has been reviewed and accepted by the student's advisor, on behalf of the advisory committee, and by the Director of Graduate Studies (DGS), on behalf of the program; we verify that this is the final, approved version of the student's dissertation including all changes required by the advisory committee. The undersigned agree to abide by the statements above.

Hsin-Fen Li, Student

Dr. Barbara Knutson, Major Professor

Dr. Stephen Rankin, Director of Graduate Studies

APPLICATION OF THIN FILM ANALYSIS TECHNIQUES AND CONTROLLED
REACTION ENVIRONMENTS TO MODEL AND ENHANCE BIOMASS UTILIZATION BY
CELLULOLYTIC BACTERIA

Dissertation

A dissertation submitted in partial fulfillment of the
requirements for the degree of Doctor of Philosophy in the
College of Engineering
at the University of Kentucky

By

Hsin-Fen Li

Lexington, Kentucky

Director: Dr. Barbara L. Knutson, Professor of Chemical Engineering

Lexington, Kentucky

2012

Copyright© Hsin-Fen Li 2012

ABSTRACT OF DISSERTATION

APPLICATION OF THIN FILM ANALYSIS TECHNIQUES AND CONTROLLED REACTION ENVIRONMENTS TO MODEL AND ENHANCE BIOMASS UTILIZATION BY CELLULOLYTIC BACTERIA

Cellulose from energy crops or agriculture residues can be utilized as a sustainable energy resource to produce biofuels such as ethanol. The process of converting cellulose into solvents and biofuels requires the saccharification of cellulose into soluble, fermentable sugars. However, challenges to cellulosic biofuel production include increasing the activity of cellulose-degrading enzymes (cellulases) and increasing solvent (ethanol) yield while minimizing the co-production of organic acids. This work applies novel surface analysis techniques and fermentation reactor perturbations to quantify, manipulate, and model enzymatic and metabolic processes critical to the efficient production of cellulosic biofuels.

Surface analysis techniques utilizing cellulose thin film as the model substrate are developed to quantify the kinetics of cellulose degradation by cellulase as well as the interactions with cellulase at the interfacial level. Quartz Crystal Microbalance with Dissipation (QCM-D) is utilized to monitor the change in mass of model cellulose thin films cast. The time-dependent frequency response of the QCM simultaneously measures both enzyme adsorption and hydrolysis of the cellulose thin film by fungal cellulases, in which a significant reduction in the extent of hydrolysis can be observed with increasing cellobiose concentrations. A mechanistic enzyme reaction scheme is successfully applied to the QCM frequency response for the first time, describing adsorption/desorption and hydrolysis events of the enzyme, inhibitor, and enzyme/inhibitor complexes. The effect of fungal cellulase concentration on hydrolysis is tested using the QCM frequency response of cellulose thin films. Atomic Force Microscopy (AFM) is also applied for the first time to the whole cell cellulases of the bacterium *C. thermocellum*, where the effect of temperature on hydrolysis activity is quantified.

Fermentation of soluble sugars to desirable products requires the optimization of product yield and selectivity of the cellulolytic bacterium, *Clostridium thermocellum*. Metabolic tools to map the phenotype toward desirable solvent production are developed through environmental perturbation. A significant change in product selectivity toward ethanol production is achieved

with exogenous hydrogen and the addition of hydrogenase inhibitors (e.g. methyl viologen). These results demonstrate compensatory product formation in which the shift in metabolic activity can be achieved through environmental perturbation without permanent change in the organism's genome.

KEYWORDS: Lignocellulosic biomass conversion, chemostat, cellulase kinetics, mechanistic model, ethanologenic bacteria.

Hsin-Fen Li

August 8, 2012

APPLICATION OF THIN FILM ANALYSIS TECHNIQUES AND CONTROLLED
REACTION ENVIRONMENTS TO MODEL AND ENHANCE BIOMASS UTILIZATION BY
CELLULOLYTIC BACTERIA

By

Hsin-Fen Li

Dr. Barbara Knutson

Director of Dissertation

Dr. Stephen E. Rankin

Director of Graduate Studies

August 8, 2012

To my family

Acknowledgement

This work is completed with much help and contributions from numerous people. I would like to first thank Dr. Barbara L. Knutson for giving me endless support, guidance, and encouragement. Her expertise and insights always inspire me and help me to be a better researcher. It is a great honor and pleasure to be her student as well as co-researcher. I would also like to thank Dr. Steve E. Rankin, Dr. Sue E. Nokes, and Dr. Herbert J. Strobel for their thoughtful inputs that helped me complete this work. I am thankful for Gloria L. Gellin who taught me analytical skills in HPLC. I am also grateful to Dr. Michael D. Flythe who not only is my science teacher but also my life mentor. He once told me that a good researcher learns and develops technological innovations by “standing on the shoulder of giants”. I would like to thank them all for lending me their shoulders.

I would also like to acknowledge my ASTeCC 223 lab family: Srivenu Seelam, Daniel Schlipf, and Utshab Chakravorty for bringing so much joy and love to this lab. Their creativity motivates me every day.

Finally, I would like to thank my parents and my sister, Grace. Without them, my life would not have been completed. Their love and caring are always my most precious and valuable assets. Thank you. Thanks to all giants!

TABLE OF CONTENTS

Acknowledgement	iii
List of Tables	vii
List of Figures	viii
Chapter 1 Introduction	1
Chapter 2 Background	7
Addressing the recalcitrance of cellulose	7
Action and Activity of Cellulases	10
Kinetic model of cellulose hydrolysis by cellulase and product inhibition	12
Surface techniques to study cellulose hydrolysis by cellulase	16
<i>QCM studies of enzymatic hydrolysis</i>	17
Model Cellulose Thin Film for Enzymatic Hydrolysis	19
<i>Model cellulose thin film: NMMO-Dissolved Cellulose</i>	20
<i>Clostridium thermocellum</i> as the model organism	21
Metabolic modulation studies on Clostridia	23
<i>Effect of H₂ on ethanol production</i>	24
<i>Effect of other hydrogenase inhibitors on ethanol production</i>	25
<i>Carbon monoxide (CO)</i>	26
<i>Methyl viologen</i>	28
Chapter 3 Modeling of enzymatic hydrolysis and cellulase inhibition by cellobiose on cellulose thin films monitored by quartz crystal microbalance	30
Summary	30
Introduction	31
Materials and Methods	34
Materials	34
Preparation of Cellulose Thin Film	34
Cellulose Thin Film Characterization by Spectroscopic Ellipsometer and Atomic Force Microscopy (AFM)	35
Cellulose Thin Films/ Cellulase Interactions Measured by Quartz Microbalance with Dissipation (QCM-D)	36
Model Development for Inhibited Enzyme-Kinetics on Cellulose Thin Films	38
Results and Discussion	44
Model cellulose thin film on QCM sensors	44
QCM Experimentation: Enzymatic Binding and Hydrolysis	46
QCM Experimentation: Enzymatic binding and hydrolysis in the presence	

of inhibitors	48
Model Analysis and Parameter Estimation	51
Conclusion	60
Chapter 4 Modeling the Effect of Enzyme Concentration Dependence on Hydrolysis of Cellulose Thin Film using Quartz Crystal Microbalance	62
Summary	62
Introduction.....	63
Materials and Methods	66
Materials	66
Preparation of Cellulose Thin Film.....	66
Cellulose Thin Film Characterization by Spectroscopic Ellipsometer and AFM.....	67
Cellulose Thin Films/ Cellulase Interactions Measured by QCM	68
Model Development for Inhibited Enzyme-Kinetics on Cellulose Thin Films	69
Results and Discussion.....	74
Hydrolysis of model cellulose thin films	74
Effect of enzyme concentration on the enzymatic hydrolysis	76
of thin films as measured by QCM	
Modeling the effect of enzyme concentration on the enzymatic	79
hydrolysis of thin films from the QCM frequency response	
Conclusion	91
Chapter 5 Direct monitoring of the temperature dependence of cellulose hydrolysis by <i>Clostridium thermocellum</i> using Quartz Crystal Microbalance (QCM) and liquid Atomic Force Microscopy (AFM)	93
Abstract.....	93
Introduction.....	94
Materials and Methods	97
Materials	97
Strain and media composition.....	98
Preparation of Cellulose Thin Films	98
Cellulose Thin Film Characterization by AFM.....	99
Cellulose Thin Films/ Cellulase Interactions Measured by QCM	100
Results and Discussion.....	102
Cellulosome binding and hydrolysis as measured by QCM	102
AFM experimentation: cellulose degradation by <i>C. thermocellum</i>	105

Conclusion	109
Chapter 6 Metabolic Control of <i>Clostridium thermocellum</i> via Inhibition of Hydrogenase Activity and the Glucose Transport Rate	111
Summary.....	111
Introduction.....	112
Materials and Methods	114
Strain and media composition.....	114
Batch culture conditions	114
Continuous culture conditions	115
High Density Washed Cell Conditions	117
Glucose transport assays	117
Product analysis (HPLC).....	118
Bioenergetic calculations	118
Results	118
Discussion.....	123
Conclusion.....	127
Chapter 7 Conclusions and Future Work	128
Future Work.....	131
Appendix A Hydrogen-adapted <i>Clostridium thermocellum</i>	135
Appendix B Use of a new buffer in <i>Clostridium thermocellum</i> culture medium.....	141
Appendix C Effect of pH and dissolved gas on cell growth and product formation.....	145
Appendix D Bioenergetic calculations	148
References	150
Vita	170

List of Tables

Table 3-1	Model parameters optimized from the frequency data for cellulose thin films treated with cellulase (0.02 mM) in the presence of cellobiose (0 to 5 g/l).....	53
Table 4-1	Alternative kinetic models to account for enzyme concentration effects	73
Table 4-2	Model parameters optimized from the frequency data for cellulose thin films treated with cellulase (0.01 % v/v to 1 % v/v)	87
Table 6-1	Products of high-density washed <i>C. thermocellum</i> cell suspensions with the addition of H ₂ , H ₂ +MV (methyl viologen, 30 µg ml ⁻¹), or N ₂ under 1 or 6.8 atm	120

List of Figures

Figure 2-1	Chemical structure of cellulose, a polysaccharide made up of β -D-glucopyranose units (<i>bracket</i>) linked by β -1,4 glycosidic bonds (<i>shaded</i>).....	8
Figure 2-2	Schematic process diagram of simultaneous saccharification and fermentation (SSF) versus consolidated bioprocessing (CBP).....	9
Figure 2-3	The modes of hydrolytic actions by each cellulase component: end-glucanase (circle), exo-glucanase (trapezoid), β -glucosidase (rectangle)	12
Figure 2-4	Mode of operation by QCM.....	18
Figure 2-5	The chemical structure of N-Methylmorpholine-N-oxide (NMMO)	21
Figure 2-6	Simplified scheme of Embden-Meyerhof-Parnas (EMF) pathway of glucose catabolism by <i>C. thermocellum</i>	23
Figure 2-7	The relationship of NAD^+_{LE} production to ATP production of <i>C. thermocellum</i> under a N_2 - (<i>open symbols</i>) or CO_2 - (<i>filled symbols</i>) headspace	27
Figure 3-1	Potential reaction pathways of enzyme inhibition during cellulose hydrolysis.....	43
Figure 3-2	AFM amplitude images (tapping mode, $5 \times 5 \mu\text{m}^2$) of (a) gold-coated quartz crystal resonator; (b) cellulose-coated quartz crystal resonator before exposure to cellulases; (c) cellulose-coated quartz crystal resonator after hydrolysis.....	45
Figure 3-3	Frequency (a) and dissipation (b) profile of cellulose hydrolysis by cellulase (0.5 % v/v) at 30 °C	47
Figure 3-4	Frequency profile of cellobiose loading at 20 g l^{-1} (--- <i>dashed line</i>), 40 g l^{-1} (— <i>gray solid line</i>), 60 g l^{-1} (--- <i>black dashed line</i>), 80 g l^{-1} (— <i>black solid line</i>)	49
Figure 3-5	Frequency profile of cellulose hydrolysis by cellulase (0.5 % v/v) in the presence cellobiose at 0 g l^{-1} (— <i>black solid line</i>), 0.1 g l^{-1} (--- <i>black dashed line</i>), 0.4 g l^{-1} (— <i>gray solid line</i>), 1 g l^{-1} (--- <i>gray dashed line</i>), 5 g l^{-1} (.... <i>gray dotted line</i>)	51
Figure 3-6	Measured frequency profile (— <i>black solid line</i>) and model frequency profile (--- <i>gray dashed line</i>) of cellulose hydrolysis by cellulase (0.5 % v/v) in the presence of 0 g l^{-1} (a), 0.1 g l^{-1} (b), 0.4 g l^{-1} (c), and 1 g l^{-1} cellobiose (d).....	52

Figure 3-7	Model concentration profile of S_i (- - - <i>black dashed line</i>), ES (— <i>black solid line</i>), and ESI (··· <i>black dotted line</i>) normalized by S_o during cellulose hydrolysis by cellulase (0.5 % v/v) in the presence of 0.1 g l^{-1} cellobiose.....	56
Figure 3-8	Measured frequency profile (— <i>black solid line</i>) and model frequency profile (- - - <i>gray dashed line</i>) of cellulose hydrolysis by cellulase (0.5 % v/v) in the presence 5 g l^{-1} cellobiose	59
Figure 4-1	Typical frequency profile of cellulose hydrolysis. The arrow indicates the injection of enzyme solution (0.05 % v/v diluted in 0.1M acetic acid, pH 5)	75
Figure 4-2	QCM frequency profile of cellulose hydrolysis by cellulase at 0.01% v/v, 0.05 % v/v, 0.1 % v/v, 0.5 % v/v, 1 % v/v.....	77
Figure 4-3	Initial hydrolysis rate of cellulose thin film for the experimental frequency profile at different cellulase concentrations (% v/v).....	78
Figure 4-4	QCM frequency profile of measured frequency profile at 0.1 % v/v (— <i>thick black solid line</i>) and model QCM frequency profile using original model (— <i>gray line</i>), fractal model (····· <i>small break line</i>), jammed model (-----), fractal jammed model (— — —), and the model accounting the enzyme-substrate interaction that leads to enzyme inactivation (—)	81
Figure 4-5	Model QCM frequency profile of cellulose hydrolysis using ES inactivation model.....	82
Figure 4-6	Model fit using a) first order kinetics or b) n^{th} ($n = 0.2$) order kinetics for the frequency response of the measured frequency change (<i>solid line</i>) and the model frequency change (<i>dotted line</i>) during adsorption at cellulase different concentrations	84
Figure 4-7	Measured frequency profile (— <i>black solid line</i>) and model frequency profile (- - - <i>dashed line</i>) of cellulose hydrolysis by cellulase to 80% conversion (<i>vertical dashed line</i>) at 0.01 % v/v (a), 0.05 % v/v (b), 0.1 % v/v (c), 0.5 % v/v (d), 1 % v/v (e), and predicted model frequency (····· <i>dotted line</i>) at 2 % v/v.....	85
Figure 4-8	Model concentration profile of S_i (- - - <i>black dashed line</i>), ES (— <i>black solid line</i>), and ESI (— <i>gray solid line</i>) normalized by initial substrate concentration, S_o , during cellulose hydrolysis by cellulase (0.1 % v/v).....	88
Figure 4-9	The adsorption term (a) and the hydrolysis term (b) of the model QCM frequency change for cellulose film hydrolysis at cellulase concentration of 0.01 % v/v (····· <i>small dotted line</i>), 0.05 % v/v (---- <i>short dash line</i>), 0.1 % v/v (- - - <i>medium dash line</i>), 0.5 % v/v (- - - <i>long dash line</i>), 1 % v/v (— <i>solid line</i>).....	89

Figure 5-1	Frequency profile of cellulose hydrolysis by 0.5 % v/v <i>T. reesei</i> cellulase (<i>black</i>) and <i>C. thermocellum</i> (<i>gray</i>) at 30 °C.....	103
Figure 5-2	Frequency profile of cellulose hydrolysis by <i>C. thermocellum</i> at 40 °C (<i>gray</i>) and 50 °C (<i>black</i>)	104
Figure 5-3	AFM topography image (5 x 5 μm ²) of cellulose-coated quartz crystal resonator in a) air or in b) liquid acetate buffer (0.1 M, pH 5) at 30 °C.....	105
Figure 5-4	AFM Topography images (tapping mode, 5 x 5 μm ²) of cellulose-coated quartz crystal resonator incubated with <i>C. thermocellum</i> at 50 °C	106
Figure 5-5	AFM topography images (left, 5 x 5 μm ²) and topography vs. distance (right) of cellulose-coated quartz crystal resonator incubated with cellulase from <i>T. reesei</i> (0.5% v/v, pH 5) at 30 °C	107
Figure 5-6	AFM Topography images (<i>top</i> , 5 x 5 μm ²) and the corresponding thickness (<i>bottom</i>) of cellulose-coated quartz crystal resonator incubated in liquid acetate buffer (0.1 M, pH 5) at 30 °C	108
Figure 6-1	Simplified glycolytic scheme (Embden–Meyerhof–Parnas) of <i>C. thermocellum</i> ..	113
Figure 6-2	Culture vessel. <i>Shaded components</i> contain media. <i>P</i> pressure gauge, <i>T</i> temperature control.....	116
Figure 6-3	The effect of sparge gas on cellobiose-limited <i>C. thermocellum</i> continuous culture	119
Figure 6-4	Glucose transport by <i>C. thermocellum</i> cell suspensions.....	121
Figure 6-5	The growth (<i>a</i>) and ethanol: acetate ratios (<i>b</i>) of <i>C. thermocellum</i> under N ₂ (<i>open circles</i>), N ₂ with 30-μg ml ⁻¹ methyl viologen (<i>black circles</i>), or under CO (<i>triangles</i>)	122
Figure 6-6	An analysis of metabolism <i>C. thermocellum</i> chemostat cultures (Fig 6-3).....	126

Chapter 1

Introduction

The world's demand for energy resources has resulted in the pursuit of alternatives to diminishing petroleum-based transportation fuels and commodity chemicals. Biofuels such as ethanol are one alternative to replace non-renewable petroleum-based energy sources. Current bio-ethanol production relies on the hydrolysis (pretreatment) of agricultural crop material into soluble sugars, and yeast (*Saccharomyces cerevisiae*) is used to convert sugars into ethanol. However, ethanol produced from grain crops like corn or wheat increases food prices due to its competition with food supplies (Pimentel and Patzek 2005; Mitchell et al. 2008). Cellulose is the most abundant, sustainable bio-polymer that can be degraded into soluble sugars for ethanol production. Due to its recalcitrant nature, most cellulose on earth is not utilized. Techniques to convert lignocellulose biomass into ethanol have been developed. Conventional cellulosic ethanol processes involve substrate pretreatment (to provide accessible cellulose), cellulase production (enzyme that degrade cellulose), cellulose hydrolysis, ethanol fermentation and product recovery. However, low ethanol yield and inefficient cellulose hydrolysis remain challenges to commercial cellulosic ethanol production (Bender et al. 1985; Taillez et al. 1989; Munasinghe and Khanal 2010).

The thermophilic anaerobic bacterium, *Clostridium thermocellum*, represents an important class of microorganisms considered for the direct conversion of cellulose in lignocellulosic materials to alcohols and organic acids (ethanol, lactate, acetate), as well as gases (carbon dioxide, and hydrogen) (Slapack et al 1985; Lovitt et al. 1988; Lynd et al. 1989). The degradation of cellulose is carried out by the complex extracellular cellulosome system

which contains 20 different catalytic subunits (Richardson et al. 2003). The specific activity of the *C. thermocellum* cellulase complex on crystalline cellulose is approximately 50 fold higher than other cellulolytic species (Raynolds and Johnson 1985). However, its hydrolytic efficiency is limited by the presence of cellulose degradation products including cellobiose. Therefore, the inhibitory effect of cellobiose on cellulose hydrolysis is investigated through a surface reaction study on the interaction of the enzyme and the substrate at the interfacial level. Influence of inhibitors on both binding and hydrolysis is the key to improve enzyme sustainability and efficiency against environmental impact.

Consolidated bioprocessing (CBP), the process of using *C. thermocellum* to integrate cellulase production, cellulose hydrolysis and fermentation in one step, offers the potential for lower cost and higher efficiency because the addition of cellulolytic enzyme is not required. However, the limitation to its practical application is its low ethanol yield and low ethanol tolerance up to 1.5% (Herrero and Gomez 1980; Tailliez et al. 1989), as well as the production of other side products including the lactate and acetate. To overcome technical barriers to commercialization, studies involving genetic modification of *C. thermocellum* have been developed, but the unanticipated product regulation and control in the expression of organism's metabolic responses (phenotype) make this approach difficult (Bailey et al. 1996). Recent works have focused on enhancing the metabolic regulatory network of microorganisms through environmental techniques. Metabolic engineering offers a distinct advantage over genetic modification due to the ability to tune product selectivity of microorganisms to enhance bioconversion rates and optimize desirable products.

A novel approach to overcome the technical barrier and enhance ethanol yield is the introduction of dissolved H₂ in the fermentation system. Ethanol yield is observed to increase

with elevated hydrostatic pressure relative to atmospheric pressure in a continuous culture system (Bothun et al. 2004). Specifically, the product ethanol to acetate ratio (E/A) increased nearly 60-fold at 7.0MPa relative to the non-growing cells in batch culture. The increase in E/A ratios is a result of a simultaneous increase in ethanol production and a decrease in acetate production (Bothun et al. 2004). Due to the reversibility of reactions involving electron carriers (NAD, NADP, and ferredoxin), the increase in end-product (hydrogen) concentration caused a shift in product selectivity (Lynd et al. 1989). While the decreased acetate production is broadly attributed to the inhibition of bacterial hydrogenases by the end-product H₂, the dramatic increase in ethanol production is unexplained. Therefore, if we can manipulate the metabolic pathway of *C. thermocellum* toward ethanol-only production through our understanding of hydrogenase inhibition we will move towards the goal of economical cellulosic ethanol production. The objectives of this work are to develop enzymatic models to predict the behavior of cellulase on cellulose using thin film surface analysis techniques, and to develop metabolic tools to map the phenotype of *C. thermocellum* toward ethanol production through environmental perturbation. Technical barriers to efficient cellulose hydrolysis are addressed through the surface reaction study of the interaction of cellulase and cellulose at the interfacial level. The effects of inhibitors and enzyme concentration are investigated to more fully understand the enzymatic kinetics and hydrolytic activity during saccharification processes. Direct visualization of cellulose hydrolysis was demonstrated with cellulases and whole cell cellulolytic bacteria. Mechanistic models are also developed based on the dynamic enzymatic reactions including cellulase binding, cellulose hydrolysis, enzyme inhibition, and enzyme inactivation. The developed models are capable of describing the impact of inhibitors and enzyme concentration on specific enzyme adsorption in the enzymatic hydrolysis of cellulose.

Chapter 2 begins with a general background of approaches to addressing the recalcitrance of cellulose to hydrolysis, the role of cellulases in cellulose hydrolysis to fermentable sugars and the kinetic models associated with enzymes, enzyme-substrate interactions, and enzymatic inhibition by-products. The surface techniques to provide *in-situ* monitoring of the hydrolysis of cellulose thin films by cellulases are also presented. In addition, a review of using *C. thermocellum* as a model organism to study the metabolic modulation on cellulolytic bacteria is provided. The review focuses on the effect of environmental perturbations, in particular the addition of hydrogen and hydrogenase inhibitors (carbon monoxide and methyl viologen), on ethanol production.

The inhibitory effect of cellobiose on cellulose hydrolysis is examined in Chapter 3. The cellulase source is fungal cellulases from *Trichoderma reesei*, which are natural non-complexed cellulase mixtures. The interaction of the inhibited enzyme and the cellulose substrate are investigated through the measurement of mass change and surface properties of cellulose thin films using Quartz Crystal Microbalance with Dissipation (QCM-D). A non-linear mechanistic model is developed using QCM frequency change measurement that describes simultaneous enzyme adsorption and desorption as well as cellulose hydrolysis. The concentration dependence of inhibition of cellulase binding and hydrolysis by cellobiose is quantified by QCM. Other kinetics properties such as affinity, inhibition constant, and adsorption/desorption rate constants are determined, which makes this model a useful tool to evaluate the hydrolysis performance and underlying reaction pathway in the enzymatic hydrolysis of cellulose.

The surface technique and kinetic model development is continued in Chapter 4, which examines the impact of enzyme concentration on hydrolysis. A maximum apparent hydrolysis rate with respect to enzyme concentration is observed, where further increased in cellulase

concentration did not enhance the hydrolysis rate. The QCM frequency response as a function of cellulase concentration was fit to hydrolysis models (i.e., fractal and jammed kinetics) models which have been proposed to capture the effects of enzyme crowding on the a heterogeneous substrate surface. Surface enzyme inactivation with an n-th order enzyme adsorption is proposed. The formation of active and inactive enzyme-substrate complexes are quantified and analyzed to explain the change in hydrolysis rate in response to different enzyme concentrations. This work presents the first study to describe enzyme surface events in mechanistic model (adsorption and enzyme inactivation) using surface analysis techniques.

Chapter 5 presents the effect of temperature on cellulose hydrolysis by *C. thermocellum* as an enzyme system. The developed surface technique (Chapter 3 and 4) is applied to observe the effect of whole cell biocatalysis on the hydrolysis of cellulose thin film for the first time. Direct monitoring of the time-dependent adsorption and subsequent hydrolysis by QCM is compared between *C. thermocellum* and free cellulases of *Trichoderma reesei*. In addition, the change in thin film surface topography during the hydrolysis is visualized through liquid atomic force microscopy (AFM) at a controlled temperature. The combination of AFM and QCM surface analysis techniques is demonstrated for the analysis of substrate interaction and hydrolysis using whole cells in liquid media

One approach to lower biofuels production cost is to increase the production of the desired product. In Chapter 6, enhanced product selectivity toward ethanol is demonstrated using *C. thermocellum* as a model organism. The yield of ethanol production is improved by the introduction of hydrogenase inhibitors, which is only expected to decrease acetate (a lower value product of *C. thermocellum*) production. The effect of these inhibitors in continuous cultures, batch cultures and high-density washed cell cultures (in the absence of growth phase-dependent

substrate and energy use) is compared to fermentations in the presence of N₂ headspace. The contribution of substrate uptake rate to enhanced ethanol production is also examined. This study presents evidence for compensatory production of lactate and/or ethanol when hydrogenases are inhibited through environmental perturbations. In addition, this chapter presents the ability of cellulolytic organisms to change its product patterns in response to environmental perturbation without the need for permanent genetic modification.

In summary, this work presents the development of surface analysis techniques and novel kinetic models required to enhance the efficiency of hydrolysis reactions by understanding the interplay between cellulose and cellulase in the presence of hydrolysis inhibitors. This research suggests that fermentation can be directed without bringing permanent change to the organism's genome, in this case by understanding the interplay of hydrogenase inhibition and substrate limitation condition to move toward ethanol only production by *C. thermocellum*. Future development to enhancing biomass utilization is suggested in Chapter 7 in which the mechanism of cellulolytic bacteria and their impact on cellulose saccharification can be further investigated to achieve environmentally and economically feasible lignocellulosic fuel and solvent production.

Chapter 2

Background

Addressing the recalcitrance of cellulose

Cellulose is a major component in most plant structure, and is the most abundant and sustainable polymer source on earth (Himmel et al. 1999; Monserrate et al. 2001). In grass, for example, cellulose content takes up 45 to 60% of the plant cell wall (Bidlack et al. 1992; Carpita and Gibeaut 1993). This naturally occurring polysaccharide consists of β -D-glucopyranose units which are linked by beta-1,4 glycosidic bonds (Fig 2-1). Native cellulose contain regions of high crystallinity (highly ordered structure) and regions with less ordered or disrupted component, referred to as amorphous cellulose. The chain length of cellulose, characterized by the number of glucose units in one polymer molecule or the degree of polymerization (*DP*) varies among different plant materials. For example, there are approximately 300 to 1,700 glucose residues in wood pulp, 800 to 10,000 units in cotton; and more than 25,000 units in other longer glucan chains (Brown et al. 1996; Klemm et al. 2005). Unlike short-chain sugars such as cellodextrin ($DP = 2\sim 7$) or other glucan polymers such as starch that are soluble in water, cellulose is insoluble (Pereira et al. 1988; Zhang and Lynd 2003). The linear β -linkage between glucose with C-O bonds on the opposite side of the chain makes the C-O bonding strongly connected. In addition, the intermolecular hydrogen bonds formed between primary hydroxyl group (-OH) at O-6' and secondary hydroxyl group (-OH) at O-2' and O-3' require a tremendous amount of energy to break. This hydrogen bond in the network involves the connection with the entire OH group in the structure which prevents hydrolysis by water molecules. It is due to this strong mechanical strength in the cellulose structure that maintains plant structural integrity.

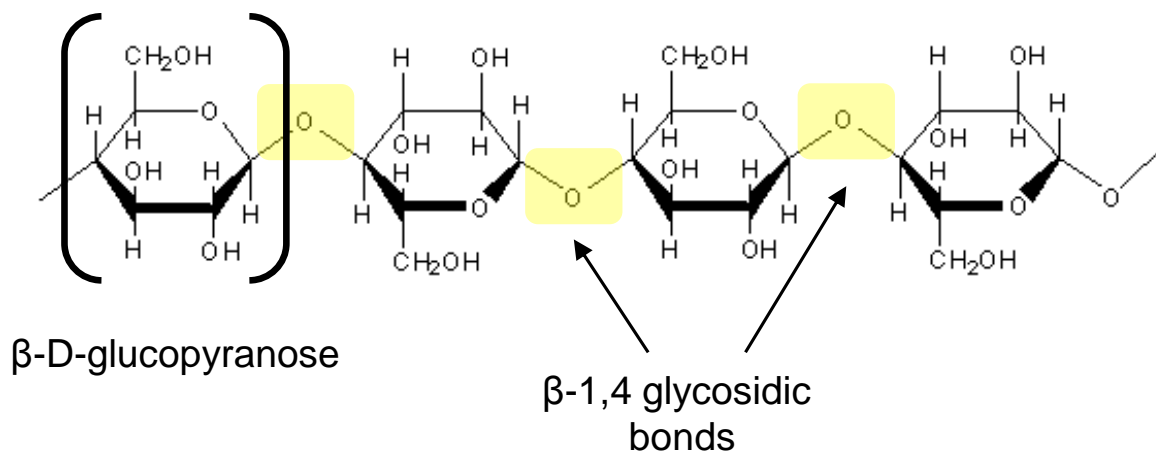


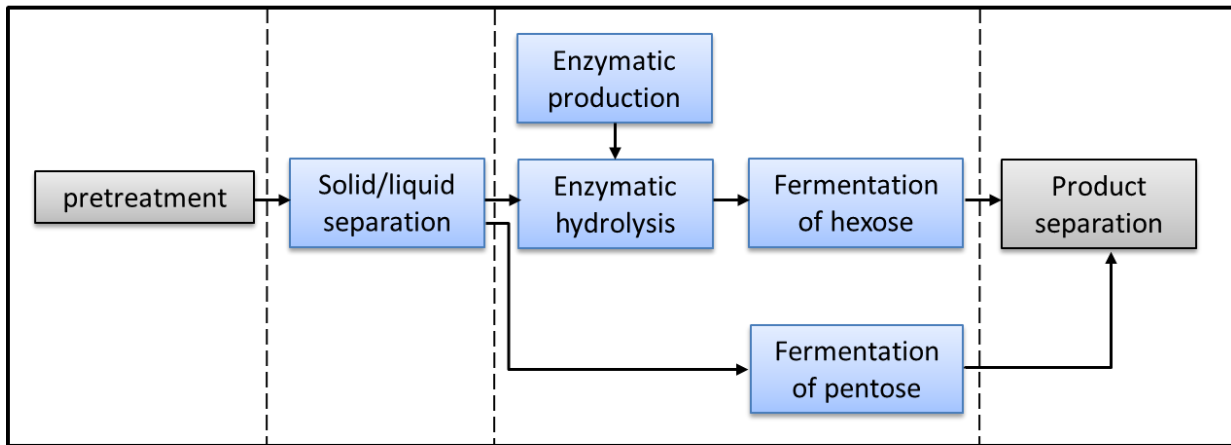
Figure 2-1 Chemical structure of cellulose, a polysaccharide made up of β -D-glucopyranose units (*bracket*) linked by β -1,4 glycosidic bonds (*shaded*). Figure modified from Royal Society of Chemistry, 2005.

Other portions of the plant biomass include hemicelluloses (25-50%), lignin (10-40%), and trace amounts of pectins, proteins, and ash (Sun and Cheng 2002; Jorgensen et al. 2007). The fraction of each component varies with plant maturity and plant material type. Xylose, arabinose (five carbon sugars) and glucose (a six carbon sugar) are the main constituents of hemicelluloses and cellulose, respectively, which can be hydrolyzed into glucose monomers. Lignin, however, is a polymer consisting of phenylpropylene (non-sugar type) subunits joined by ether and carbon-carbon linkage. Lignin is not biodegradable and cannot be hydrolyzed into glucose. The presence of lignin is often limits the accessibility to cellulose and therefore its hydrolysis to soluble sugars.

Cellulose in plant materials contains large fraction of fermentable sugars, but a complex pretreatment step is required to make the native form of multi-component biomass more accessible to enzyme degradation. Effective pretreatment process can increase the hydrolysis yield from 20 % to 90 % (Lynd 1996). Common pretreatment processes involve physical

(grinding), thermal (steam-explosion), or chemical (dilute acid or organic acid) treatments followed by enzymatic hydrolysis of pre-treated substrate into glucose monomers. The liberated sugars can then be fermented into products such as ethanol. Consolidated bioprocessing (CBP) is an alternative approach which is developed to reduce the processing steps by ‘consolidating’ enzyme production, cellulose hydrolysis and ethanol fermentation in one reactor (Fig 2-2). CBP offers the potential to reduce processing cost, lower energy input and increase conversion efficiency (Carere et al. 2008).

Simultaneous saccharification and fermentation



Consolidated bioprocessing

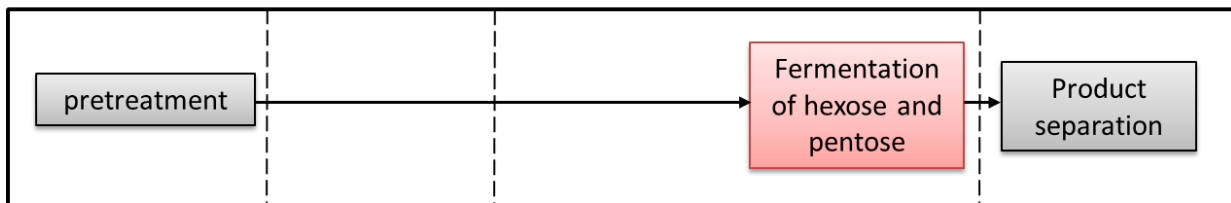


Figure 2-2 Schematic process diagram of simultaneous saccharification and fermentation (SSF) versus consolidated bioprocessing (CBP). Figures adapted from Xu et al (2009).

Action and Activity of Cellulases

Cellulolytic micro-organisms obtain their carbon food source by producing multiple enzymes known as cellulases to breakdown plant cell walls into simple carbohydrates. Cellulase activity can be found not only in plants but also the digestive tracts of ruminant animals where cellulose- and hemicellulose-rich feed is broken down to glucose (Beauchemin et al. 2003). The ability of cellulases to hydrolyze cellulose makes them important biocatalysts for the conversion of lignocellulosic material to fermentable sugars.

Cellulase systems are categorized by two types: complexed or non-complexed cellulases. Complexed cellulases are often produced by anaerobic bacteria, and these enzymes remain attached to the cells (Shoham et al. 1999; Schwarz 2001; Lynd et al. 2002). Non-complexed cellulases are produced by fungi and some bacteria, from which they are secreted freely and separately from the cells (Wood 1992; Teeri 1997). Individual component of the cellulase are classified by their modes of actions and structural properties (Henrissat et al. 1998). In general, three types of cellulases are known: i) endo-glucanase, ii) exo-glucanase (cellobiohydrolases), and iii) β -glucosidase.

- i) Endo-glucanase breaks the internal 1-4 β -glycosidic bond in the amorphous region of cellulose (Mosier et al. 1999) and forms free intermediate compounds (oligosacharrides of various lengths) (Lynd et al. 2002). This catalytic action creates greater specific surface area of the substrate and better accessibility of the chain ends for other cellulases for further depolymerization (Bravo et al. 2002). Endo-glucanase is active on amorphous or disordered region of cellulose but act poorly on crystalline substrate.

- ii) Exo-glucanase with a tunnel-like catalytic site that acts processively and degrades the crystalline region of cellulose from the reducing and non-reducing end and releases cellobiose as their main products (Lynd et al. 2002).
- iii) β -glucosidase then converts the produced cellobiose unit into glucose. The catalytic activity of β -glucosidase is inversely proportional to the degree of substrate polymerization.

These cellulase isomers work simultaneously and synergistically to breakdown cellulose into soluble sugars (Berghem and Petterss 1973; Fägerstam and Pettersson 1980). For example, endo-glucanases break the cellulose polymer chain and make the non-reducing end available for exo-glucanase hydrolysis (Rabinovich et al. 2002).

Cellulolytic bacteria such as *C. thermocellum* are known to produce cellulolytic enzymes. Other fungal species include *Trichoderma reesei* and *Trichoderma koningii* are also able to secrete cellulolytic enzymes, but *C. thermocellum* enzymes have the highest hydrolytic activity on crystalline cellulose among all species (Ng and Zeikus 1981; Johnson et al. 1982). The multi-component enzyme system consisting of a carbohydrate binding module (CBM) (previous classified as cellulose binding domain (CBD)) and several catalytic domains are all linked in an external organelle known as a cellulosome (Bayer et al. 1994; Beguin and Alzari 1998; Schwarz 2001; Demain et al. 2005). The two main functions of cellulosome are binding and catalysis (Bayer et al. 2004; Demain et al. 2005). Prior to cellulose degradation, enzymes are adsorbed onto the substrate by a cellulose-binding factor (CBF), a component of the cellulosome (Bayer et al. 1983).

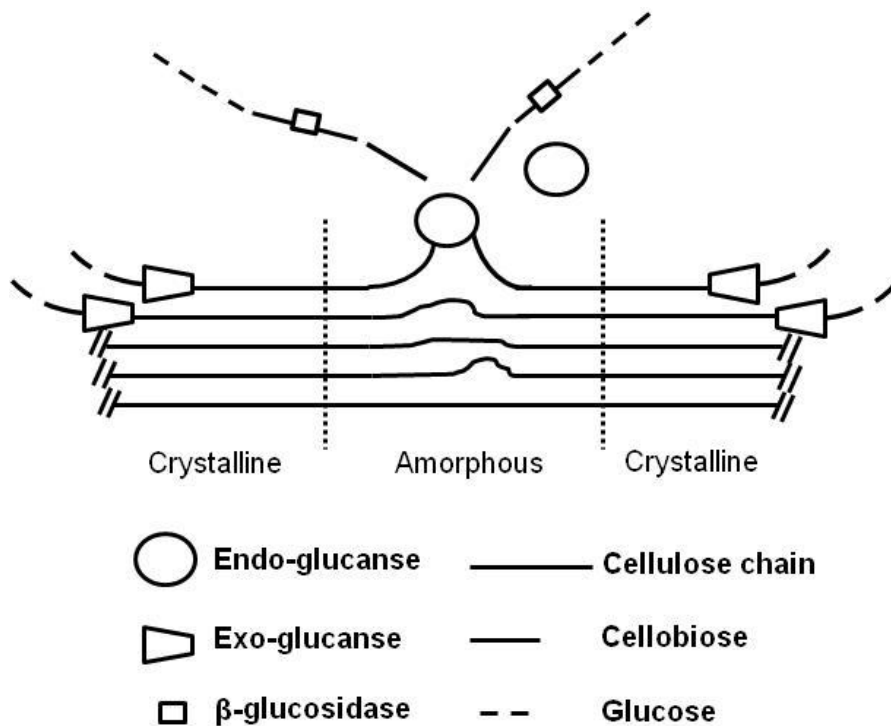


Figure 2-3 The modes of hydrolytic actions by each cellulase component: end-glucanase (circle), exo-glucanase (trapezoid), β -glucosidase (rectangle). Amorphous and crystalline region of cellulose is indicated. The figure is adapted from Lynd (2002).

Kinetic model of cellulose hydrolysis by cellulase and product inhibition

The main challenges to efficient enzymatic hydrolysis include high cellulase cost and low hydrolysis rate (Bommarius et al. 2008; Bansal et al. 2009). One way to enhance the reaction rate is to understand the kinetics associated with the enzyme hydrolysis on lignocellulosic substrate. Models have been developed to describe the enzymatic kinetics. The advantage of modeling includes the identification of kinetics expression and parameters which contribute to various reactor system properties useful for designing or optimizing the hydrolytic process. For example, models of enzymatic hydrolysis have been applied to continuous and fed-batch processes to model stage reactor configurations (Hodge et al. 2009; Shao et al. 2009). Most of the enzyme catalysis models are developed to address the following major processes: 1)

adsorption of cellulases and/or location of a bond susceptible to hydrolysis, 3) formation of enzyme-substrate complex, 4) hydrolysis of the β -glycosidic bond, 5) desorption of cellulases from the substrate, and 6) hydrolysis of cellobiose to glucose by β -glucosidase (Bansal et al. 2009). In general, enzymatic models on cellulosic substrate are categorized into three types: empirical, Michaelis-Menten (reaction-pathway) based and Langmuir-based adsorption models.

Empirical models are used most commonly in quantifying the effect of hydrolysis in pretreatment processes. Usually, empirical models are developed based on fitting a mathematical equation to the data curve that describes the substrate conversion, enzyme adsorption, or product formation with respect to time (Ohmine et al. 1983; Ooshima et al. 1991; Kurakake et al. 1995; Parajó et al. 1996; Tarantili et al. 1996; Moldes et al. 1999; Park et al. 2002; Berlin et al. 2007; Kim et al. 2008). These models are helpful in providing the measures of quantitative analysis for substrate properties, initial hydrolysis rate estimation, optimization of reaction conditions and spectroscopic data required for statistical models (Bansal et al. 2009). However, empirical models are limited to the experimental conditions, and do not provide mechanistic details of the hydrolysis process (Bansal et al. 2009).

The Michaelis-Menten equation, which was first proposed in 1913, suggests the formation of an enzyme-substrate complex as an intermediate before product formation (Michaelis and Menten 1913). This mechanistic model was further developed and proven applicable in many complex systems (Briggs 1925). Since then, considerable kinetic studies based on Michaelis-Menten equations have been applied to cellulases (Whitaker 1956; Li et al. 1965; Toda et al. 1968; Reese and Mandel 1971). The purpose of these models is to identify the rate limiting adsorption/hydrolysis steps and describe the action of enzymes on cellulosic substrates. However, the kinetic behavior differs significantly in the presence of more complex

and highly crystalline cellulose. Recently, models incorporating fractal and jamming kinetics have been developed to account for the decrease in hydrolysis rate in the heterogeneous, spatial-limited substrate (Valjamae et al. 2003; Xu and Ding 2007). These models accounts for processive enzyme activity on the cellulose chain and demonstrate the effect of overcrowding on the substrate surfaces.

Enzyme adsorption models based on Langmuir adsorption have also been applied to account for the enzyme adsorbed onto the substrate surface with the assumption that the hydrolysis rate is proportional to the adsorbed enzyme concentration, and the adsorption equilibrium is established faster than the hydrolysis reaction (Huang 1975; Dwivedi and Ghose 1979; Movagarnejad et al. 2000; Gan et al. 2003; Kadam et al. 2004). The Langmuir adsorption model provides a quantitative estimation of the maximum adsorption capacity and the adsorbed enzymes per weight of cellulose. The adsorbed enzyme concentration can be incorporated into the hydrolysis kinetic equations to model limited accessibility of lignocellulosic substrate (Kadam et al. 2004). However, this model may not be applicable in many conditions such as irreversible reaction, interacting adsorbed species, heterogeneous binding sites and non-uniform composition of adsorbed cellulase mixture (Zhang and Lynd 2004).

Kinetics studies based on the Michaelis-Menten model and other combined model equations have been applied to show the effect of product inhibition (Lynd et al. 2002; Zhang and Lynd 2004). The decreased in cellulose hydrolysis rate is often associated with the inhibition of enzyme by the metabolic products (ethanol and acetate) or degradation products (glucose and cellobiose) (Woodward and Arnold 1981; Ghosh et al. 2002; Gruno et al. 2004; Xiao et al. 2004). This work focused on the effect of cellobiose because it is highly inhibitory to cellulase enzyme activity (Mandels and Reese 1965; Holtzaple et al. 1990). The mechanism of

cellobiose inhibition on cellulase for soluble substrate has been suggested to be both competitive (Ghose and Das 1971; Ohmine et al. 1983; Kruus et al. 1995; Gruno et al. 2004) and non-competitive (Howell and Stuck 1975; Holtzapple et al. 1990). A competitive inhibitor binds to the active site of the enzyme and prevents substrate from binding to that site. This inhibition reaction may be reversible when sufficient substrate is available and the inhibitor is replaced by the enzymes. Therefore, the rate of reaction is a function of inhibitor and substrate concentration. A non-competitive inhibitor, on the other hand, interacts with the enzyme and binds to sites other than the enzyme active sites. This binding can occur before or after the enzyme binds to the substrate, and cause a conformational change in the enzyme active site to prevent product formation. It has been difficult to draw a conclusive interpretation on the type of inhibition mechanism of cellobiose due to highly complex property of cellulose and multiplicity of the cellulase enzyme system (Ryu and Mandels 1980).

Due to the recalcitrant nature of cellulose, modeling of enzymatic hydrolysis has been challenging. Also, it is difficult to draw direct comparison of parameters across different models because cellulose comes in different forms and sources. The kinetics of cellulose hydrolysis is heavily dependent on relevant enzyme and substrate properties such as crystallinity, degree of polymerization, accessibility to cellulose, substrate/enzyme concentration, size distribution of chains, and cellulase composition (Bansal et al. 2009). In addition to structural and physical features of cellulose, modeling enzyme kinetics on cellulose hydrolysis requires the consideration of mechanistic modes of enzyme action (including synergism), interaction between substrate and enzyme as well as the formation of multi enzyme-substrate complexes (Lee et al. 1980).

Surface techniques to study cellulose hydrolysis by cellulase

Due to the heterogeneous nature of the cellulose hydrolysis and various types of cellulose substrates with different physical properties, techniques have been developed to measure cellulase activity in bulk by: 1) product formation, 2) reduction in substrate quantity, and 3) physical/structural change in substrate (Zhang et al. 2006). Among these methods, assays associated with product accumulation are most commonly used because they do not require tedious preparation processes (Wood and Bhat 1988; Zhang et al. 2006). Hydrolysis products such as cellobiose or glucose are usually measured using HPLC (high pressure liquid chromatograph) or enzymatic glucose assays. Extra conversion steps to glucose are required for the enzyme assay if the degraded products are longer-chain cellodextrins. Assays involving cellulose quantification are usually measured through gravimetric or chemical means. They are less commonly used because these methods require more sample processing such as centrifugation, filtration, and drying, etc. Physical changes in cellulose are also used to infer the extent of hydrolysis, where the substrate's structural integrity is described through the swollen factor, fiber strength, structure collapse, turbidity, and viscosity (Zhang et al. 2006).

Measures of cellulase activity from bulk cellulose degradation offer information to evaluate enzyme activity, but are not usually sufficiently precise to provide closely-spaced time dependent data appropriate for testing mechanistic models of cellulase activity. Recently, novel surface analysis techniques such as Quartz Crystal Microbalance with Dissipation (QCM-D) and Atomic Force Microscopy (AFM) have been developed to provide more direct measures of cellulase interactions and activity on model cellulose thin films (Josefsson et al. 2007; Rojas Rejon et al. 2007; Turon et al. 2008; Aulin et al. 2009; Hu et al. 2009). The distinct advantage of these surface techniques relative to bulk cellulose degradation experiments is the potential to

observe and delineate cellulase adsorption and hydrolysis steps, where both enzymatic steps affect the observed hydrolysis rate.

QCM studies of enzymatic hydrolysis

Quartz crystal microbalance with dissipation (QCM-D) is a piezoelectric device that measures the change in resonance frequency (Δf) and dissipation (D) of a film deposited on a quartz crystal resonator. The output of frequency signal provides information regarding mass adsorbed/desorbed (ng cm^2) on the crystal resonator. Dissipation signal is associated with the viscoelasticity that gives structural/conformational information (softness/rigidity) of the surface molecule studied. The mode of operation by QCM is shown in Figure 2-4. A piece of circular quartz is sandwiched between two metal electrodes, and AC voltage is applied across the electrodes to make the quartz crystal oscillate. The AC voltage is alternatively switched on and off. When the voltage is turned off, the oscillating frequency and dissipation undergo decay (Fig 2-4b). The change in frequency decreases as mass is added to the surface of the acoustic resonator (Fig 2-4c). Increase in mass deposition on the substrate surface contributes to greater oscillatory decay (Fig 2-4d).

Because of ultra-sensitive measurement in mass, QCM has been widely used to provide simultaneous and direct measurement of the ultrasensitive mass and surface property changes of model cellulose thin films deposited on a quartz crystal resonator (Tammelin et al. 2006; Saarinen et al. 2008; Nyfors et al. 2009; Song et al. 2009; Mohan et al. 2012). In the presence of the cellulolytic enzyme, the corresponding change in mass is due to enzyme binding and/or cellulose hydrolysis. The flow-through system in the QCM chamber allows highly controlled

conditions of cellulose hydrolysis with variable parameters such as operating temperature, substrate/enzyme concentration, and type of substrate thin film.

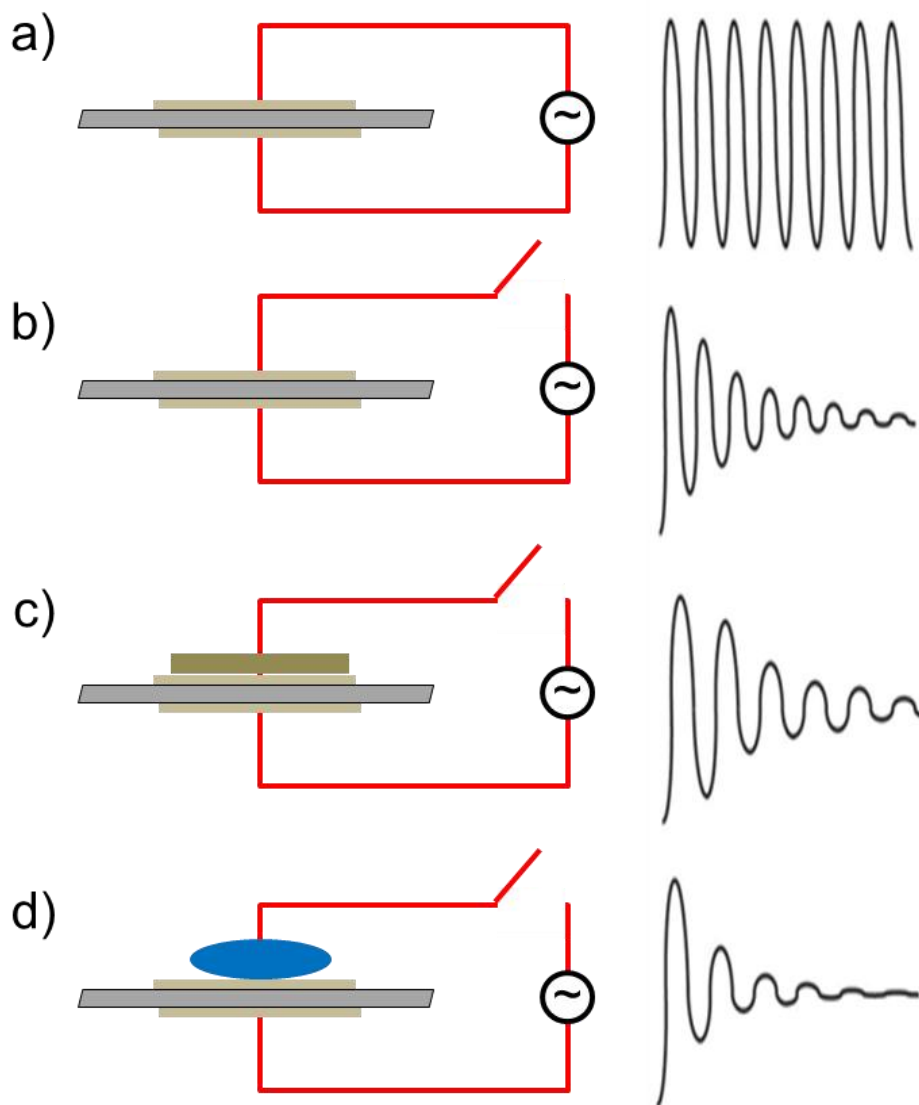


Figure 2-4 Mode of operation by QCM. Figures adapted from Andreas Dahlin, Chalmers Applied Physics (2011).

The application of QCM data to cellulase kinetic studies has used empirical hydrolysis models coupled with adsorption models to describe the dynamic events as cellulose film was

hydrolyzed by cellulase solution. Turon (Turon et al. 2008) modeled the frequency response in two-part functions: exponential decay function (to describe the initial frequency drop by enzyme adsorption) and Boltzmann-sigmoidal equation (to describe frequency increase due to cellulose hydrolysis). Ahola (2008) used the same empirical models to compare the kinetic parameters among different enzyme concentrations and type of cellulose substrate during the degradation of cellulose thin film by cellulase. Similarly, Hu et al (2009) applied a Langmuir based model to fit the adsorption data and a sigmoidal dose-response model to fit the hydrolysis response of the QCM frequency. Further model development is necessary to combine the two events because enzyme adsorption and desorption during cellulose hydrolysis is a simultaneous process.

Model Cellulose Thin Film for Enzymatic Hydrolysis

Surface analysis by QCM requires the synthesis of thin film substrates that adhere to the QCM sensor. Cellulose thin films are generally prepared by direct dissolution in organic solvent such as N-methylmorpholine-N-oxide (NMMO) or dimethylacetamide with lithium chloride (DMAc-LiCl) (Gunnars et al. 2002; Adelwoehrer et al. 2009; Aulin et al. 2009). Other solvents such as 1-butyl-3-methylimidazolium Cl (Swatloski et al. 2002) and hydrophilic ionic solutions have also been shown to dissolve cellulose (Klein and Snodgrass 1993; Krassig, 1993; (O'sullivan 1997). Cellulose is deposited on a solid surface support by Langmuir-Blodgett method (Schaub et al 1993) or spin-coating (Gunnars et al. 2002; Kontturi et al. 2003). For the purpose of enzymatic hydrolysis studies by QCM, a model cellulose thin film (Avicel) is prepared using NMMO with spin-coating techniques. Details of cellulose solubilization by NMMO are described below.

Model cellulose thin film: NMMO-Dissolved Cellulose

N-Methylmorpholine-N-oxide (NMMO) monohydrate has been demonstrated to dissolve cellulose (Chanzy et al. 1979; Dube et al. 1984; Buijtenhuijs et al. 1986). This organic compound, containing a heterocyclic amine oxide (Fig 2-5), is used in water mixtures to dissolve pulp to make industrial fibers, films, membranes, and flexible regenerated cellulose (Schurz 1994). The procedure to obtain dissolved cellulose requires four major steps:

- i) Preparation of cellulose in an NMMO-water mixture
- ii) Thermal control of the mixture until cellulose is dissolved
- iii) Regeneration of cellulose in precipitation bath (water or alcohol)
- iv) Washing and drying of the cellulose fiber

The process depends critically on the diffusion-driven precipitation of cellulose from cellulose-NMMO-water mixture with coagulating agent such as water or alcohol that is soluble with NMMO but insoluble with cellulose. The kinetic of the precipitation process is heavily dependent on the solvent strength, cellulose concentration and the interaction between the solvent and cellulose (Biganska and Navard 2005). Although the mechanism of the dissolution process is not clearly understood, it is thought that the dissolution takes place when the hydrogen bond is formed between the oxygen (from N-O dipole in NMMO) and the hydroxyl group of the cellulose (Chanzy et al. 1982). The melting temperature of the anhydrous NMMO is approximately 170 °C but the addition of hydrate decreases the melting point. However, water content must remain low during the dissolution process because water can compete with cellulose for NMMO molecules (Fink et al. 2001), and results in cellulose swelling.

Native cellulose contains both crystalline (cellulose I) and amorphous regions. The regenerated cellulose is partially crystalline antiparallel structure (cellulose II) (Chanzy et al.

1979; Osullivan 1997; Dubé and Blackwell 1983) but the other cellulose type may be observed under different process conditions (Dubé and Blackwell 1983). The mechanisms for cellulose dissolution by other solvents (DMAc-LiCl, 1-butyl-3-methylimidazolium Cl (Swatloski et al. 2002), and hydrophilic ionic solution) are also associated with the disruption of hydrogen bonding network in cellulose structure (McCormick and Shen 1982; McCormick et al. 1985).

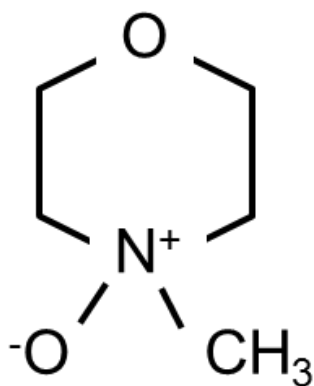


Figure 2-5 The chemical structure of N-Methylmorpholine-N-oxide (NMMO)

***Clostridium thermocellum* as the model organism**

C. thermocellum is of interest for biofuel production because it produces extracellular cellulase enzyme capable of degrading inexpensive cellulosic substrates into ethanol (Wiegel 1980; Payton 1984; Lynd et al. 1989; Lee 1997; Hendriks and Zeeman 2009). Liquid fermentation products (acetate, ethanol, lactate, formate), and gaseous products (hydrogen, carbon dioxide) are also co-produced through anaerobic fermentation. *C. thermocellum* has high specific growth (Ng et al. 1977) and metabolic rates (Payton 1984; Lynd et al. 1989), and grow at elevated temperatures (65° C). Growth at elevated temperatures offers a distinct advantage for bioprocessing fermentation because it increases the solubility of soluble substrates and reduces the issue of contamination because most microorganisms grow at mesophilic temperature (Clark

and Kelly 1990). However, a technical barrier that prevents large-scale bioethanol production using *C. thermocellum* is the low ethanol yield due to the co-production of other products. Metabolic approaches involving environmental perturbation have been demonstrated to alter product selectivity toward ethanol yield (Knutson et al. 1999; Bothun et al. 2004; Bothun et al. 2005; Collet et al. 2005; Li et al. 2012). In addition, the utilization of the highly-active enzyme system of *C. thermocellum* is also key to enhance lignocellulosic biomass conversion, even if its direct fermentation to ethanol is not the desired outcome.

Solvent and organic acid production by *C. thermocellum* is described in Figure 2-6. Glycolysis proceeds by the Embden-Meyerhof-Parnas pathway. Glucose (produced by cellobiose phosphorylase upon translocation) is catabolized into pyruvate. The energy released from the process is used to form adenosine-5'-triphosphate (ATP) from adenosine diphosphate (ADP) and inorganic phosphate through substrate-level phosphorylation. ATP contains phosphoryl bonds of high free energy. Upon converting ATP to ADP, energy is released for cellular repair and the excretion of internal molecules through active transport. The conversion of pyruvate to ethanol, acetate, and lactate is controlled by the regulation of nicotinamide adenine dinucleotide (NAD^+) and reduced nicotinamide adenine dinucleotide (NADH), which are also coupled to the synthesis of ATP. Therefore, the product formation of the bacteria can be altered to meet the need for energy-efficient metabolism. Ethanol is produced via ethanol dehydrogenase and NADH as a metabolic end-product. However, ethanol production is limited by the co-production of other end-products such as acetate and lactate (Lynd et al. 1989). An estimated ethanol production by wild type *C. thermocellum* ranges from 0.08 to 0.37 g ethanol g⁻¹ glucose equivalents fermented (Bender et al. 1985; Freier et al. 1988; Sai Ram and Seenayya 1989; Mori 1990; Sato et al. 1992; Sudha Rani et al. 1996).

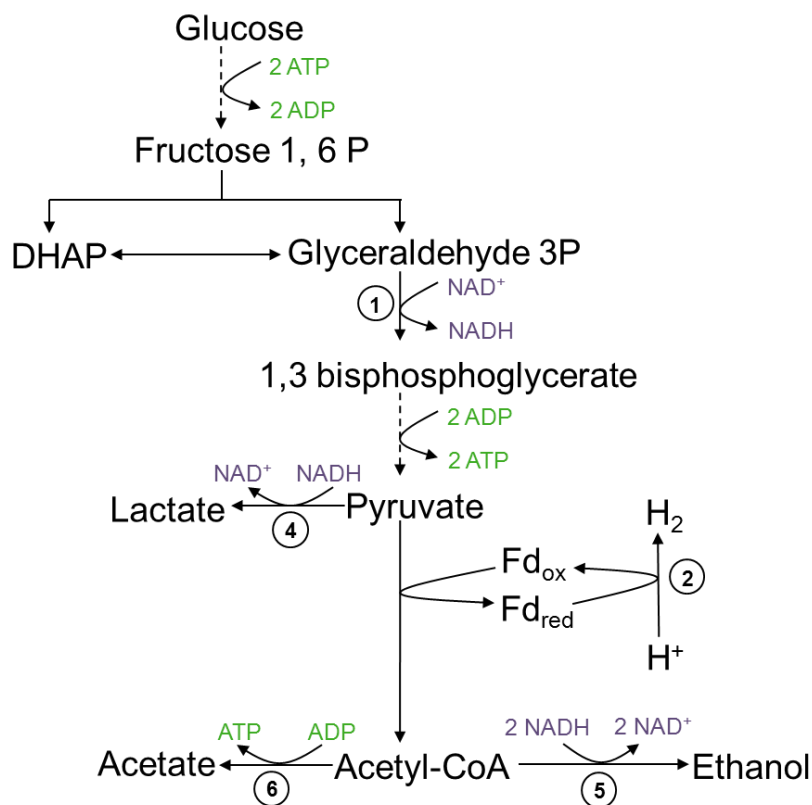


Figure 2-6 Simplified scheme of Embden-Meyerhof-Parnas (EMF) pathway of glucose catabolism by *C.thermocellum*. Numerals indicate enzymes: 1) glyceraldehyde 3-phosphate dehydrogenase, 2) ferredoxin-dependent hydrogenases, 3) NADH-ferredoxin oxidoreductase, 4) lactate dehydrogenase, 5) acetaldehyde-ethanol, 6) acetate kinase.

Metabolic modulation studies on Clostridia

The metabolism of *C.thermocellum* has been shown to exhibit versatile product pattern in response to the change in end-product concentrations (Lynd et al. 1989). Herrero (1982) presented various cases when the addition of fermentation end products caused a decreased in the accumulated product but an increased in other end-products. This mechanism is regulated through electron flows between redox intermediates in a pathway that lead to a particular product (Lynd et al. 1989). The metabolic flexibility of *C. thermocellum* to exhibit different product selectivity in response to environmental stimuli poses a unique opportunity for tunable product

selectivity toward ethanol production. Previous experiments (Bothun et al. 2004) revealed that elevated hydrostatic pressure decreases the acetate:ethanol ratios in continuous cultures as a result of a simultaneous increase in ethanol production and a decrease in acetate production. This is consistent with the observation of decreased acetate production by Lamed and Bayer (1988) in batch experiments with the addition of exogenous hydrogen (H_2), which is broadly attributed to the inhibition of bacterial hydrogenases by the end product H_2 . While the decreased acetate production is not unexpected, the dramatic increase in ethanol production is unexplained. With a goal of probing the underlying mechanism of H_2 partial pressure on ethanol production and manipulating the fermentation towards high ethanol selectivity, we examine the growth and end product formation of *C. thermocellum* in cultures perturbed with H_2 and several known hydrogenase inhibitors (carbon monoxide and methyl viologen).

Effect of H_2 on ethanol production

The presence of exogenous H_2 , a metabolic product of *C. thermocellum*, is suggested to alter the product pattern of the organism and increase ethanol yield. The mechanism by which hydrogen affects the ethanol production was proposed in earlier research. Lamed et al (1980) considered the H_2 production via hydrogenase activity inversely correlated to ferredoxin-NAD reductase. When the accumulation of hydrogen inhibits hydrogenase, ferredoxin-NAD reductase is allowed to produce more NADH, which is required by the reduction of acetyl CoA to ethanol. Lamed and Zeikus (1980) demonstrated a near 70% increase in ethanol to acetate ratio when exogenous H_2 is added to *C. thermocellum* AS 39 during culture growth on cellobiose. Similar results were reported by Bothun and colleagues (Bothun et al. 2004) when elevated pressure was applied to increase the dissolved H_2 concentration in *C. thermocellum* fermentation broth. At

high hydrostatic pressure (17.3 MPa), ethanol production was enhanced and acetate production decreased. Under those conditions, the solubility of H₂ was 130.4 mM rather than 0.7 mM near ambient pressure (Harvey 1996). This observation was consistent with the hypothesis that H₂ accumulation caused an end-product inhibition on hydrogenase, and a shift in product selectivity toward ethanol (Bothun et al. 2004).

Correspondingly, previous literature suggested that the decrease in hydrogen concentration permitted conversion of acetyl-CoA to acetate and ATP production. Weimer and Ng et al. (1977) demonstrated that acetate production by *C. thermocellum* was enhanced by co-culture with a methanogen. Methanogens convert carbon dioxide and hydrogen to methane. Weimer and Zeikus concluded that the increase in acetate was attributable to the activity of the methanogen. They observed a shift in the conversion of acetyl-CoA from ethanol to acetic acid when they co-cultured the *Clostridium* with *M. thermoautotrophicum* on cellulose (Ng et al. 1977). It is well known that enzymes can be inhibited by the products that they produce, and this concept is called end product inhibition. These latter results indicate that the absence of hydrogen is detrimental to ethanol production.

Effect of other hydrogenase inhibitors on ethanol production

Hydrogenase is an enzyme responsible for catalyzing the reversible hydrogen oxidation with reduced ferredoxin as the physiological electron donor (Gray and Gest 1965). Hydrogenase can exist in different forms based on their binding ligand: NiFe, NiFeSe, Fe-only, or non-metal (Adams 1990; Przybyla et al. 1992; Thauer et al. 1996). Hydrogenases liganded with Ni are often involved in the reversible oxidation of hydrogen, but Fe-liganded hydrogenases such as the Ferredoxin (Fd)-dependent NiFe hydrogenase or NAD(P)H-dependent Fe-only hydrogenases

from *C. thermocellum* are mostly associated with the reduction of protons to molecular hydrogen (Lemon and Peters 1999). Ethanol production is greatly influenced by the regulation of hydrogenase activity because hydrogen production utilizes NADH which is required for ethanol production. Therefore, the inhibition of hydrogenase activity has the potential to redirect electrons for NAD/NADH balance that leads to higher ethanol production. A search for a number of hydrogenase inhibitors and their effect on cellular growth and production is conducted to achieve greater solvent yield.

Carbon monoxide (CO)

Carbon monoxide is known to inhibit hydrogenase from *Clostridia*. The inhibition of hydrogen production by CO has been demonstrated in *Clostridium butyricum* (Kempner and Kubowitz 1933), *Clostridium pasteurianum* (Thauer et al. 1974), and *Clostridium acetobutylicum* (Kim et al. 1984). The increased partial pressure of carbon monoxide (2 to 10%) could significantly reduce the growth and hydrogen production in *C. acetobutylicum* by 90% (at 10% CO). CO is shown to compete with proton to the iron binding site of hydrogenase (Kempner and Kubowitz 1933; Lemon and Peters 1999). For example, the hydrolysis of iron pentacarbonyl to iron tetracarbonyl and carbon dioxide, $\text{Fe}(\text{CO})_5 + \text{H}_2\text{O} \rightarrow \text{Fe}(\text{CO})_4\text{H}_2 + \text{CO}_2$, shows that CO and 2H are interchangeable ligands (Thauer et al. 1974). However, carbon monoxide is only inhibitory when it is bound to the site of reversible hydrogen oxidation (Lemon and Peters 1999).

As a result of hydrogenase inhibition, an enhanced solvent production is observed. Kim et al (1984) reported an increase in butanol concentration and productivity by 63 % and 31 % in batch *C. acetobutylicum* under 15 % CO in gas phase. Meyer (Meyer et al. 1986) also reported

an increased in butanol specific production rate from initially 0 mmol g⁻¹ h⁻¹ to 10 mmol g⁻¹ h⁻¹ upon sparging CO in continuous fermentation. Incubation of the same organism in CO at elevated pressure again increased the butanol concentration by 9% and ethanol production by 178% (Datta and Zeikus 1985). The general proposed mechanism suggests that the hydrogenase inhibition by CO leads to the transfer of electrons from ferredoxin reduction to NAD⁺ reduction (via NAD: ferredoxin oxidoreductase). As a result, more NADH is available for butanol and ethanol production.

The increased in solvent yield was also demonstrated in our recent work in *C. thermocellum* batch cultures (Fig 2-7). An inverse relationship between the NAD⁺_{LE} (NAD⁺ from ethanol and lactate) and ATP production was observed when the cultures grew under N₂. However, when CO was present, a greater proportion of the pyruvate was dedicated to NAD⁺ recovery via ethanol and lactate. This work presents the case when the organism compensated for the loss of hydrogenase-dependent NAD⁺ production by converting a greater proportion of pyruvate to ethanol rather than acetate.

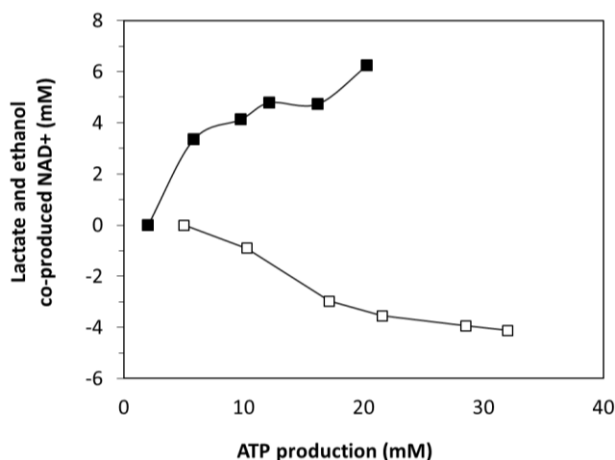


Figure 2-7 The relationship of NAD⁺_{LE} production to ATP production of *C. thermocellum* under a N₂- (open symbols) or CO- (filled symbols) headspace. NAD⁺_{LE} production and ATP production were calculated from the concentrations of cellobiose, acetate, ethanol, and lactate. Representative data are shown (Unpublished results).

Methyl viologen

Methyl viologen (MV) has also been used to enhance solvent production (Rao and Mutharasan 1987; Peguin and Soucaille 1996). The mechanistic effect of MV on solvent production is yet to be determined but is suggested to involve electrochemical reactions. MV, an artificial electron carrier, has the same electron carrier system as ferredoxin (Fd) to accept electrons from pyruvate: ferredoxin oxidoreductase. The reduction of MV is mediated through hydrogenase which is also a mediator for the oxidation of ferredoxin (Fd_{red}). Therefore, both MV and Fd_{red} are competing for an active site on the hydrogenase (Adams et al 1981; Yu and Wolin 1969). Consequently, the inhibition of Fd_{red} oxidation via hydrogenase leads to the activation of ferredoxin reductase which re-generates oxidized Fd (Fd_{oxi}) required for pyruvate catabolism. However, NADH at high level inhibits ferredoxin reductase unless it is eliminated through solvent production.

Based on this metabolic flexibility in *Clostridia*, MV has been used to increase solvent yield. Peguin and Soucaille (1996) demonstrated that the addition of MV to *Clostridium acetobutylicum* continuous cultures caused an increase in ethanol production from approximately 0 to 2 mM and butanol production from 2 to 10 mM. Similar result is observed by Rao and Mutharasan (1987) who recorded an increase of butanol productivity by 28% and ethanol productivity by 154% for the same organism. Despite the established effect of hydrogenase inhibitors (H₂ and CO) on ethanol yield in many *Clostridia*, there have been no definitive studies on the influence of methyl viologen on ethanol productivity in *C. thermocellum*.

Hydrogenases are very sensitive to carbon monoxide and end-product inhibition. The use of hydrogenase inhibitors in microbial fermentation takes the advantage of this characteristic in

hydrogenase to alter product distribution. Perturbation by hydrogenase inhibitors reduces NAD^+ production from ferredoxin-dependent hydrogenases, in which production of NAD^+ from other metabolic reactions must occur for glycolysis to proceed. This metabolic approach to elicit the desired phenotype of the microorganism offers an alternative strategy for enhancing product yield.

Chapter 3

Modeling of enzymatic hydrolysis and cellulase inhibition by cellobiose on cellulose thin films monitored by quartz crystal microbalance

Summary

Soluble sugars produced from the hydrolysis of cellulose are one of the most promising feedstocks for production of fuels and commodity chemicals from renewable plant-based resources. Fungal cellulase mixtures consisting of exoglucanase, endoglucanase, and β -glucosidase are capable of the efficient production of soluble sugars from the hydrolysis of accessible cellulose. The reduced efficiency of cellulases in the presence of cellobiose, an intermediate product of glucose formation, has been widely documented in the conversion of bulk biomass to soluble sugars. The reduced efficiency is interpreted at the interfacial level using the Quartz Crystal Microbalance with Dissipation (QCM-D) to monitor the change in mass and surface properties of model cellulose thin films cast from NMMO solutions. The time-dependent frequency response of the QCM simultaneously measures both enzyme adsorption and hydrolysis of the cellulose thin film by cellulase (from *Trichoderma reesei*, 0.5 % v/v), in which significant reduction in the extent of hydrolysis can be observed with increasing cellobiose concentrations (0, 0.1, 0.4, 1, or 5 g l⁻¹). The effect of inhibitor on enzyme adsorption and hydrolysis is modeled to 80 % conversion based on the QCM frequency response using a reaction scheme describing adsorption/desorption and hydrolysis events of the enzyme, inhibitor, and enzyme/inhibitor complexes. The relative value of adsorption and desorption constant of enzyme-substrate complex (ES) indicates an irreversible formation of ES complex. Strong

binding strength of inhibited cellulase to cellulose is also revealed through the estimation of rate constant ratio ($k_3/k_{-3}=2.1\times 10^2 \text{ mM}^{-1}$). The dissociation constant for the enzyme-inhibitor complex was determined to be $0.21 \pm 0.01 \text{ mM}$, which is comparable to that measured previously in bulk. The hydrolysis rate coefficient of adsorbed enzyme on the model films is estimated to be $0.057\pm 0.03 \text{ min}^{-1}$. The developed model is capable of predicting the hydrolysis performance of cellulase at different level of inhibitor and quantifies the impact of inhibitors on specific enzyme adsorption and reaction pathways in the enzymatic hydrolysis of cellulose.

Introduction

Cellulose is the most abundant polymer on earth (Lee and Fan 1982) and is a component in most sustainable biological resources, including agricultural and forestry biomass. Pretreatment and enzymatic degradation of cellulose from lignocellulosic biomass can be used to depolymerize cellulose and release utilizable soluble sugars. The multi-component cellulase enzyme mixture consisting of exoglucanase, endoglucanase, and β -glucosidase are capable of hydrolyzing the β -1, 4-glycosidic bond between monosaccharide units in cellulose. The enzymes work synergistically during cellulosic hydrolysis. Exoglucanase attacks the cellulose chain from the reducing and non-reducing end to produce cellobiose, while endoglucanase splits the cellulose away from chain end. β -glucosidase then converts the produced cellobiose into glucose.

The performance of cellulases is critical to achieving efficient and economical biomass conversion; cellulase is a major contributor to the cost of biomass conversion processes, accounting in some proposed processes for more than 50% of the cost (Howard et al. 2003; Sun et al. 2011). Byproducts of pretreatment of lignin and hemicellulose, including organic acids,

sugar degradation products (such as furfural) and lignin degradation products (such as vanillin) are microbial and cellulase inhibitors (García-Aparicio et al. 2006; Kim et al. 2006; Pienkos and Zhang 2009). Intermediate products of the conversion of cellulose to glucose, such as cellobiose (the disaccharide of glucose) are also cellulase inhibitor, decreasing the observed rate and extent of cellulose hydrolysis in bulk lignocellulosic materials (Holtzapfle et al. 1990; Gruno et al. 2004).

The mechanism of catalytic inhibition of cellulases is of significant interest, with the goal of enhancing enzyme recovery and yield of soluble sugars from cellulose. Fundamental biochemical and computational investigations of cellulase inhibition focus on understanding the role of the carbohydrate binding module (CBM) of cellulases, which gives it a strong binding ability to cellulose, and the catalytic core module (Bayer et al. 2004; Hildén and Johansson 2004; Demain et al. 2005; Josefsson et al. 2007). Traditional techniques such as enzyme assay, calorimetric measurement, and enzyme kinetics measurement in bulk solution with inhibitors have been used to study the inhibitory effects on hydrolysis (Beran and Paulicek 1992; Cantarella et al. 2004). The link between biochemical-level investigations of cellulase binding, hydrolysis, inhibition, and the corresponding effects of inhibition observed on bulk substrates is made tenuous by the difficulty of directly measuring enzyme-surface binding and hydrolysis events for these complex and heterogeneous cellulosic substrates.

Advanced surface measurement techniques suggest alternative methods to directly measure enzyme–substrate interactions (including adsorption and hydrolysis), and to determine the specific hydrolysis rate and the interaction between the enzyme-substrate complexes. Quartz crystal microbalance with dissipation (QCM-D) is a piezoelectric device that employs a quartz crystal resonator to measure the change in resonance frequency (Δf) and dissipation (D). The

ultrasensitive detection capability of QCM-D allows it to measure mass change (sensitivity of 1.8 ng cm^{-2}) or thickness change on the surface of the resonator (Q-Sense AB, Västra, Frölunda, Sweden).(Rodahl et al. 1995) QCM-D has been used widely for analyzing molecular mass adsorption, (Rodahl et al. 1997) enzyme degradation, (Yamashita et al. 2005; Hou et al. 2007) biofilm formation, (Nivens et al. 1993) and the interaction of macromolecules with proteins (Hianik et al. 2005) on model surfaces. Recent studies (Josefsson et al. 2007; Ahola et al. 2008; Turon et al. 2008; Hu et al. 2009) have reported the in situ measurement and monitoring of cellulose hydrolysis and cellulase adsorption, and empirical enzyme kinetics models on model cellulose thin film using QCM-D.

Enzyme kinetics models have been widely used to study the mechanism and rate of chemical reactions in the presence of inhibitors (Cornish-Bowden 1995). The advantage of using enzyme kinetics-based model over empirical models is the ability to describe the kinetics of enzymes and their interaction with inhibitors at the molecular level. Numerous mechanistic and empirical models have been used to describe the activity of cellulase enzymes on bulk cellulosic substrates (Bansal et al. 2009). These models provide quantitative comparison of enzymatic activities on various substrates. However, the mechanistic details (such as adsorption, binding affinity and hydrolysis rate) in the event of product inhibition have not been taken into account in the current models (Bansal et al. 2009).

In the present work, the adsorption and hydrolytic activity of cellulases from *Trichoderma reesei* on spin-coated cellulose thin films are measured by QCM from the change in resonance frequency. The hydrolytic activity of cellulases on cellulose thin films is quantified in the presence of cellobiose, a product of cellulose hydrolysis and a known inhibitor of cellulase activity. The effect of inhibitor (0, 0.1, 0.4, 1, or 5 g l^{-1}) on enzyme adsorption and activity is

modeled using a reaction scheme describing adsorption/desorption and hydrolysis events of the enzyme, inhibitor, and enzyme/inhibitor complexes. Parameters of the model are obtained by fitting the QCM resonance frequency response as a function of inhibitor concentration. The developed model is capable of predicting the hydrolysis performance of cellulase at different inhibitor concentrations and quantifies the impact of inhibitors on specific enzyme adsorption and reaction pathways in the enzymatic hydrolysis of cellulose.

Materials and Methods

Materials. Microcrystalline cellulose (MCC, 20 μ m) was purchased from Aldrich. N-methylmorpholine N-oxide (NMMO), dimethyl sulfoxide (DMSO, $\geq 99.8\%$), and polyethyleneimine (PEI, 50 wt. % aqueous solution) were supplied by Acros Organics. Acetate buffer (0.1 M, pH 5) was prepared by diluting glacial acetic acid (Fisher Scientific) in Milli-Q de-ionized water (Millipore Corporation). Cellulase (an aqueous mixture consisting of *endo*-glucanases, *exo*-glucanases, cellobiohydrolases, and β -glucosidases) from *Trichoderma reesei* 26921 (Celluclast®) was purchased from Sigma Aldrich. Cellulase (0.5 % v/v) was diluted in acetate buffer (0.1 M, pH 5). The protein content of cellulase (E_0 , mM) was determined by the Peterson method (Peterson 1977) protocol provided by Sigma with purchase of kit. Cellobiose (98% D(+)-cellobiose, Acros Organics) was dissolved in acetate buffer (0.1 M, pH 5) to make the cellobiose solution (in concentrations as indicated). The inhibited enzyme solutions were prepared by dissolving cellulase (0.5 % v/v) in the cellobiose solution.

Preparation of Cellulose Thin Film. The procedures to make cellulose thin films were slightly modified from the previous investigations (Gunnars et al. 2002; Fält et al. 2004). Gold-coated

QCM-D resonators (QSX 301, Q-Sense) were treated with ultraviolet cleaner (BioForce, Ames, IA) for 10 minutes to decompose and volatilize organic contaminants on the sensor surface. The UV-treated QCM-D sensors were immersed in diluted (0.2 % v/v) polyethyleneimine (PEI, 50 wt. % aqueous solution) for 15 minutes. PEI was used as an anchoring polymer (Ahola et al. 2008; Aulin et al. 2009) to attach the cellulose to the QCM-D sensor (QSX 301 Gold, Q-Sense AB, Göteborg, Sweden). The QCM-D sensors were contacted with de-ionized water (pH adjusted with sodium hydroxide to that of the polymer solution, ~ pH 10) for an additional 10 minutes, during which time the polymer precipitated on the surface of the sensor. The PEI-coated sensors were dried in the oven (50° C, 30 min), then kept in a desiccator (room temperature) for storage. A solution of microcrystalline cellulose in N-methylmorpholine-N-Oxide (NMMO 50 wt. % aqueous solution in water) was prepared by adding cellulose (2 wt. %) to NMMO preheated to 110 °C and continuing to heat the mixture to 115 °C. The addition of cellulose at high temperature solution prevented the agglomeration of fine microcrystalline cellulose. A clear solution was obtained at 115 °C after approximately one hour. Dimethyl sulfoxide (DMSO, ≥99.8%) was slowly added to the mixture to make a final solution of 0.5 wt. % cellulose. The temperature of the cellulose solution was reduced to 70° C, prior to spin coating. Cellulose solution (0.1 ml) was spin-coated (4500 rpm, 40 sec, WS-400BZ-6NPP/Lite, Laurell Technologies) on the PEI-coated QCM-D sensors. After spin-coating, the sensors were immersed in deionized water (30 min), and then dried in the oven (50° C, 30 min). The cellulose-coated sensors were stored in a desiccator at room temperature prior to use.

Cellulose Thin Film Characterization by Spectroscopic Ellipsometer and Atomic Force Microscopy (AFM). The thickness of model cellulose thin film was measured using a variable

angle spectroscopic ellipsometer (M-2000, JA Woollam Co., Inc.). The surface topography and material distribution of the cellulose thin film on QCM sensor (QSX301) was measured by AFM in air (Series 4500, Agilent Technologies). The support base (QSX301) and the cellulose thin layer coating on the sensor (QSX301) were scanned in tapping mode using a silicon cantilever (TAP 300AI-G, Budget Sensors) with a spring constant of 40 N/m and a driving frequency of 300 kHz. The acquired scan area ranged from 2×2 μm to 50×50 μm. At least three sensors were scanned to confirm reproducibility.

Cellulose Thin Films/ Cellulase Interactions Measured by Quartz Microbalance with Dissipation (QCM-D). A quartz crystal microbalance (Q-Sense E4) equipped with four temperature controlled flow modules was used to measure changes in mass per unit area and in the viscoelasticity properties of the cellulose thin films from the change in frequency (Δf) and dissipation (D) of the cellulose-coated quartz crystal resonator. The oscillation frequency and dissipation energy were measured simultaneously from the application of an AC voltage across the electrode, causing the piezoelectric quartz crystal to vibrate (Rodahl et al. 1995). The resonance frequency change (Δf) can be used to calculate the proportional mass absorbed on the crystal surface by the Sauerbrey equation:

$$\Delta m = -\frac{c}{n} \Delta f \quad (1)$$

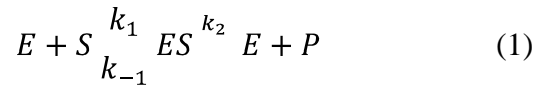
where c is the constant for mass sensitivity and n is the overtone number. “ c ” varies for different type of sensors. For the 4.95 MHz AT-cut sensor used in this study, c is equal to 17.8 ng cm⁻² Hz⁻¹. The QCM acquires frequency signal at the fundamental resonance (5 MHz) and at a multiple of resonance (overtone frequency). Third overtone frequency was used to avoid edge effect (unstable frequency signal at the edge of the sensor measured by the fundamental

frequency). The Sauerbrey equation (Rodahl et al. 1995) is valid for the following conditions: 1) the surface film is flat and uniformly distributed, 2) the mass change of the crystal surface is much smaller than the mass of the quartz resonator, 3) the film is rigid, meaning that the mass absorbed on to the surface must be firmly attached with no oscillatory effect ($D < 10^{-6}$ per 10 Hz). In this study, the Sauerbrey equation is valid because the change in dissipation during cellulase treatment on ultrathin cellulose films prepared with the dissolved cellulose was relatively small ($2-6 \times 10^{-6}$ dissipation units).

The mass change of cellulase thin films in response to cellulase, cellobiose (enzyme inhibitor) and cellulase/cellobiose mixtures was measured by QCM. Prior to contacting the cellulose thin films with cellulase/cellobiose solutions, the cellulose-coated QCM sensors were incubated with the acetate buffer (0.1 M, pH 5) at a flow rate of 0.2 ml min^{-1} until a constant baseline in frequency measurement was reached ($< 2 \text{ Hz hr}^{-1}$), which was obtained in approximately 30 min. The temperature of the QCM chamber was controlled at $30 \text{ }^\circ\text{C}$. All liquid solutions were degassed for 30 min using an ultra-sonicator (Cole-Parmer 8890, IL) prior to injection in the flow cell. The adsorption of cellobiose on cellulose thin films was measured from cellobiose solutions (20, 40, 60, and 80 g l^{-1}) which were injected into the QCM chamber in continuous flow mode (0.2 ml min^{-1}). When enzyme solutions (0.5 % v/v cellulase in the presence of 0, 0.1, 0.4, 1, or 5 g l^{-1} cellobiose) were injected (0.2 ml min^{-1}) into the QCM flow module containing the cellulose thin films, both cellulase/cellobiose binding and cellulose hydrolysis were monitored simultaneously. The change in oscillation frequency and dissipation energy was recorded throughout the experiment. When the frequency signal and dissipation had no significant change ($< 2 \text{ Hz h}^{-1}$), the injection solution was switched to acetate buffer to rinse and remove any remaining hydrolysate on the sensor surface.

Model Development for Inhibited Enzyme-Kinetics on Cellulose Thin Films. A model was developed to describe cellulase adsorption and hydrolysis on thin cellulose films in the presence of inhibitor (cellobiose) using a series of differential equations describing the concentration of the system species based on reaction kinetics. The QCM frequency profiles from inhibited enzyme catalyzed reactions were linked to the reaction scheme and used to fit the kinetic parameters.

A traditional Michaelis-Menten kinetic scheme assumes homogenous reaction in which the enzyme (E) binds to the soluble substrate (S) to form a substrate-bound enzyme (ES) and the enzyme is recovered after the product (P) is formed. A translation of this kinetic scheme is presented in eq 1. In the presence of inhibitor, the inhibited enzyme complex (EI) is formed (eq 2). Both EI and the inhibitor (I) may also bind to the substrate (eq 3 and eq 4) to form inhibited enzyme-substrate complex (ESI) or inhibitor-substrate complex (SI), respectively. Binding to the substrate is reversible, as described for ES , ESI and SI formation and dissociation (eq 1, eq 3, and eq 4).



The concentration of substrate (S), enzyme (E) and inhibitor (I) are unknown and are determined by eq 5 to eq 7. S_i is the instantaneous concentration of hydrolyzable substrate. When time equals to zero, the initial substrate coverage on the sensor is S_o . E_o is the initial

enzyme concentration in solution and was determined from Peterson Method (Peterson et al. 1977). I_o is the total inhibitor concentration (mM) in solution, which is varied across experiments.

$$S = [S_i] - ES - ESI - [SI] \quad (5)$$

$$E = [E_o] - EI \quad (6)$$

$$I = [I_o] - EI \quad (7)$$

The kinetic scheme (eq 1 to eq 4) leads to the set of differential equations describing cellulase adsorption and hydrolysis (eq 8 to eq 11). In this set of equations, the enzyme/inhibitor complexation reaction (eq 2) is assumed to be at quasi-equilibrium because the enzyme and inhibitor are present together in the solution that is introduced to QCM cell. The equilibrium constant for the enzyme-inhibitor complex, K_I , is defined by eq 12.

$$\frac{d[ES]}{dt} = k_1 E S - k_{-1} ES - k_2 ES \quad (8)$$

$$\frac{d[S_i]}{dt} = -k_2 ES \quad (9)$$

$$\frac{d[ESI]}{dt} = k_3 EI S - k_{-3}[ESI] \quad (10)$$

$$\frac{d[SI]}{dt} = k_4 I S - k_{-4}[SI] \quad (11)$$

$$K_I = \frac{E I}{EI} \quad (12)$$

The rate parameters in the model were fit to the experimentally measured change in frequency, where the change in mass of the film can be expressed as a sum of the change in mass due to enzyme and enzyme complex adsorption on the substrate, the adsorption of inhibitor, and the mass loss due to hydrolysis:

$$\Delta f = -A \underset{\text{enzyme adsorption}}{ES} + [ESI] + B \underset{\text{hydrolysis}}{[S_o] - [S_i]} - C \underset{\text{inhibitor binding}}{[SI]} \quad (13)$$

A represents the frequency change per bound enzyme and inhibited enzyme (which were assumed to contribute similarly to the frequency change), B represents the frequency change per substrate lost, and C represents the frequency change per bound inhibitor.

The initial substrate concentration of each individual film, S_o , is slightly different for each hydrolysis experiment (because of slight sample-to-sample variability during spin coating). The units of S_i and S_o are reported in a standardized hydrolysable “substrate unit,” SU. The value of S_o for the hydrolysis experiment with no cellobiose is normalized to 1 SU, and the remaining S_o for each hydrolysis experiment is presented relative to this surface concentration. The “substrate unit” represents the hydrolysable amount of cellulose in this multilayered film. The frequency response described using a normalized initial substrate concentration is:

$$\Delta f = -A S_o \left(\frac{ES}{S_o} + \frac{ESI}{S_o} \right) + B S_o \left(\frac{S_o}{S_o} - \frac{S_i}{S_o} \right) - C S_o \left(\frac{SI}{S_o} \right) \quad (14)$$

The rate events describing potential modes of enzyme inhibition (i.e. inhibitor binding to the substrate and the inhibitor-bound enzyme binding to the substrate) are described by this model. Time- and concentration-dependent enzyme deactivation and non-productive enzyme-enzyme interactions, such as enzyme jamming or overcrowding effect, are not accounted for in rate equations in this model. In addition, the complex surface effects and enzyme-enzyme interactions that occur as the cellulose substrate is depleted and the processive cellulase enzymes encounter other enzymes warrant further fundamental investigation and are not described in the kinetic model. For this reason, kinetic parameters were fit to frequencies corresponding up to 80% substrate conversion ($S_i/S_o = 0.2$), where the impact of these additional enzyme processes should be limited. This is consistent with bulk kinetic investigations of cellulose hydrolysis by cellulases, which the validated conversion range was generally below 70% (Bansal et al. 2009).

The thin layer of cellulose film and the enzyme solutions were contacted in a flow-through cell, thus the free enzyme concentration (E) and inhibitor concentration (I) in solution were assumed to be constant. This is distinctly different from traditional Michaelis-Menten kinetics, in which there is a fixed total enzyme concentration distributed between free enzyme and bound enzyme. The free substrate concentration (S) in our analysis can be represented by eq 5 where S_i denotes the instantaneous concentration of hydrolysable substrate. The hydrolysable substrate is lost by hydrolysis (eq 9). The initial concentrations of complex ES , ESI , and SI are assumed to be zero, and the initial substrate concentration (S_0) on an individual QCM sensor is unknown and is treated as a different fitting parameter for each experiment. The rest of the coefficients in the model are found by fitting to all experiments simultaneously.

The parameters of the model were determined in two nonlinear regression steps. First, inhibitor adsorption experiments were conducted to decouple the effect of mass adsorption due to inhibitor and the effect of mass adsorption due to enzyme/enzyme complex. These experiments were performed by introducing only cellobiose (20, 40, 60, 80 g l⁻¹) to the cellulose-coated QCM resonator and measuring the frequency response as a function of concentration. Because the experiments only measured the frequency change due to cellobiose, eq 14 can be simplified to $\Delta f = -CS_0 \frac{SI}{S_0}$ where the adsorbed inhibitor on the substrate, SI , can be calculated from eq 11. Parameters C , k_4 , and k_{-4} were determined by minimizing the squared difference between the modeled and measured frequency response at a large number of time points using *lsqcurvefit* function in MATLAB Curve Fitting Toolbox. Data from all four cellobiose concentration experiments were used simultaneously for regression and error analysis.

The frequency response of the cellulose-coated QCM resonator in the presence of cellulase/inhibitor mixtures (0.5 % v/v cellulase in the presence of 0, 0.1, 0.4, 1, or 5 g l⁻¹

cellobiose) was used to determine the additional kinetic parameters, holding the values of C , k_4 , and k_{-4} constant. Parameters (k_1 , k_{-1} , k_2 , k_3 , k_{-3} , K_1 , A , B , and S_o for the individual experiment) were determined by nonlinear regression using the *lsqcurvefit* function in MATLAB Curve Fitting Toolbox. All parameters, except for S_o , were held constant across experiments and all five data sets were used for simultaneous nonlinear regression. S_o values were determined for each experiment due to the potential for different surface coverage of cellulose on each QCM resonator. The standard errors associated with the kinetic parameters were calculated from the 95% confidence interval determined by the *nlparci* function in the MATLAB Nonlinear Statistics Toolbox. The model was not parameterized to fit the frequency response curve beyond 80% substrate conversion.

The inhibition model proposed in Equations 1-7 are shown schematically in Figure 3-1a. Alternative models for enzyme inhibition (Fig 3-1b-d) can also be proposed. The ability to describe the QCM frequency response as a function of inhibitor concentration with these alternative models was investigated. For example, classical competitive inhibition, in which the inhibitor competes with the substrate for the active site on the enzyme, is represented by Fig 3-1b. However, this model does not fully reflect the inhibitory effect observed in the experimental data, and was therefore poorly fit to the data ($R^2 < 0.8$). Cellobiose inhibition via non-competitive inhibition (Fig 3-1c) was also evaluated, but the adsorption constant for cellobiose binding to the enzyme-substrate complex (K_{ib}) was negligible according to the values found by regression (data not shown). Similarly, when *ESI* was allowed to form products (Fig 3-1d), the forward reaction constant was also negligible according to the values found by regression. The results of models containing additional parameters of negligible significance to the fit are not reported. Thus, the parameters represented by Fig 3-1a are our final form of the model.

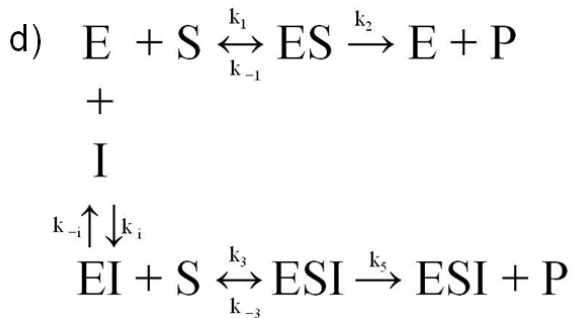
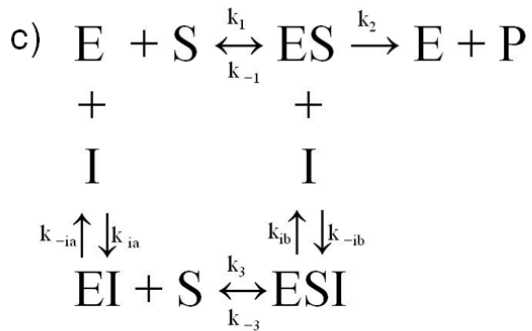
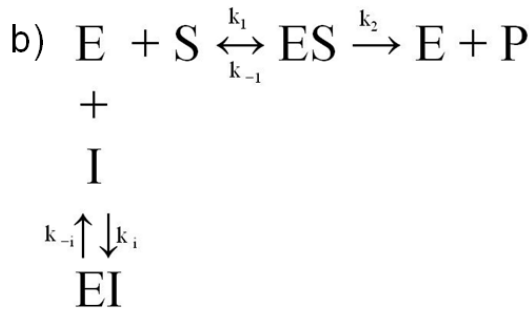
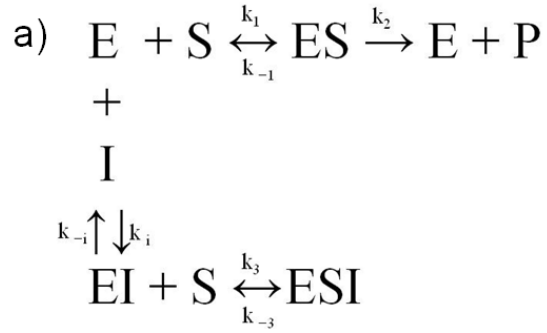


Figure 3-1 Potential reaction pathways of enzyme inhibition during cellulose hydrolysis. a) Pathway represented by equations 1-7, as reported in this paper; b) Competitive inhibition model; c) Non-competitive inhibition model; and d) Reactive substrate/enzyme/inhibitor complex model.

Results and Discussion

Model cellulose thin film on QCM sensors

The thickness of the model cellulose films was characterized by a variable angle spectroscopic ellipsometer. Under the experimental and spin coating conditions employed in this study, the thickness of the polyethyleneimine layer was approximately 3 nm, and the cellulose layer was approximately 21 nm. The thickness of cellulose thin films prepared by previous researchers using similar techniques (Gunnars et al. 2002; Freudenberg et al. 2005; Notley et al. 2006; Eriksson et al. 2007; Rojas Orlando et al. 2007) ranged from 10 to 280 nm. The results of the film thickness depend heavily on preparation procedure (i.e. cellulose dissolution process, deposition technique, surface coating speed, etc.) and the materials utilized (i.e. cellulose type, cellulose solvent, cellulose-to-solvent ratio, etc.) (Gunnars et al. 2002; Kontturi et al. 2006). The amount of spin-coated cellulose on the QCM sensor was approximately 641 ± 24 ng, quantified by identifying the frequency difference between the cellulose + polyethyleneimine coated sensor and polyethyleneimine coated sensor only using QCM. Therefore, one substrate unit (SU) for substrate concentration represents approximately 640 ng of cellulose on the QCM sensors.

AFM images (Fig 3-2) of the bare gold and cellulose-coated sensor before and after the incubation with cellulases validate the presence of a cellulose thin film on the QCM-D resonator. The bare gold QCM sensors (Fig 3-2a) have a globular texture, which is typical for colloidal gold particles. After the anchoring polymer (polyethyleneimine) was adsorbed onto the gold surface by immersing the QCM sensor (15 min), the dissolved cellulose was coated on the sensor, and ridge-like filaments of cellulose are deposited on the surface (Fig 3-2b). The morphological image of the spin-coated cellulose film is comparable to that reported for microcrystalline cellulose thin films in previous work (Kontturi et al. 2006; Aulin et al. 2009).

After the cellulose-coated sensor was treated with cellulase (30°C, pH 5), the cellulose filaments were no longer visible (Fig 3-2c).

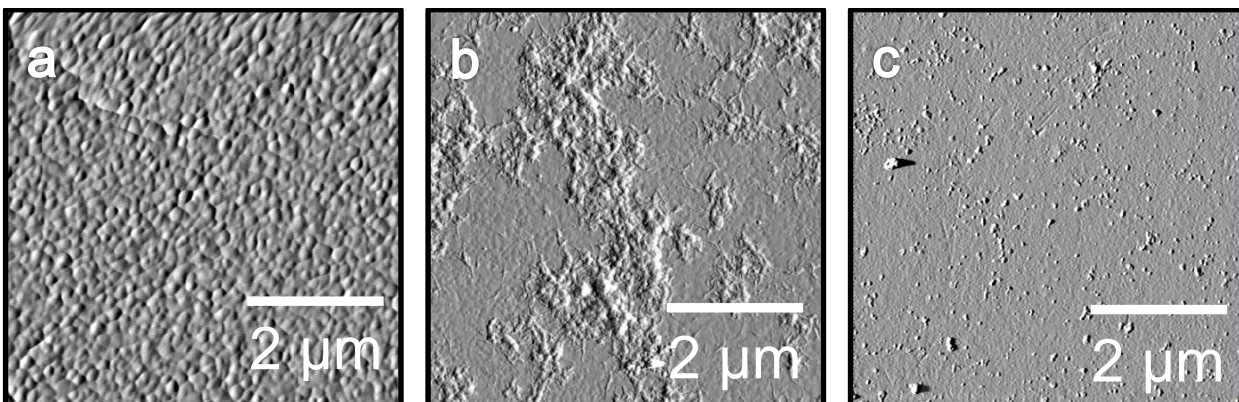


Figure 3-2 AFM amplitude images (tapping mode, $5 \times 5 \mu\text{m}^2$) of (a) gold-coated quartz crystal resonator; (b) cellulose-coated quartz crystal resonator before exposure to cellulases; (c) cellulose-coated quartz crystal resonator after hydrolysis.

The dissolution of cellulose in NMMO/water system, which was used to produce the cellulose thin films, is the result of breaking the intramolecular hydrogen bonds within the cellulose chains and forming the complex between NMMO and hydroxyl groups of cellulose (Maia et al. 1981; Fink et al. 2001; Bocek 2003; Jie et al. 2005). Elevated temperature greatly reduces the molecular dipoles and hydrogen bonds between cellulose chains (Fink et al. 2001). Previous investigations have demonstrated that the formation of hydrogen bonds between NMMO and the hydroxyl group of cellulose did not derivatize the cellulose structure, but dissolves the cellulose to form a homogenous solution (Berger et al. 1988). The process converts crystalline cellulose to amorphous cellulose (Zhao et al. 2007; El-Wakil and Hassan 2008). Upon diluting with excess water, the cellulose loses its preference for interaction with the NMMO molecule, and precipitates on the surface of the QCM resonator. Cellulose II (containing amorphous and crystalline structure) is obtained according to prior work with this

type of NMMO-based cellulose model film. Aulin et al (2009) showed that the NMMO-dissolved microcrystalline cellulose has approximately 60% degree of crystallinity. Therefore, the cellulose filaments observed on the QCM resonator are expected to have both amorphous and crystalline regions.

QCM Experimentation: Enzymatic Binding and Hydrolysis

QCM-D was employed to provide quantitative measurements on enzyme binding and hydrolysis on the cellulose thin film. A sample frequency and dissipation profile (using the 3rd overtone) is presented for cellulase solution (0.5 % v/v) in the absence of inhibitor (Fig 3-3a), in which the flowing enzyme solution replaces acetate buffer (0.1 M, pH 5) 3 min after the start of the plot. A rapid drop in frequency (to a minimum of -38 Hz) was observed due to the rapid adsorption/binding of cellulase onto the cellulose surface. After enzyme loading on the cellulose surface (approximately 6 min after the introduction of cellulase), the frequency increases with time due to the reduction of mass of the film. This reduction in mass is attributed to the loss of cellulose by enzymatic hydrolysis. Finally, the maximum frequency reaches a plateau when the available substrate was hydrolyzed. The AFM image of the film (Fig 3-2c) also reveals a much smoother surface after the enzymatic treatment. Turon et al (2008) reported an approximately 60% decrease in roughness of the hydrolyzed film due to the action of the cellulase enzyme. This previous investigation suggested that the residual cellulose (with higher crystalline region) may remain on the surface, and was not able to be degraded by the enzyme.

The energy dissipation describes the change in structural property of cellulose thin film during the enzyme binding and hydrolysis. A dissipation signal responds to the viscoelastical change of the film, which is dependent upon the thickness, the softness/rigidity, and the density

of the film. When cellulase was introduced on the substrate surface (3 min), the dissipation signal increased (Fig 3-3b). This is indicative of a soft film caused by the cellulase attaching to the cellulose chains. The maximum dissipation energy occurs during the linear increase of the frequency, and the dissipation decreases as the frequency curve slowly flattened out. This is consistent with high surface coverage of available cellulose when hydrolysis is dominant, followed by a decrease in cellulose availability, causing a thinner and more rigid surface. Eventually, the dissipation signal becomes relatively constant ($< 5 \text{ Hz hr}^{-1}$), a trend that mirrors the frequency signal at large times and is consistent with removal of most or all of the cellulose by hydrolysis.

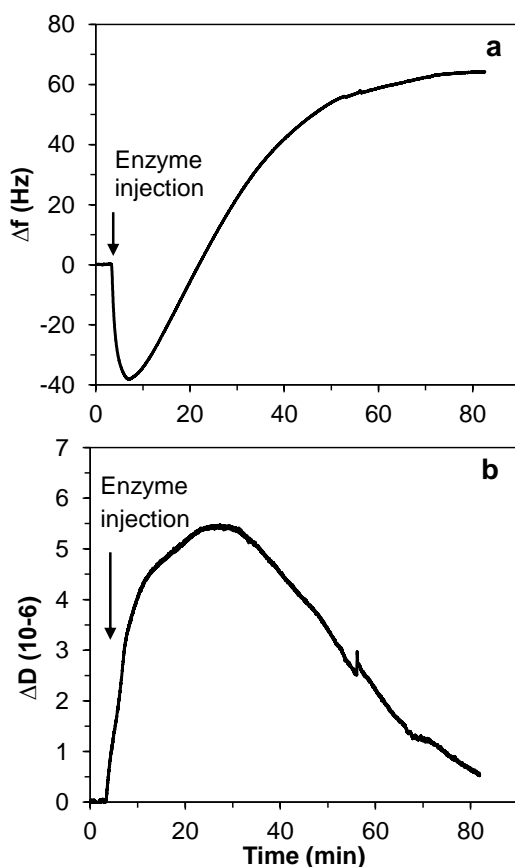


Figure 3-3 Frequency (a) and dissipation (b) profile of cellulose hydrolysis by cellulase (0.5 % v/v) at 30 °C.

The observed trends in frequency and dissipation responses are typical for cellulose film hydrolysis by cellulase (Ahola et al. 2008; Turon et al. 2008; Hu et al. 2009). The rate of the initial frequency decrease is usually fast (< 5 min) due to the rapid adsorption of cellulase to the cellulose surface. The extent of frequency increase due to hydrolysis depends on the crystallinity, the surface distribution and the thickness of the cellulose thin film prepared. Ahola et al (2008) showed that the cellulose nanocrystal (highly crystalline cellulose) was more difficult hydrolyze by the cellulase enzyme and therefore resulted in longer degradation time and less mass degraded from the surface. The change in the dissipation signal is a result of the change in viscoelastic property of the film. When immersed in liquid, the amorphous region of the cellulose layer swells and causes the dissipation signal to increase (Aulin et al. 2009). The binding of the enzyme to the cellulase surface further increases the energy dissipation until the effect of hydrolysis begins to dominate over enzyme binding. The corresponding decrease in dissipation is the result of thinning of the cellulose film due to hydrolysis by cellulase. In this study, small clusters of unhydrolyzed cellulose are observed by AFM (Fig 3-2c) following enzyme hydrolysis. Similar observation by Turon et al (2008) also suggests that residual cellulose remains on the sensor surface after long incubation time (> 2 h).

QCM Experimentation: Enzymatic binding and hydrolysis in the presence of inhibitors

The successful use of QCM to observe enzyme binding and hydrolysis of cellulose thin films is extended to investigate the effect of a cellulase inhibitor, cellobiose. Inhibitor binding experiments were conducted to account for the QCM-D frequency decrease due to the binding of cellobiose to the cellulose surface. Figure 3-4a shows the frequency response of the cellulose-coated resonator with the addition of cellobiose (20, 40, 60, or 80 g l⁻¹). When the loading

cellobiose concentration increases, the drop in frequency signal is approximately proportional to the concentration of cellobiose in solution (Fig 3-4a). The relative frequency drops in response to the cellobiose (20, 40, 60, 80 g l⁻¹) adsorption are -14.3, -31.3, -41.5, -56.7 Hz, respectively. These frequency drops correspond to 85, 185, 246, 336 ng cm⁻² of adsorbed cellobiose, as calculated by the Sauerbrey equation. When the cellobiose concentration increases, the increase in dissipation signal indicates that the film is softened by the attached layer of cellobiose, but the adsorbed film does not dissolve.

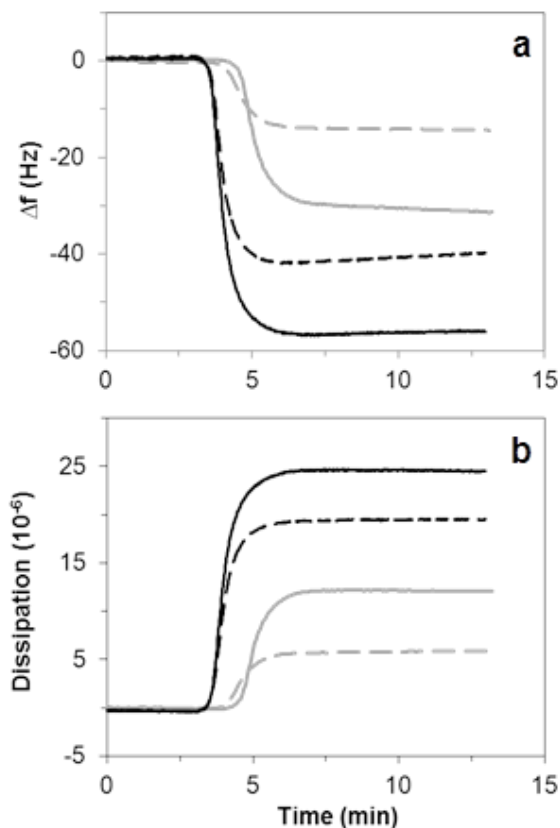


Figure 3-4 Frequency profile of cellobiose loading at 20 g l⁻¹ (--- dashed line), 40 g l⁻¹ (— gray solid line), 60 g l⁻¹ (--- black dashed line), 80 g l⁻¹ (— black solid line).

Cellobiose (0, 0.1, 0.4, or 1, 5 g l⁻¹) was added to the cellulase solutions (0.5 v% v/v) in the flow through QCM cell to study the effect of product inhibition on the rate of cellulose

degradation, as interpreted from the frequency response of the QCM (Figure 3-5). The addition of cellobiose in the enzyme solution did not alter the solution pH (data not shown). Similar to the frequency response in the absence of cellobiose, the binding of cellulase to the cellulose surface (i.e. decrease in Δf) was followed by the cellulose hydrolysis (i.e. increase in Δf), which was evident within 5 min after the injection of the enzyme solution. The increased concentration of inhibitor does not result in a significant initial reduction in resonance frequency, which is consistent with minimal adsorption of cellobiose on the cellulose films due to the low inhibitor concentrations ($\leq 1 \text{ g l}^{-1}$) employed. Changes in hydrolysis rate can be inferred from changes in the slope of the QCM frequency curve following the initial minimum. The slope decreases as the inhibitor concentration increases, consistent with cellobiose concentration-dependent inhibition resulting in a slower rate of loss of film mass due to hydrolysis. At higher concentrations of cellobiose (5 g/l cellobiose), the decrease in frequency due to enzyme adsorption is followed by a plateau, with no evidence of hydrolysis. Complete inactivation of the enzyme is suggested by the frequency response curve in the presence of greater than 5 g/l cellobiose.

Cellobiose was selected because it is a known inhibitor of cellulase activity (Mandels and Reese 1965; Lee and Fan 1982; Holtzapple et al. 1990; Gusakov et al. 1992; Gruno et al. 2004). Cellobiose concentrations of 3.75 g/l were found to reduce the activity of crude cellulase from *Trichoderma reesei* by 50% (Ryu and Lee 1986). At 5 g/l, cellobiose was found to almost completely inhibit (92 %) the purified recombinant *Clostridium thermocellum* CelS (endoglucanase) in *Escharichia coli* (Kruus et al. 1995). Similar degrees of inhibition are observed in QCM with the addition of 5 g/l cellobiose, as measured by steady state flow (Fig 3-

5), supporting our use of QCM to obtain and interpret the kinetics of cellulose hydrolysis in the presence of enzyme inhibitors.

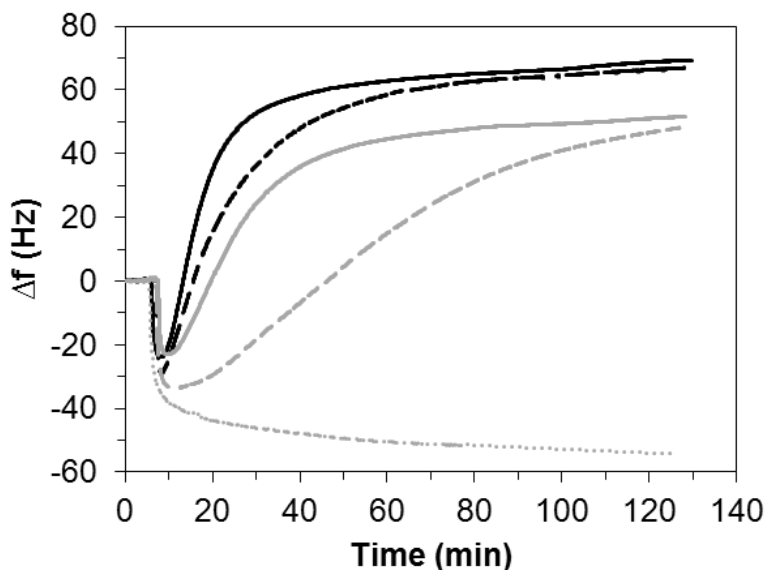


Figure 3-5 Frequency profile of cellulose hydrolysis by cellulase (0.5 % v/v) in the presence cellobiose at 0 g l^{-1} (— *black solid line*), 0.1 g l^{-1} (- - - *black dashed line*), 0.4 g l^{-1} (— *gray solid line*), 1 g l^{-1} (- - - *gray dashed line*), 5 g l^{-1} (..... *gray dotted line*).

Model Analysis and Parameter Estimation

A non-linear kinetic model was developed to describe the surface phenomena of binding and hydrolysis by cellulase in the presence of inhibitor. This model makes use of the environmental control of the QCM flow cell (allowing for constant free enzyme and inhibitor concentrations) and is capable of describing adsorption and reaction of a heterogeneous substrate. The enzymatic mechanisms of cellulose hydrolysis on the model cellulose film were described by eq 1 to eq 4. The model frequency equation (eq 14) accounts for adsorption (of inhibited and active cellulase), hydrolysis (of cellulose) and binding (of inhibitors). The model parameters are eight kinetic and equilibrium constants ($k_1, k_{-1}, k_2, k_3, k_{-3}, k_4, k_{-4}, K_I$), three frequency constants (A, B, C ; related to the sensitivity of the QCM to the individual species), and

an initial cellulose surface coverage parameter (S_0) (Table 3-1). A single constant was determined across experiments by simultaneously fitting the QCM frequency response curves obtained as a function of cellobiose concentration (0, 0.1, 0.4, 1, and 5 g/l) (Fig 3-6).

The exception is S_0 , which represents the initial surface coverage of the cellulose thin film and is a unique parameter for each frequency response curve. S_0 is expected to vary slightly from experiment to experiment due to the slight change in cellulose distribution on each QCM sensor. The model parameters giving the best fits shown in Figure 3-6 are summarized in Table 3-1.

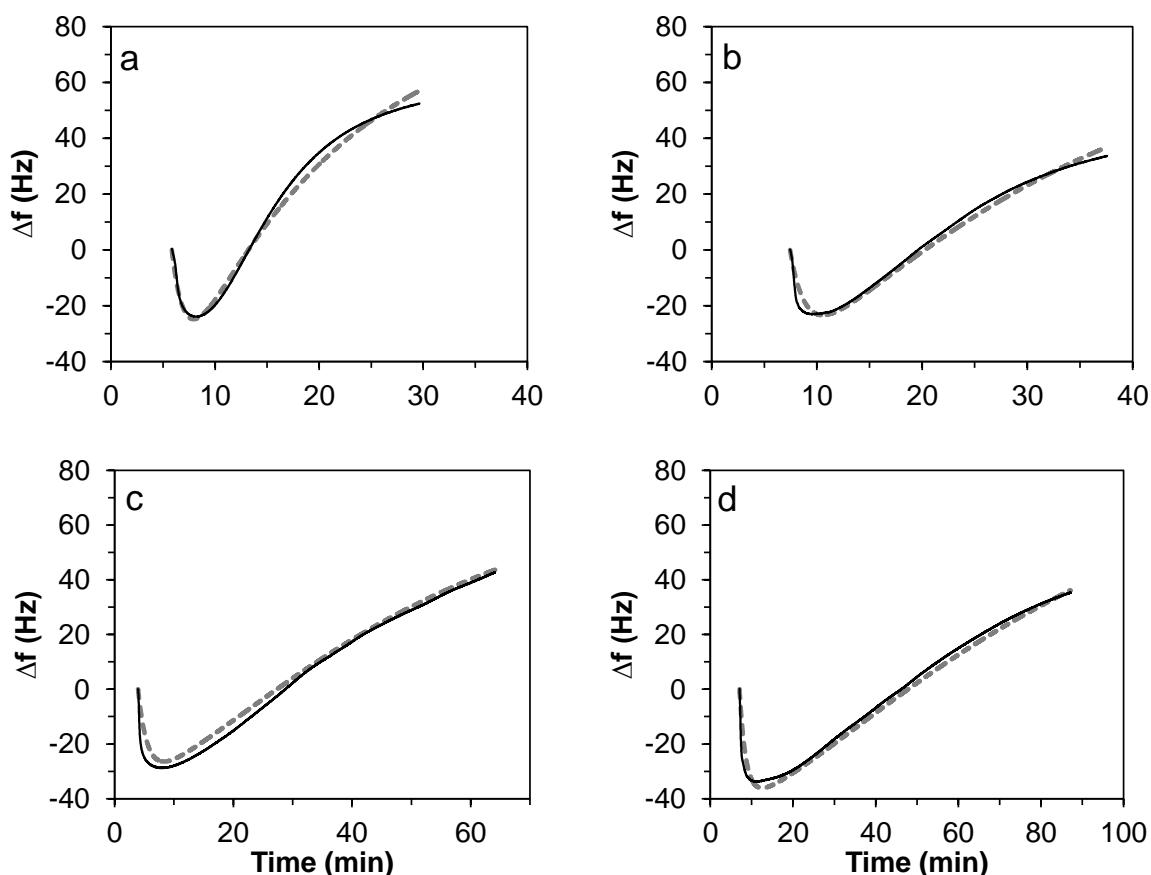


Figure 3-6 Measured frequency profile (— *black solid line*) and model frequency profile (- - - *gray dashed line*) of cellulose hydrolysis by cellulase (0.5 % v/v) in the presence of 0 g l⁻¹ (a), 0.1 g l⁻¹ (b), 0.4 g l⁻¹ (c), and 1 g l⁻¹ cellobiose (d).

Table 3-1 Model parameters optimized from the frequency data for cellulose thin films treated with cellulase (0.02 mM) in the presence of cellobiose (0 to 5 g/l)

Parameters	Name	Values
<i>Enzyme kinetics parameters</i>		
k_1	enzyme adsorption constant ($\text{mM}^{-1} \text{min}^{-1}$)	47.8 (3.5)
k_{-1}	enzyme desorption constant (min^{-1})	0
k_2	rate constant of enzyme hydrolysis (min^{-1})	0.057 (0.003)
k_3	inhibited-enzyme adsorption constants ($\text{mM}^{-1} \text{min}^{-1}$)	28.8 (2.8)
k_{-3}	inhibited-enzyme desorption constants (min^{-1})	0.14 (0.05)
k_4	inhibitor adsorption constants ($\text{mM}^{-1} \text{min}^{-1}$)	0.0054(0.0002)
k_{-4}	inhibitor desorption constants (min^{-1})	0.80 (0.05)
K_I	dissociation constant for cellobiose binding to the hydrolysable substrate (mM)	0.21 (0.01)
<i>QCM-specific response parameters</i>		
A	frequency response for bound enzyme (Hz SU^{-1})	56.0 (1.0)
B	frequency response for substrate lost (Hz SU^{-1})	114.2 (1.8)
C	frequency response for bound cellobiose (Hz SU^{-1})	46.3 (12.3)
S_o (CB = 0 g l^{-1})	initial substrate concentration (SU)	1
S_o (CB = 0.1 g l^{-1})	initial substrate concentration (SU)	0.64 (0.01)
S_o (CB = 0.4 g l^{-1})	initial substrate concentration (SU)	0.68 (0.01)
S_o (CB = 1 g l^{-1})	initial substrate concentration (SU)	0.89 (0.02)
S_o (CB = 5 g l^{-1})	initial substrate concentration (SU)	1.35 (0.02)

The adsorption and desorption constants for cellobiose on the cellulose thin films and the cellobiose-dependent frequency change (k_a , k_d and C) were determined independently from the frequency response curves as a function of cellobiose concentration (20, 40, 60, 80 g l⁻¹) in the absence of cellulase (Fig 3-4a). The inhibitor binding term ($-CS_0 \frac{SI}{S_0}$ in eq 14) describes to the frequency drop caused by cellobiose loading, and SI is calculated by eq 11. The value of k_a , k_d and C were determined first by fitting the model frequency to the measured frequency data obtained when only the cellobiose solution (20, 40, 60, 80 g/l of cellobiose in pH 5 0.1M acetate buffer) was introduced on the immobilized cellulose surface (Fig 3-4). The optimized parameters (k_a , k_d and C) were then used as constants in the full model frequency equations (eq 14) to obtain the remainder parameters. The inhibitor adsorption/desorption constant ($k_a = 0.005 \pm 0.002$ (mM⁻¹ min⁻¹) and $k_d = 0.80 \pm 0.05$ (min⁻¹) and frequency change per bound cellobiose ($C = 46.3 \pm 12.3$ Hz SU⁻¹) were obtained by fitting model frequency (eq 14) to the corresponding QCM-frequency measurement (taken to steady state) using least square estimation. Although the corresponding frequency change is minimal at low inhibitor concentrations (< 1 g/l), the term becomes significant at higher inhibitor concentrations.

The remainder of the optimized parameters were determined by fitting model parameters simultaneously to all QCM frequency curves obtained at different concentrations of inhibitor (0, 0.1, 0.4, 1, or 5 g/l cellobiose) in the presence of cellulase (0.5 % v/v) using least square estimation (Fig 3-6). The optimized parameters (Table 3-1) resulted in correlation coefficients for each curve fittings were greater than $R^2 = 0.98$ (data not shown). The frequency change per bound enzyme (ES) or enzyme/inhibitor complex (ESI) is specific to the experimental setup (QCM and sensor system). The frequency change per unit substrate ($B = 114.2 \pm 1.8$ Hz SU⁻¹)

describes the sensitivity of the experimental setup to the reduction of substrate lost from hydrolysis. The modeled initial substrate concentration was denoted by S_o , which was different for each experiment because the surface coverage of solubilized cellulose on each QCM sensor varied. Parameters related to enzyme adsorption and activity ($k_1, k_{-1}, k_2, k_3, k_{-3}, k_4, k_{-4}, K_I$) provide insight into the relative binding strengths and hydrolysis rates of inhibited and uninhibited enzymes. The modeled enzyme adsorption constant (k_1) is $47.8 \pm 3.5 \text{ mM}^{-1} \text{ min}^{-1}$ but the desorption constant (k_{-1}) is 0 indicating an irreversibility of ES formation. Based on the relative ratio of adsorption/desorption, cellulase complexed with cellobiose has strong binding affinity toward cellulose ($k_3/k_{-3}=2.1 \times 10^2 \text{ mM}^{-1}$). Conversely, the binding affinity of cellobiose for the substrate is orders of magnitude less than that of the inhibited enzyme ($k_4/k_{-4}=0.0068 \text{ mM}^{-1}$).

Using the model parameters, the time-dependent concentrations of hydrolysable substrate (S_i), enzyme-substrate complex (ES), and inhibited enzyme-substrate complex (ESI) can be predicted, as shown for the case of 0.1 g l^{-1} cellobiose and 0.5% v/v cellulase in Figure 3-7. ES formation (from free enzyme and available substrate) is greater than ESI formation (from inhibited enzyme and available substrate); at their maximum levels, approximately twice the amount of ES exists relative to ESI . At 80% conversion, almost all of the hydrolysable substrate (S_i) exists bound with an enzyme or inhibited enzyme. At this concentration of cellobiose, the normalized ratio of SI/S_i is approximately 0.00002, which is negligible relative to the bound enzyme. As time progresses, both (ES and ESI) decrease due to hydrolysis of available substrate S_i . The hydrolysable substrate (S_i) decreases with the rate of first-order enzyme hydrolysis constant ($k_2 = 0.057 \pm 0.003 \text{ min}^{-1}$).

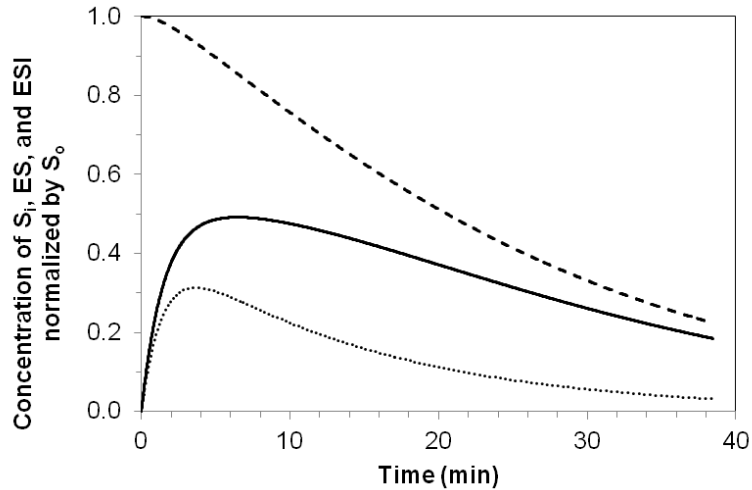


Figure 3-7 Model concentration profile of S_i (--- black dashed line), ES (—black solid line), and ESI (⋯ black dotted line) normalized by S_o during cellulose hydrolysis by cellulase (0.5 % v/v) in the presence of 0.1 g l^{-1} cellobiose. The concentration profile of SI normalized by S_o was plotted on the secondary axis.

The dynamic kinetic constants for cellulase adsorption and desorption on cellulose have been reported through model simulations for combinations of cellulase systems and cellulose substrates (Wald et al. 1984). Levine et al (2010) found that the experimental parameter of adsorption for both endoglucanase II and cellobiohydrolase I on Avicel to be approximately $8640 \text{ L mol}^{-1} \text{ hr}^{-1}$. In the same experiment, the desorption constants for endoglucanase II and cellobiohydrolase I was found 19.3 hr^{-1} and 164 hr^{-1} , respectively. Similarly, Converse and Optekar (1993) used a dynamic adsorption model and reported the adsorption rate constant of adsorption for both endoglucanase and cellobiohydrolases on Avicel to be $5 \times 10^3 \text{ L mol}^{-1} \text{ hr}^{-1}$. In the same simulation, the desorption rate constant for endoglucanase and cellobiohydrolase is approximately 0.5 hr^{-1} and 5 hr^{-1} , respectively. In this study, the kinetic constant of adsorption and desorption for cellulase (reported as a single component) on microcrystalline cellulose is $47.8 \text{ L mol}^{-1} \text{ min}^{-1}$ (or $2868 \text{ L mol}^{-1} \text{ hr}^{-1}$) and 0.0003 min^{-1} (or 0.018 hr^{-1}), respectively. Although the mode of adsorption and desorption for individual enzyme were not directly

compared, the values which describe the cellulase affinity to cellulose was in the same range of magnitude.

The rate at which the product formed or the substrate hydrolyzed is also determined from the model. When the enzyme-substrate complex (ES) was converted to product, the available substrate (S_i) decreases with the first-order enzyme hydrolysis constant ($k_2 = 0.057 \pm 0.003 \text{ min}^{-1}$). The value of k_2 is specific to type of substrate and enzyme. Howell and Mangat (Howell and Mangat 1978) proposed a model describing the hydrolysis of cellulose (Solka-Floc) by *Trichoderma viride* cellulase and found the hydrolysis rate constant to be 0.15 min^{-1} . The dissociation constant (or inhibition constant, K_i) is widely used across kinetic studies to measure the binding affinity of the inhibitor to the enzyme. A strong inhibitor has low value of K_i which is a result of a strong binding affinity to the enzyme. Typical determination of K_i from bulk solution requires the measurement of the initial hydrolysis rate with different substrate concentration in the presence and absence of inhibitor. Rate measurements are taken during the initial rate of hydrolysis to avoid complication of high product formation that influences the analysis of kinetic data (Gruno et al. 2004). Our model was developed based on 80% substrate conversion and assumes no additional complication from product accumulation (due to a flow-through cell in the QCM). The value of K_I , which is the dissociation constant for cellobiose binding to the enzyme (Eq. 12), is obtained directly as an optimized parameter used to model the frequency response of the QCM. The value of K_I is estimated to be $0.21 \pm 0.01 \text{ mM}$ or approximately 0.6 g/l and is specific to the reaction pathway represented by equations 1 – 4.

The mechanism of cellobiose inhibition on cellulase for soluble substrate has been suggested to be both competitive (Ghose and Das 1971; Kruus et al. 1995; Gruno et al. 2004) and non-competitive (Howell and Stuck 1975; Holtzapple et al. 1990). Competitive inhibition

occurs when the action of inhibition is achieved through the binding of the inhibitor to the active site of the enzyme to form an enzyme-inhibitor complex of reduced activity, as suggested by eq 2 of the model. When the binding of inhibitor occurs on different sites of the enzyme during adsorption or hydrolysis processes, non-competitive mechanism, represented by eq 3 of the model, is more applicable. For insoluble substrate such as cellulose, the observed mechanism of inhibition may depend on the diffusivity of the substrate to access the enzyme (Holtzaple et al. 1990). For example, amorphous and more accessible (swollen) cellulosic substrate allowed the enzyme to diffuse quickly and bind competitively with inhibitors for the active sites, and therefore, competitive inhibition resulted (Huang 1975). Crystalline cellulose or more ordered region of cellulose made the enzyme difficult to access even at high substrate concentration. The inability of the substrate to compete for the active site of the low-molecular-weight enzyme results in a noncompetitive inhibition.

The reported inhibition constant of cellulase by cellobiose vary due to different model (ie. type of inhibition) or experimental approach (ie. type of substrate, type of enzyme, temperature, etc). Philippidis et al (1993) developed a mathematical model based on an initial rate measurement under simultaneous saccharification and fermentation condition and found the noncompetitive inhibition constant of cellulase (Laminex, synthesized by a *T. reesei* strain) by cellobiose to be 5.85 g l^{-1} (or 17.1 mM). Gruno et al (2004) applied initial rate-based quantitative analysis using [^3H]-labeled bacterial cellulose and found the competitive inhibition constant for Cel7A (cellobiohydrolases) of *T. reesei* to be 1.6 mM. In comparison to these bulk studies, our results for inhibited cellulase kinetics on thin cellulose films indicate that competitive inhibition by a cellulase/cellobiose complex does not capture the effect of cellobiose

concentration on hydrolysis kinetics. This investigation quantifies the effect of an inactive enzyme/substrate complex in reducing the hydrolysis rate (Fig 3-6).

The model successfully describes the effect of inhibitor concentration (cellobiose) on enzymatic hydrolysis by *T. reesei* cellulases at inhibitor concentrations where hydrolysis is still evident. However, the model is unable to describe the observed QCM frequency responses at high inhibitor concentrations (i.e., 5 g l⁻¹ cellobiose (Fig 3-8)). When cellulase was inhibited by 5 g l⁻¹ cellobiose, the measured QCM resonance frequency decreases rapidly to approximately -50 Hz, consistent with the adsorption of the enzyme and inhibitor on the cellulose thin film. However, the response leveled off without an increase in frequency that indicates cellulose hydrolysis. While the model predicts a similar frequency decrease due to enzyme adsorption, it also predicts a measurable cellulose hydrolysis rate (as depicted by the slow increase in frequency signal in Figure 3-8). Specific events that may occur in enzyme inhibition that are not explicitly described in the kinetic model include structural changes, multi-enzyme complex formation and/or inactivation of the enzyme on the surface in the presence of high inhibitor concentrations (Philippidis et al. 1993; Gan et al. 2003; Zhang and Lynd 2004).

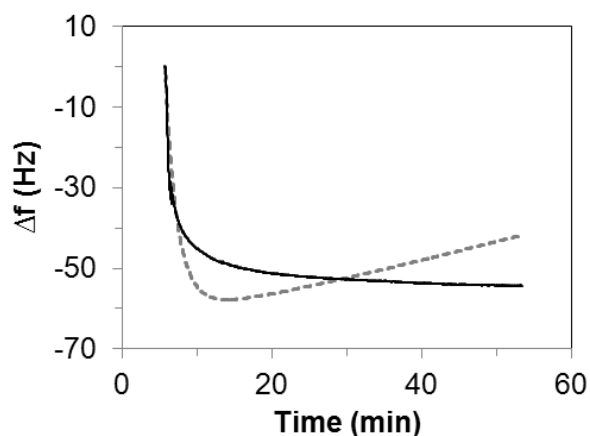


Figure 3-8 Measured frequency profile (— *black solid line*) and model frequency profile (- - - *gray dashed line*) of cellulose hydrolysis by cellulase (0.5 % v/v) in the presence 5 g l⁻¹ cellobiose.

Cellulose hydrolysis by fungal cellulases is a complex process involving sequential mechanism from three types of cellulases: endoglucanase, exoglucanase and β -glucosidase. These enzymes, when used together, works most effectively in synergistic manner. In this study, the enzyme mixture (Celluclast, cellulase from *T. reesei* 26921, Sigma Aldrich) was used in the QCM experiments also consists of all three type of cellulases. The intended use of cellulase mixture was to resemble the natural process of cellulose hydrolysis by fungi or other bacterial cellulases that behave in cooperative action. Therefore, the model developed in this study reflects the results of the overall adsorption and hydrolysis by a native cellulase mixture, and, as first step, treating the enzyme mixture as a single species. The model does not specifically address multi-enzyme interactions and synergy in this natural system. Success of this modeling approach suggests opportunities to investigate the hydrolysis kinetics of individual cellulase components and for the optimization of non-natural enzyme cocktails to tailor biomass conversion.

Conclusion

The concentration dependence of inhibition of cellulase binding and subsequent cellulose hydrolysis by cellobiose is quantifiable by QCM with *in-situ* monitoring of the changes in frequency due to change in mass of the cellulose thin film. The rate of enzymatic degradation of the cellulosic thin film was slowed by partially inhibited cellulase (0.5 % v/v cellulase in the presence of 0.1, 0.4, or 1 g l⁻¹ cellobiose) and completely inhibited with an excess of inhibitor (5 g l⁻¹ cellobiose). The inhibition as a function of cellobiose concentration is comparable to inhibition levels observed in bulk studies of cellulose degradation by *T. reesei* cellulase in the presence of cellobiose, as quantified by the inhibition constant K_I .

The ability to simultaneously monitor thin film mass change due to both adsorption and hydrolysis events using QCM presents unique opportunities to evaluate the kinetics of inhibited enzymes (cellulases) relative to bulk cellulose hydrolysis experiments. An enzyme kinetics model is developed to describe the surface phenomenon of binding and hydrolysis by cellulase. This model accounts for mass change of the model cellulose thin film due to the adsorption and desorption of enzyme, enzyme complex, and inhibitor on the substrate, as well as enzymatic hydrolysis. The kinetic parameters that result from fitting the adsorption/hydrolysis/inhibition model to the QCM frequency response of cellulose thin films provide for the interpretation of the underlying mechanism of observed changes in cellulose hydrolysis as a result of environmental perturbations, such as inhibitor concentration.

Chapter 4

Modeling the Effect of Enzyme Concentration Dependence on Hydrolysis of Cellulose Thin Film using Quartz Crystal Microbalance

Summary

Cellulose is the most abundant and readily available renewable feedstock for the production of biofuels and solvents from soluble and fermentable sugars. The enzymatic hydrolysis of cellulose requires the depolymerization of the solid cellulose substrate by cellulases. Observed decreases in hydrolysis rate of bulk lignocellulose with enzyme loading have led to kinetic models that account for the heterogeneity of the adsorbed cellulase-cellulose substrate surface as well as traditional enzyme adsorption and hydrolysis steps. In this study, the effect of enzyme concentration (cellulase from *Trichoderma reesei* at 0.34, 1.7, 3.4, 17, 34, and 68 μM) on the adsorption and the hydrolysis of cellulose is investigated using model cellulose thin films and measured as a mass change in the film using Quartz Crystal Microbalance with Dissipation (QCM-D). Increasing enzyme concentration results in a plateau of apparent hydrolysis rate with increasing enzyme concentration beyond 0.05 % v/v. The ability of several models of cellulase adsorption, cellulose hydrolysis, and enzyme inactivation to fit the mass response of the cellulose thin film as a function of enzyme concentration is compared, focusing on models that describe the effect of enzyme crowding on the surface. The successful model of enzymatic hydrolysis of cellulose thin films employs an n-th order adsorption model with respect to enzyme concentration and accounts for surface inactivation explicitly. The combination of surface analysis techniques and mechanistic modeling provides more detailed insight into cellulose hydrolysis kinetics than can be obtained from bulk experiments, and therefore an alternative approach to guide the selection of conditions that enhance cellulase activity.

Introduction

Cellulose from wide range of agriculture waste or residual plant materials can be utilized as a sustainable energy resource to produce biofuels such as ethanol. The process of degrading cellulose into fermentable sugars for biofuel production generally requires four main steps: i) pretreatment of the lignocellulosic biomass to reduce lignin content, ii) hydrolysis of the delignified cellulose (by thermal, chemical or enzymatic means) into soluble sugars, iii) microbial fermentation of hydrolyzed sugars into ethanol, and iv) separation of solvent products from the broth mixture. The enzymes required to address the recalcitrance of cellulose to hydrolysis are a major cost component in the production of lignocellulosic biofuels (Zhang et al. 2006; Bansal et al. 2009). Enhancing cellulase activity is of critical importance to realizing the next generation of biofuels and solvent production based on renewable lignocellulosic biomass. Therefore, recent studies have been focused on improving the efficiency of the cellulase performance on cellulose (Zhang et al. 2006; Sukumaran et al. 2009).

Cellulase enzymes work synergistically to hydrolyze recalcitrant chains of cellulose polymers into soluble sugars. Cellulases are classified into three types: endoglucanases that split the cellulose from the chain end, exoglucanases (or cellobiohydrolases) that attack the cellulose chain from the reducing and non-reducing end to produce cellobiose, and β -glucosidases that convert cellobiose into glucose. The hydrolyzed products including disaccharides (cellobiose) and monosachharides (glucose) can be fermented by microbes such as *Saccharomyces cerevisiae* or solvent-producing bacterial strains to produce soluble products such as ethanol or butanol.

The efficiency of cellulose saccharification relies significantly on the ability of the enzymes to adsorb to the available substrate surface and diffuse to the active cellulose binding sites. However, the accessibility of enzyme to the cellulose binding sites may be limited by

many factors (i.e. non-Fickian diffusion, molecular collision, and enzyme-enzyme interaction), which makes it even more difficult to access the already limited cellulose in the lignocellulose material (Xu et al. 2009). This work focused on pure cellulose and its reactivity with cellulases as a function of concentration.

Hydrolysis of cellulosic substrates is greatly influenced by cellulase concentrations. At low enzyme concentrations, the hydrolysis rate is proportional to the fraction of productively adsorbed cellulases (Bansal et al. 2009). At higher enzyme concentration, the productivity levels off due to the saturation of the hydrolysable cellulose with cellulases on the cellulose surface (Hogan et al. 1990; Spindler et al. 1991). Cellulase activity is often measured in bulk experiments by taking the rate at which the products are formed (or the substrate is consumed) or the substrate change its physical property (Zhang et al. 2006). However, the level of detail and precision measured in bulk is not sufficient to delineate adsorption and kinetic events, making testing and parameterizing the models of reaction pathways difficult.

Kinetics models have been developed to describe and predict the interaction between cellulase and cellulose during cellulase binding and cellulose hydrolysis. The kinetics of enzymatic cellulose hydrolysis are most commonly described by i) empirical models, ii) Michaelis-Menten based reaction pathway models, iii) models focusing on cellulase adsorption processes, and iv) models for soluble substrates (Bansal et al. 2009). For example, Langmuir-based model of enzyme adsorption to the substrate coupled with traditional hydrolysis kinetics was proposed to describe the adsorption of cellulase to cellulose at the liquid-surface interface (Kadam et al. 2004). However, the implicit assumption of the Langmuir adsorption model is not consistent with experimental observations from the complex interaction between the enzyme and the substrate (Zhang and Lynd 2004). A recently developed empirical model applying fractal

and jamming theory is used to describe the limited cellulose surface accessibility by enzyme-enzyme interaction when large quantities of cellulase are loaded onto the cellulose surface (Xu et al. 2009). While fractal and jamming theories of enzyme kinetics do not provide mechanistic details of the reduced hydrolysis rate due to surface enzyme-enzyme interactions, the models capture time-dependent hydrolysis rates with simple kinetic parameters that can be fit to bulk cellulose hydrolysis data.

A kinetic-based model detailing the combined effect of binding and hydrolysis by inhibited cellulases in the presence of cellobiose has been developed previously using the experimental mass-dependent frequency data obtained from quartz crystal microbalance (QCM) (Chapter 3). The advantage of using QCM relative to bulk cellulose hydrolysis studies is the ability to simultaneously observe mass changes due to enzyme adsorption and subsequent hydrolysis of the cellulose thin film over the course of the hydrolysis. The kinetic parameters were fit to the frequency response of thin cellulose films in the presence of cellulases, where the mass dependency captures both mass increase due to enzyme adsorption and mass decrease due to cellulose hydrolysis. However, the effect of enzyme concentration on binding and hydrolysis, particularly the potential for enzyme interactions and crowding on the cellulase surface was not addressed.

In this study, the change in mass of cellulose thin films due to enzymatic binding and hydrolysis is measured by QCM as a function of cellulase concentration (0.01, 0.05, 0.1, 0.5, 1, and 2 % v/v). The QCM frequency response (up to 1% v/v) is used to fit and compare kinetic modeling approaches over a range of enzyme concentrations. The frequency measured with 2 % v/v cellulase is used to validate the predictive capability of the model. Enzyme adsorption models (traditional first-order Langmuir-based adsorption and n-th order adsorption models) as

well as hydrolysis models that account for enzyme distribution on the cellulose surface are examined (fractal, jammed, fractal jammed and inactivation at the surface). The results are consistent with enzyme inactivation due to enzyme overloading effect during the hydrolysis process. The developed model is capable of evaluating the balance between adsorption and hydrolysis events that maximizes hydrolysis with respect to enzyme concentration.

Materials and Methods

Materials. Microcrystalline cellulose (MCC, 20 μ m) was purchased from Aldrich. N-Methylmorpholine N-oxide (NMMO), dimethyl sulfoxide (DMSO, $\geq 99.8\%$), and polyethyleneimine (PEI, 50 wt. % aqueous solution) was supplied by Acros Organics. Acetate buffer (0.1 M, pH 5) was prepared by diluting glacial acetic acid (Fisher Scientific) in Milli-Q de-ionized water (Millipore Corporation). Cellulase (aqueous mixture consists of *endo*-glucanases, *exo*-glucanases, cellobiohydrolases, and β -glucosidases) from *Trichoderma reesei* 26921 (Celluclast®) was purchased from Sigma Aldrich. Cellulase was diluted in acetate buffer (0.1 M, pH 5) to the desired final concentration of 0.01, 0.05, 0.1, 0.5, 1 and 2 % v/v. Protein content of cellulase (E_o , mM) was determined by Peterson Method (Peterson 1977) protocol provided by Sigma). Based on protein content, the cellulase concentrations correspond to 0.34 μ M, 1.7 μ M, 3.4 μ M, 17 μ M, 34 μ M, and 68 μ M, respectively.

Preparation of Cellulose Thin Film. The procedures to make cellulose thin films were described in previous investigation (Chapter 3). Gold-coated QCM-D resonators (Qsx 301, Q-Sense) were treated with ultraviolet cleaner (BioForce, Ames, IA) for 10 minutes to decompose and volatilize organic contaminants on the sensor surface. The UV-treated QCM-D sensors were

immersed in diluted (0.2 % v/v) polyethyleneimine (PEI, 50 wt. % aqueous solution) for 15 minutes. PEI was used as an anchoring polymer (Ahola et al. 2008; Aulin et al. 2009) to attach the cellulose to the QCM-D sensor (QSX 301 Gold, Q-Sense AB, Göteborg, Sweden). The QCM-D sensors were contacted with de-ionized water (pH adjusted with sodium hydroxide to that of the polymer solution, ~ pH 10) for an additional 10 minutes, during which time the polymer precipitated on the surface of the sensor. The PEI-coated sensors were dried in the oven (50° C, 30 min), then in a desiccator (room temperature) for storage. A solution of microcrystalline cellulose in N-methylmorpholine-N-Oxide (NMMO 50 wt. % aqueous solution in water) was prepared by adding cellulose (2 wt. %) to NMMO preheated to 110 °C and continuing to heat the mixture to 115 °C. The addition of cellulose at high temperature solution prevented the agglomeration of fine microcrystalline cellulose. A clear solution was obtained at 115 °C after approximately one hour. Dimethyl sulfoxide (DMSO, ≥99.8%) was slowly added to the mixture to make a final solution of 0.5 wt. % cellulose. The temperature of the cellulose solution was reduced to 70° C, prior to spin coating. Cellulose solution (0.1 ml) was spin-coated (4500 rpm, 40 sec, WS-400BZ-6NPP/Lite, Laurell Technologies) on the PEI-coated QCM-D sensors. After spin-coating, the sensors were immersed in deionized water (30 min), and then dried in the oven (50° C, 30 min). The cellulose-coated sensors were stored in a desiccator at room temperature prior to use.

Cellulose Thin Film Characterization by Spectroscopic Ellipsometer and Atomic Force Microscopy (AFM). The thickness of model cellulose thin film was measured using a variable angle spectroscopic ellipsometer (M-2000, JA Woollam Co., Inc.). The surface topography and material distribution of the cellulose thin film on QCM sensor (QSX301) was captured by the

AFM (Series 4500, Agilent Technologies). The support base (QSX301) and the cellulose thin layer coating on the sensor (QSX301) were scanned in tapping mode using a silicon cantilever (TAP 300AI-G, Budget Sensors) with a spring constant of 40 N/m and a driving frequency of 300 kHz. The acquired scan area ranged from 2×2 μm to 50×50 μm. At least three sensors were scanned to confirm reproducibility.

Cellulose Thin Films/ Cellulase Interactions Measured by Quartz Microbalance with

Dissipation (QCM-D). A quartz crystal microbalance (Q-Sense E4) equipped with four temperature controlled flow modules was used to measure changes in mass per unit area and in the viscoelasticity properties of the cellulose thin films from the change in frequency (Δf) and dissipation (D) of the cellulose-coated quartz crystal resonator. The oscillation frequency and dissipation energy were measured simultaneously from the application of an AC voltage across the electrode, causing the piezoelectric quartz crystal vibrate (Rodahl et al. 1995). The resonance frequency change (Δf) can be used to calculate the proportional mass absorbed on the crystal surface by the Sauerbrey equation:

$$\Delta m = -\frac{c}{n} \Delta f \quad (1)$$

where c is the constant for mass sensitivity and n is the overtone number. “ c ” varies with different type of sensors. For the 4.95 MHz AT-cut sensor used in this study, c is equal to 17.8 ng cm⁻² Hz⁻¹. The QCM acquires frequency signal at the fundamental resonance (5 MHz) and at a multiple of resonance (overtone frequency). Third overtone frequency was used to avoid edge effect (unstable frequency signal at the edge of the sensor measured by the fundamental frequency). The Sauerbrey’s equation (Rodahl et al. 1995) is valid for the following conditions: 1) the surface film is flat and uniformly distributed, 2) the mass change of the crystal surface is

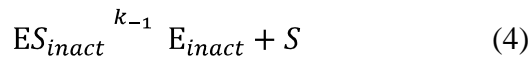
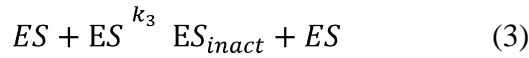
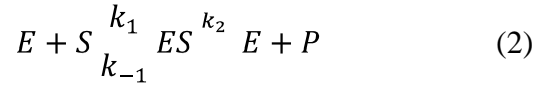
much smaller than the mass of the quartz resonator, 3) the film is rigid, meaning that the mass absorbed on to the surface must be firmly attached with no oscillatory effect ($D < 10^{-6}$ per 10 Hz). In this study, the Sauerbrey equation is valid because the change in dissipation was relatively small ($2-6 \times 10^{-6}$) during cellulase treatment on ultrathin cellulose films prepared with the dissolved cellulose.

The mass change of cellulase thin films in response to cellulase concentration (0.01, 0.05, 0.1, 0.5, 1 and 2 % v/v) was measured by QCM. Prior to contacting the cellulose thin films with cellulase, the cellulose-coated QCM sensors were incubated with the acetate buffer (0.1 M, pH 5) at a flow rate of 0.2 ml min^{-1} until a constant baseline in frequency measurement was reached ($< 2 \text{ Hz hr}^{-1}$), which was obtained in approximately 30 min. The temperature of the QCM chamber was controlled at $30 \text{ }^\circ\text{C}$. All liquid solutions were degassed for 30 min using an ultrasonicator (Cole-Parmer 8890, IL) prior to injection in the flow cell. When enzyme solutions (concentration as indicated) were injected (0.2 ml min^{-1}) into the QCM flow module containing the cellulose thin films, both cellulase binding and cellulose hydrolysis were monitored simultaneously. The change in oscillation frequency and dissipation energy was recorded throughout the experiment. When the frequency signal and dissipation had no significant change ($< 2 \text{ Hz h}^{-1}$), the injection solution was switched to acetate buffer to rinse and remove any remaining hydrolysate on the sensor surface.

Model Development for Inhibited Enzyme-Kinetics on Cellulose Thin Films. A non-linear model was developed to describe cellulase adsorption and hydrolysis on thin cellulose films as a function of cellulase concentration using a series of differential equations describing the concentration of the system species based on reaction kinetics. The QCM frequency profiles

from enzyme catalyzed reactions were linked to the reaction scheme and used to fit the kinetic parameters.

Traditional enzyme kinetic scheme assumes homogenous reaction in which the enzyme (E) binds to the soluble substrate (S) to form a substrate-bound enzyme (ES) and the enzyme is recovered after the product (P) is formed. A translation of this kinetic scheme is presented in eq 2. The binding scheme may be reversible for the complex ES formation and dissociation (eq 2). An ES complex formed on the surface may encounter other ES complexes, depending on the surface coverage. Enzyme-enzyme interactions on the surface can result in deactivation of ES complex (ES_{inact}), as shown in eq 3. The inactive ES complex (ES_{inact}) may dissociate and become inactive enzyme in solution (E_{inact}), leaving the substrate available for hydrolysis (eq 4). In this model, the rate at which ES_{inact} dissociates resembles the rate at which ES dissociated with the enzyme dissociation constant k_{-1} .



The thin layer of cellulose film and the enzyme solutions were contacted in a flow-through cell, thus the free enzyme concentration (E) was assumed to be constant. The concentration of free substrate (S) is unknown and is defined by eq 5. S_i is the instantaneous concentration of hydrolyzable substrate. When time equals to zero, the initial substrate coverage on the sensor is S_0 .

$$S = [S_i] - [ES] - [ES_{inact}] \quad (5)$$

The kinetic scheme (eq 2, 3, and 4) leads to the derived rate expressions (eq 6, 7, and 8) where enzyme adsorption on the cellulose surface is described by n -th order reaction.

$$\frac{d[ES]}{dt} = k_1[E]^n S - k_{-1} ES - k_2 ES - k_3 ES^2 \quad (6)$$

$$\frac{d[S_i]}{dt} = -k_2 ES \quad (7)$$

$$\frac{d[ES_{inact}]}{dt} = k_3 ES^2 - k_{-1}[ES_{inact}] \quad (8)$$

The rate parameters in the model were fit to the experimentally measured change in frequency, where the change in mass of the film can be expressed as a sum of the change in mass due to enzyme and inactivate enzyme complex adsorption on the substrate, and the mass loss of hydrolysis:

$$\Delta f = -A \underbrace{ES}_{\text{enzyme adsorption}} + \underbrace{ES_{inact}}_{\text{enzyme adsorption}} + B \underbrace{S_o - S_i}_{\text{hydrolysis}} \quad (9)$$

A represents the frequency change per bound enzyme and inactive ES complex (which were assumed to contribute similarly to the frequency change), and B represents the frequency change per substrate lost. The initial substrate concentration, S_o , is unknown and will be determined from the expression normalized by S_o (eq 10). The initial substrate concentration of each individual film is slightly different for each hydrolysis experiment (because of slight sample-to-sample variability during spin coating). The units of S_i and S_o are reported in a standardized hydrolysable “substrate unit”, SU. The value of S_o for the hydrolysis experiment at 0.01 % v/v cellulase is normalized to 1 SU, and the remaining S_o for each hydrolysis experiment is a model parameter that is normalized relative to the surface concentration of 1 SU. The “substrate unit” represents the hydrolysable amount of cellulose in this multilayered film.

$$\Delta f = -AS_o \frac{ES+ES_{inact}}{S_o} + BS_o \frac{S_o}{S_o} - \frac{S_i}{S_o} \quad (10)$$

The rate events describing potential modes of enzyme adsorption and hydrolysis are described by this model. Time- and concentration-dependent enzyme deactivation due to overcrowding effect is accounted for in rate equations in this model. In addition, the complex surface effects and enzyme-substrate complexes interactions that occur as the cellulose substrate is hydrolyzed and the cellulase enzymes encounter other enzymes are described in the form of inactivation of enzymes on the surface. The kinetic parameters were fit to frequencies corresponding up to 80% substrate conversion ($S_i/S_o = 0.2$). This is consistent with bulk investigations of cellulose conversion, in which hydrolysis kinetics are generally examined in the conversion range below 70% (Bansal et al. 2009).

The frequency response of the cellulose-coated QCM resonator in the various cellulase concentrations (0.01, 0.05, 0.1, 0.5, 1 % v/v cellulase) was used to fit the kinetic constants (k_1, k_{-1}, k_2, k_3) and other model parameters (A, B, S_o , and n). Frequency response measured at 2 % v/v cellulase was not included in the fit. It was later used to validate the predictive capability of the model. All parameters, except for S_o , were held constant across experiments, and optimized by *lsqcurvefit* function in Matlab Curve Fitting Toolbox. S_o values were determined for each experiment due to the potential different surface coverage of cellulose on each QCM resonator.

Other kinetic models are also proposed to account for the crowding effect on cellulose substrate at higher enzyme concentrations (Xu et al. 2009). Table 4-1 summarized the formulism investigated for each proposed model. QCM frequency response modeled with the hydrolysis rate constant k_2 (in equation 2) using the fractal, jammed and fractal jammed formulism was investigated. Our model developed at a single enzyme concentration (Chapter 3), fit using a constant k_2 , was also used to fit the enzyme-concentration dependent data. Fractal analysis describing the “fractional” dimensions in which the molecules collide, diffuse, and react in the

heterogeneous system is represented by Formulism 1 (Table 4-1), where the observed hydrolysis rate is the product of k_2 and a time-dependent exponential factor (f) resulting in a decrease with time (t) (Xu et al. 2009). Jamming is proposed when the enzymes are packed among the confined cellulose interchain spacing (Bommarius et al. 2008; Xu et al. 2009). The jamming model is represented by Formulism 2, where the observed hydrolysis rate is the product of k_2 and a term account for enzyme surface coverage, $1 - \frac{[E]}{j[S]}$. The jamming factor, “ j ” is an additional fit parameter. Jamming effect is observed when the enzyme concentration $[E]$ approaches $j[S]$. When enzyme concentration $[E]$ is much less than $j[S]$, the jamming effect become negligible. The combined effect of jamming and fractal kinetics is described by the “jammed fractal” model (Formulism 3, Table 4-1) (Xu et al. 2009), requiring the fit of k_2 , j and f from the QCM frequency response data. Surface enzyme inactivation (equations 3 and 4) was not considered when the fractal, jammed, and fractal jammed models (Formulism 1-3) were used to account for the effect of enzyme concentration on the hydrolysis rate.

Table 4-1 Alternative kinetic models to account for enzyme concentration effects

Kinetic model	Formulism
Constant k_2 (unmodified model, Chapter 3)	k_2 constant
Enzyme inactivation by ES-ES interaction	k_2 constant, surface enzyme inactivation
Fractal	$k_2 \rightarrow t^{-f} k_2$ (1)
Jammed	$k_2 \rightarrow 1 - \frac{[E]}{j[S]} k_2$ (2)
Fractal jammed	$k_2 \rightarrow 1 - \frac{[E]}{j[S]} t^{-f} k_2$ (3)

Results and Discussion

Hydrolysis of model cellulose thin films

Cellulose thin films were prepared by dissolving the microcrystalline cellulose (Avicel) in NMMO/water system, which results in breaking the intra-molecular hydrogen bonds within the cellulose chains and forming the complex between NMMO and hydroxyl groups of cellulose (Maia et al. 1981; Fink et al. 2001; Bocek 2003; Jie et al. 2005). Previous investigations have demonstrated that the formation of hydrogen bonds between NMMO and the hydroxyl group of cellulose does not derivatize the cellulose structure, but dissolves the cellulose to form a homogenous solution (Berger et al. 1988). The process converts crystalline cellulose to regenerated cellulose (Zhao et al. 2007; El-Wakil and Hassan 2008). Upon diluting with excess water, the cellulose lost its competitiveness for NMMO molecule, and precipitated on the surface of the QCM resonator. Cellulose II (containing amorphous and crystalline structures) was obtained. Aulin et al (2009) showed that the NMMO-dissolved microcrystalline cellulose has approximately 60% degree of crystallinity. Therefore, the deposited cellulose thin film is expected to have both amorphous and crystalline regions.

The average thickness of cellulose prepared in this work is approximately 21 nm. The amount of spin-coated cellulose on the QCM sensor was approximately 641 ± 24 ng, quantified by measuring the frequency difference between the cellulose + polyethyleneimine coated sensor and polyethyleneimine coated sensor only using QCM.

The spin-coated cellulose thin film is used in the QCM as a surface substrate. When the cellulase solution (diluted in 0.1M acetate buffer, pH 5) is injected into the QCM chamber, the frequency signal is recorded with time. Figure 4-1 shows the typical frequency profile that reflects the events when the enzyme is adsorbed onto the cellulose surface (mass increase;

frequency decrease) followed by the hydrolysis of the cellulose thin film by cellulase (mass loss; frequency increase). Enzyme adsorption and hydrolysis occurs simultaneously, but the slope of the frequency curve in the linear range indicates that the initial adsorption is surpassed by the hydrolytic reaction. As available substrate is depleted, the slope of the frequency curve slowly decreases, and eventually flattens, suggesting that the thin film surface remains unchanged due to substrate depletion.

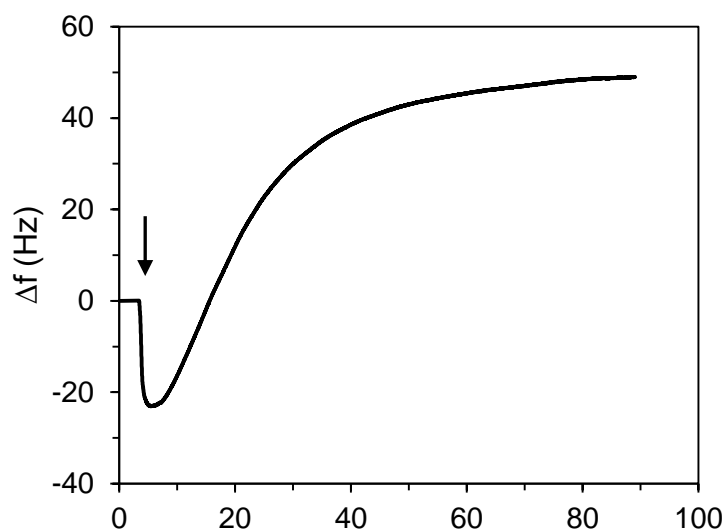


Figure 4-1 Typical frequency profile of cellulose hydrolysis. The arrow indicates the injection of enzyme solution (0.05 % v/v diluted in 0.1M acetic acid, pH 5).

Hydrolysis of cellulose thin film by cellulase is also evident by atomic force microscopy (AFM). The AFM image of the cellulose thin film shows ridge-like filaments of cellulose on the surface before hydrolysis experiment (image shown in Chapter 3). The morphological image of the spin-coated cellulose film is comparable to the microcrystalline cellulose thin film prepared from previous work (Kontturi et al. 2006; Aulin et al. 2009). After cellulose-coated sensor are treated with cellulase (30°C, pH 5), the filaments are no longer visible. The surface topography of the hydrolyzed surface appears smooth, which was a result of cellulose hydrolysis.

This work employs fungal cellulases, which are known to produce free cellulases consisting of endoglucanases, exoglucanases and β -glucosidases. These enzymes work synergistically toward degrading cellulosic material. The synergetic mechanism of cellulase makes the hydrolysis process very effective in biological systems. The advantage of using the fungal cellulase mixture as opposed to an individual enzyme is the better resemblance to the natural process of cellulose hydrolysis by cellulolytic organisms. For the purpose of model development, the fungal cellulases are treated as a single species with respect to their adsorption and hydrolysis kinetics. Therefore, the model does not take into account the effect of synergy or more complex enzyme interactions

Effect of enzyme concentration on the enzymatic hydrolysis of thin films as measured by QCM

QCM-D was successfully applied to observe the effect of enzyme concentration on enzyme binding and hydrolysis of cellulose thin film. Figure 4-2 shows the QCM frequency response (3rd overtone) of the cellulose-coated resonator with different enzyme concentrations (0.01, 0.05, 0.1, 0.5, 1, 2 % v/v). Reductions in the QCM frequency response (25~35 Hz) are observed due to the adsorption of cellulase onto the cellulose surface. As enzyme concentration increases from 0.01 % v/v to 1 % v/v, a slightly greater reduction in frequency signal was observed, suggesting adsorption greater mass of enzyme has adsorbed. After initial enzyme loading on the cellulose surface (approximately 6 min), the frequency signal increases with time due to the reduction of mass of the film. This reduction in mass is attributed to the loss of available cellulose by enzymatic hydrolysis. In this study, the least amount of initial enzyme adsorption (corresponding to the minimum in the frequency) and the lowest hydrolysis rate (as

suggested by the slope of the initial QCM frequency) occurs at the lowest enzyme concentration, 0.01 % v/v cellulase (shown in the inset of Fig 4-2), as expected. However, with increasing enzyme concentration (to 0.05, 0.1, 0.5 and 1 % v/v) more complex effects on the QCM frequency response are observed with respect to apparent adsorption, hydrolysis, and extent of reaction (Fig 4-2). For example, enzyme concentrations of 0.05 and 0.1 %v/v have similar initial enzyme adsorption, but hydrolysis at the lower enzyme concentration appears to be faster and occur to a greater extent. Further increasing the enzyme concentration to 0.5 and 1 % v/v results in similar adsorption, hydrolysis, and extent of reaction, suggesting that the cellulose surface is saturated with enzyme at these concentrations. The observed frequency response trends reflect the combination of enzyme adsorption and hydrolysis events, and the overall conversion (change in mass) is influenced by the thickness of the deposited cellulose film, which varies slightly across sensors. Therefore, modeling is critical to further interpretation of the raw QCM data.

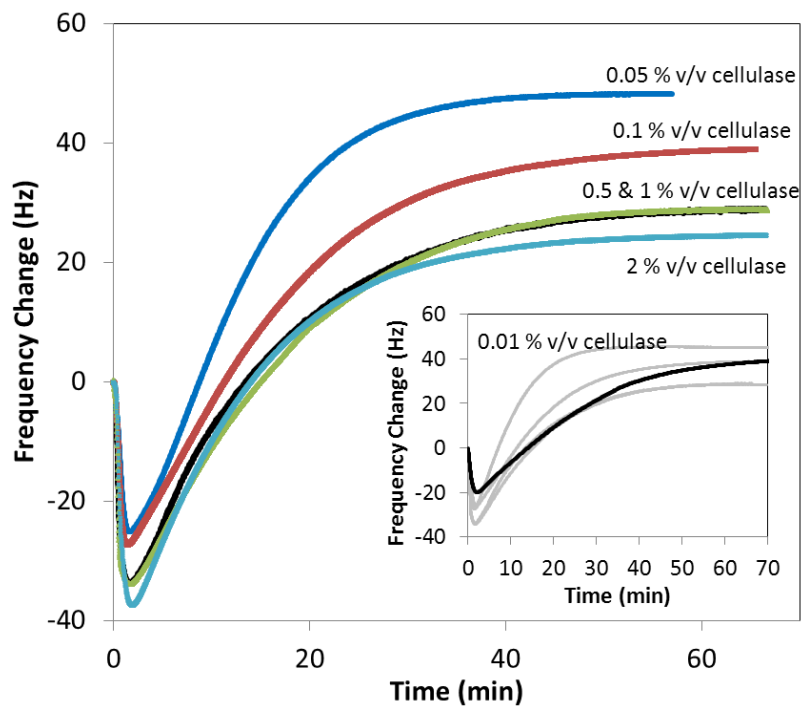


Figure 4-2 QCM frequency profile of cellulose hydrolysis by cellulase at 0.01% v/v, 0.05 % v/v, 0.1 % v/v, 0.5 % v/v, 1 % v/v

Initial rates for cellulose hydrolysis are used frequently as the basis for enzymatic kinetics models (Bernardez et al. 1994; Nidetzky et al. 1994; Mosier et al. 1999). The initial slope of the QCM frequency curve (after the frequency reached a minimum) can be taken as a measure of initial hydrolysis rate, as it reflects the amount of cellulose hydrolyzed after enzyme adsorption (Suchy et al 2011). The initial rate measurement reflects the rate at which the enzyme reacts with the surface of the substrate in which the surface coverage is assumed to be identical. Therefore, the rate is independent of the thickness of the cellulose film, and thus provides a good measure of the apparent hydrolysis rate. The change in hydrolysis rate with respect to different cellulase concentrations is shown in Figure 4-3. The initial hydrolysis rate increases approximately linearly with the enzyme concentration until 0.1 % v/v. At higher concentration (0.5 and 1 % v/v), the initial rate reaches a relatively constant level. This suggests that the enzyme loaded on the surface was fully covered with the available adsorption sites, and the rate has attained maximum level of capacity. This result consistent with other cellulase kinetic studies that observed a maximum apparent hydrolysis rate with high enzyme loading (Woodward et al. 1988; Bernardez et al. 1994; Nidetzky et al. 1994; Bansal et al. 2009).

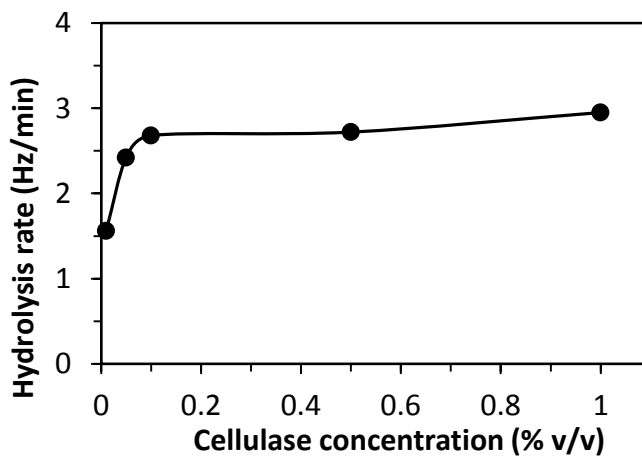


Figure 4-3 Initial hydrolysis rate of cellulose thin film for the experimental frequency profile at different cellulase concentrations (% v/v).

Modeling the effect of enzyme concentration on the enzymatic hydrolysis of thin films from the QCM frequency response

Previous studies have investigated the effect of enzyme loading on the efficiency of cellulose hydrolysis by cellulase (Tengborg et al. 2001; Mussatto et al. 2008; Chandra et al. 2011). Kinetics model have been developed to describe enzyme concentration effect of bulk cellulose hydrolysis by cellulases (Kim et al. 2008). Often the observation of a decreased rate of cellulose hydrolysis with conversion is associated with saturated enzyme on the cellulose surface which causes an overcrowding effect (Woodward et al. 1988; Bansal et al. 2009; Warden et al. 2011). The rate-limiting factor has been suggested by a fractal or jamming theory, and is applied to modeling cellulase kinetics on cellulosic substrate (Valjamae et al. 2003; Bommarius et al. 2008; Xu et al. 2009). The cellulase enzyme occupying the surface of the cellulose moves along the spatial-confined (fractal) cellulose chain and results in competitive adsorption (jamming). A general formulism to represent fractal kinetics replaces the hydrolysis rate constant (k_2) with a time-dependent expression with a fractal constant (f): $k_2 t^{-f}$ (Table 4-1, Formulism 1) and the hydrolysis rate decreases with time. Jamming assumes that cellulases act processively on cellulose polymer chains, and thus, the hydrolysis rate is dependent on the enzyme to substrate ratio with a jamming factor (j): $k_2 \left(1 - \frac{E}{jS}\right)$ (Table 4-1, Formulism 2). Therefore, changing enzymatic reaction rate in spatially constrained substrate is characteristic of fractal and jammed kinetics (Kopelman 1986; Valjamae et al. 2003; Bansal et al. 2009; Xu et al. 2009).

Other kinetics models have been developed to account for enzyme concentration effects which result in enzyme inactivation during processes other than product inhibition (Howell and Mangat 1978; Ohmine et al. 1983; Hong et al. 2007). The proposed mechanism include the inactivation of adsorbed enzyme (Howell and Mangat 1978; Scheiding et al. 1984; Gusakov et

al. 1985; Converse et al. 1988; Lin et al. 2005) and the loss of enzyme through mechanical means such as shear stress (Gan et al. 2003). For example, Lin et al (2005) considered adsorbed enzymes with reversible and irreversible interaction with the cellulose substrate, where irreversible adsorption leads to enzyme inactivation. Converse (1988) suggested that enzyme can be adsorbed on to the surface of the cellulose (active enzymes) or inside the cellulose fibril (inactive enzymes). The distinct advantage of enzyme inactivation mechanisms over fractal/jammed models is that they suggest more mechanistic reasons that enzyme and time decrease the hydrolysis rate.

Five models were initially fit to the QCM frequency responses as a function of enzyme concentration (Table 1): i) the original model with constant k_2 and no additional terms applied to account for the overcrowding effect; ii) a fractal model where k_2 is replaced by $k_2 t^{-f}$; iii) a jammed model where k_2 is replaced by $k_2(1-[E]/j[S])$; iv) a fractal jammed model; and v) a model accounting for the enzyme-substrate interaction that leads to enzyme inactivation (eq 3 and eq 4). The models investigated assumed first order kinetics with respect to enzyme concentration ($n=1$ in eq 6), which corresponds to a traditional Langmuir-based adsorption isotherm. While the models were fit to all the data, the experimental and model results are compared at 0.1 % v/v cellulase in Figure 4-4. Across the modeling approaches, the resulting model frequency profiles fit the initial adsorption of the experimental frequency data poorly. The adsorption is modeled as a smooth upward concave curve with a sharp-turn increase, and does not depict the transition from adsorption to hydrolysis effectively. Among the models investigated, only the model accounting for surface enzyme inactivation shows a smooth transition curve, but the extent of frequency drop and the linearity of the hydrolysis curve are not captured.

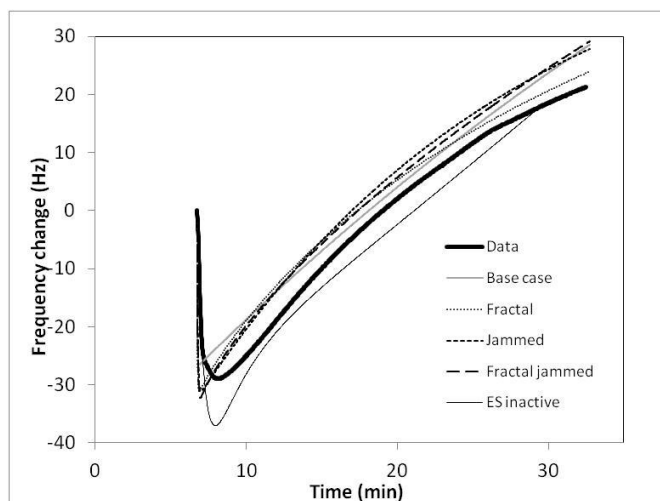


Figure 4-4 QCM frequency profile of measured frequency profile at 0.1 % v/v (— *thick black solid line*) and model QCM frequency profile using original model (— gray line), fractal model (····· small break line), jammed model (-----), fractal jammed model (- - -), and the model accounting the enzyme-substrate interaction that leads to enzyme inactivation (—).

The ability of the models to fit the hydrolysis portion of the data is also summarized in Figure 4-4, where results are shown only at an enzyme concentration of 0.1 % v/v cellulase. The original model fit poorly to the experimental frequencies because the model frequency showed only a minimal frequency increase at the lowest enzyme concentration (0.01% v/v), and over-estimated the hydrolysis curve at higher enzyme concentrations. When fractal kinetics is applied, the change in hydrolysis rate is proportional to the enzyme concentration. However, the QCM frequency response indicates that the hydrolysis rate does not further increase beyond an enzyme concentration of 0.1 % v/v. Jammed kinetics shows the same proportional change in hydrolysis rate with respect to enzyme concentration. In addition to the inconsistency between model and experimental frequency response, the applicability of the jammed and fractal jammed kinetics is limited because they are not able to predict accurate hydrolysis trend at higher enzyme concentrations. The jammed model, in particular, predicts negative hydrolysis kinetics (negative k_2) when $[E] > j[S]$. From the jammed model parameters obtained, this occurs when predicting

hydrolysis rates slightly greater [E] equal to 2% v/v suggesting that the model predictions are not relevant at enzyme concentrations slightly higher than those used in the experiment. Only the surface enzyme inactivation model is able to capture the observed trend in hydrolysis rate with respect to enzyme concentration.

The model predictions for the QCM frequency response of cellulose thin film hydrolysis based on the inactivation model is shown in Figure 4-5 as a function of cellulase concentrations (0.01, 0.05, 0.1, 0.5, and 1 % v/v). Model frequency curve for 2 % v/v is similar to 1 % v/v, and is not shown in the figure. With increasing enzyme concentration, the initial predicted drop in frequency signal due to adsorption dramatically increases, but the hydrolysis rates indicated by the upward slope of the curve does not change significantly. This indicates that the surface enzyme inactivation model correctly predicts that enzymes loading exceeding the capacity of the available substrate will not contribute to further increase in hydrolysis rate.

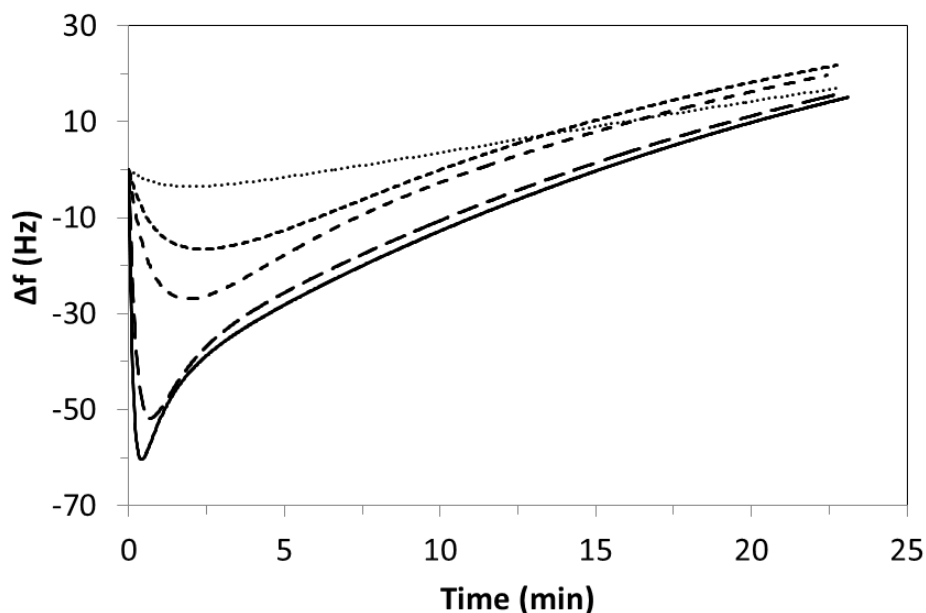


Figure 4-5 Model QCM frequency profile of cellulose hydrolysis using ES inactivation model. Cellulase concentrations represented are 0.01 % v/v (..... small dotted line), 0.05 % v/v (---- short dash line), 0.1 % v/v (- - - medium dash line), 0.5 % v/v (- - - - long dash line), 1 % v/v (— solid line).

While the enzyme surface inactivation model best describes the hydrolysis kinetics, all the modeling approaches employing the first order kinetics with respect to enzyme adsorption ($n = 1$ in eq 6) fail to predict the sensitivity and the surface saturation of the adsorption profile from the QCM frequency response to enzyme concentration. This is highlighted in Figure 4-5 for the enzyme surface inactivation model, in which increasing enzyme concentration incorrectly results in increased enzyme adsorption at high enzyme concentrations. Alternative adsorption models are investigated and fit using only the adsorption portion of the QCM frequency response. Figure 4-6a compares the observed frequency data (adsorption portion only) with model QCM frequency curves only in the QCM response region dominated by the adsorption of enzyme to the substrate. The frequency response of the model is predicted from the following expressions:

$$\Delta f = -AS_o \frac{ES}{S_o} \quad (11)$$

$$\frac{d[ES]}{dt} = k_1 E^n S - k_{-1} ES \quad (12)$$

Two enzyme adsorption models are compared: traditional first order enzyme adsorption model (in which k_f and k_r are fit to the adsorption data over all enzyme concentrations), and an n -th order adsorption model (fitting k_f , k_r , and n to the QCM adsorption data). When the rate of ES formation is first order with respect to enzyme concentration, ($n = 1$ in eq 12), the amount of enzyme adsorbed the model does not match the slope of the experimental frequency decrease (rate of the adsorption) and the extent of the frequency drop (amount of enzyme adsorbed) (Fig 4-6a). This is particularly evident at the lowest cellulase concentration (0.01 % v/v). Figure 4-6b shows the result of the modified model frequency profile ($n = 0.2$) after fitting the experimental QCM frequency curves simultaneously across experiments at different cellulase concentrations. The modified QCM frequency response results in significantly improved fit (from an average $R^2 = 0.65$ to $R^2 = 0.95$). The fact that the n -th order reaction constant with

respect to the enzyme concentration is less than 1 suggests diffusion limitation during the heterogeneous reaction at the interfaces of cellulose by liquid enzyme.

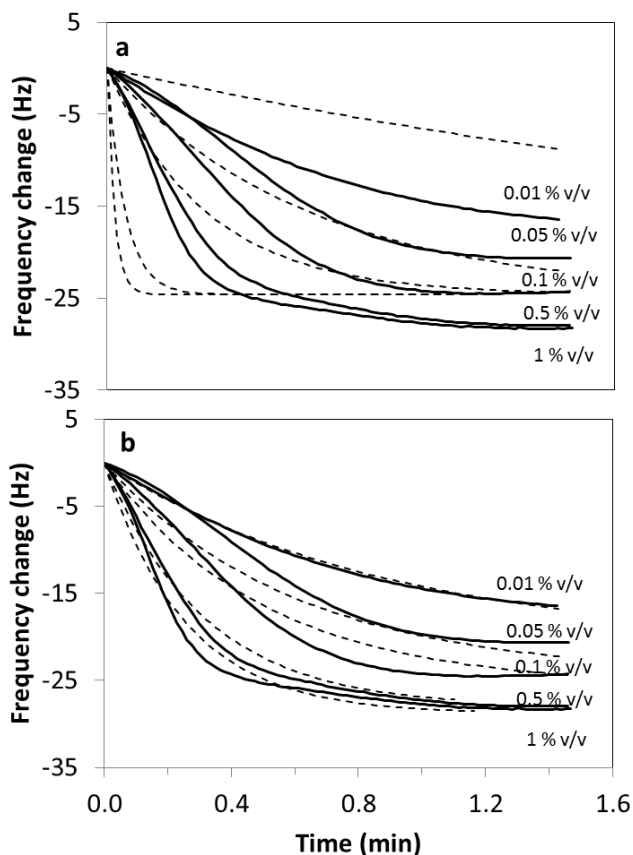


Figure 4-6 Model fit using a) first order kinetics or b) n^{th} ($n = 0.2$) order kinetics for the frequency response of the measured frequency change (*solid line*) and the model frequency change (*dotted line*) during adsorption at cellulase different concentrations.

The n -th order adsorption model and kinetics model with enzyme surface inactivation were applied simultaneously to fit the QCM frequency responses at all enzyme concentrations. The model parameters are four rate constants (k_1, k_{-1}, k_2, k_3), two frequency constants (A, B ; related to the sensitivity of the QCM to the individual species), a kinetic reaction order with respect to the enzyme concentration (n), and an initial cellulose surface coverage parameter for four of the individual experiments (S_o), where S_o was fixed to a value of one at the enzyme

concentration of 0.01% v/v. A single constant was determined across experiments by simultaneously fitting the QCM frequency response curves obtained as a function of cellulase concentration (0.01, 0.05, 0.1, 0.5, and 1 % v/v) (Fig 4-7). When the model was used to predict the frequency response with cellulase concentration of 2 % v/v, the model frequency curve showed a good fit to the experimental frequency data (Fig 4-7f). The kinetic parameters were fit to frequencies corresponding up to 80% substrate conversion ($S_i/S_o = 0.2$).

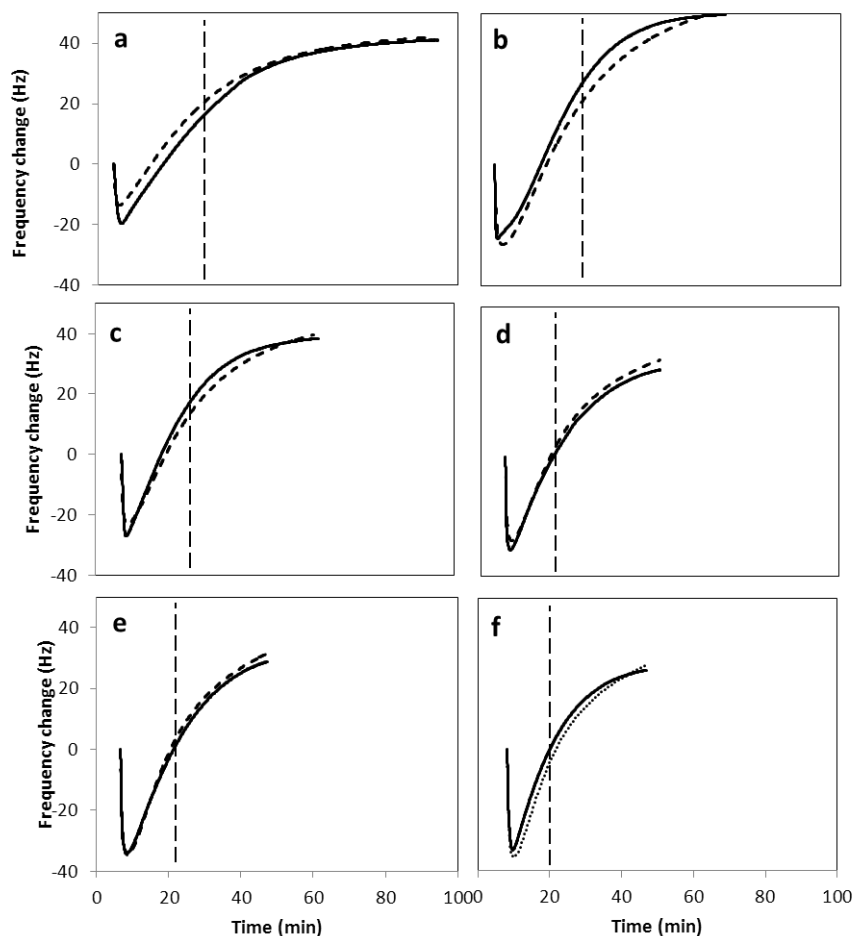


Figure 4-7 Measured frequency profile (— *black solid line*) and model frequency profile (- - - *dashed line*) of cellulose hydrolysis by cellulase to 80% conversion (*vertical dashed line*) at 0.01 % v/v (a), 0.05 % v/v (b), 0.1 % v/v (c), 0.5 % v/v (d), 1 % v/v (e), and predicted model frequency (*···· dotted line*) at 2 % v/v. The fit was extended to 100 % conversion (right side of the vertical dashed line). The average R^2 values are 0.95.

The original cellulase kinetics model developed in Chapter 3 also makes use of the environmental control of the QCM flow cell to describe the adsorption and hydrolysis of cellulose thin film using cellulose (0.5 % v/v) in the presence of cellobiose (as the inhibitor). The previous modeling effort focused on cellulase inhibition kinetics, and was intended to fit the frequency response curve up to 80% substrate conversion. The potential for additional enzyme-enzyme interactions, such as the enzyme inactivation at the surface, is expected later in the hydrolysis process and was not accounted for in the original model. The addition of inactivation of enzymes at the surface allows us to better capture the experimental frequency data at increased cellulose conversion, as shown in the model predictions over the entire data range, where the prediction past 80% conversion is provided in Figure 4-7.

The optimized model parameters fit to the QCM frequency curves at different cellulase concentration (0.01 % v/v, 0.05 % v/v, 0.1 % v/v, 0.5 % v/v, 1 % v/v) are summarized in Table 4-2. The frequency change per bound enzyme (active or non-active) represented by A ($=434.5 \text{ Hz SU}^{-1}$) is specific to the experimental setup (QCM and sensor system). The frequency change per unit substrate ($B = 43.7 \text{ Hz SU}^{-1}$) describes the sensitivity of the QCM experimental setup to the reduction of substrate lost from hydrolysis. The parameters, k_1 , k_{-1} , k_2 , k_3 , n , determined from the model, provide insight into the relative binding strength and hydrolysis rates of cellulase on microcrystalline cellulose. The resulting n , the order of the adsorption process with respect to enzyme concentration, is similar for the complete hydrolysis model ($n=0.18$) and the adsorption data only ($n=0.2$). The relative ratios of the adsorption/desorption rates (k_1/k_{-1}) do not describe equilibrium affinities of the cellulase for the cellulose, as they would in a first order process. Therefore, they are not directly comparable to our original model (Chapter 3). The rate at which the substrate (S_i) is hydrolyzed by cellulase follows first-order enzyme hydrolysis rate constant

Table 4-2 Model parameters optimized from the frequency data for cellulose thin films treated with cellulase (0.01 % v/v to 1 % v/v)

Parameters	Name	Values
<i>Enzyme kinetics parameters</i>		
k_1	enzyme adsorption constant ($\text{mM}^{-1} \text{min}^{-1}$)	0.31
k_{-1}	enzyme desorption constant (min^{-1})	0.03
k_2	rate constant of enzyme hydrolysis (min^{-1})	1.77
k_3	Inactive enzyme formation constant ($\text{mM}^{-1} \text{min}^{-1}$)	4.85
n	Order of reaction constant with respect to enzyme concentration (mM)	0.18
<i>QCM-specific response parameters</i>		
A	frequency change per bound enzyme (Hz SU^{-1})	434.5
B	frequency change per unit substrate lost (Hz SU^{-1})	43.7
S_o ([E] = 0.01% v/v)	initial substrate concentration (SU)	1
S_o (E] = 0.01% v/v)	initial substrate concentration (SU)	1.36
S_o (E] = 0.01% v/v)	initial substrate concentration (SU)	1.10
S_o (E] = 0.01% v/v)	initial substrate concentration (SU)	1.02
S_o (E] = 0.01% v/v)	initial substrate concentration (SU)	1.08

($k_2 = 1.77 \text{ min}^{-1}$). Previous model (Chapter 3) found a relatively lower hydrolysis rate constant $k_2 = 0.06 \text{ min}^{-1}$. Because surface inactivation further reduces the observed hydrolysis rate, it is expected that the hydrolysis rate is higher in this model than the original model. The value of k_2 is reported in ranges that are specific to experimental condition, model approach and different type of substrate and enzymes. Howell and Mangat (1978) proposed a model describing the hydrolysis of cellulose (Solka-Floc) by *Trichoderma viride* cellulase and found the hydrolysis rate constant to be 9.05 hr^{-1} (or 0.15 min^{-1}). Luterbacher et al (2012) developed three kinetic

models based on the fluorescence intensity signal to model the de-polymerization of bacterial microcrystalline cellulose using the β -glucosidase supplemented cellulase cocktail. The three models gave similar hydrolysis rate constants of $k_2 = 0.068 \text{ min}^{-1}$.

The advantage of the applying a mechanistic model to fit the QCM frequency responses is the ability to predict the time-dependent concentrations of available substrate (S_i), enzyme-substrate complex (ES), and inactive enzyme-substrate complex (ES_{inact}). Figure 4-8 shows the concentration profile (normalized by $S_o=1$) for the case of 0.1 % v/v cellulase. During the onset of cellulose hydrolysis, ES quickly forms and is slowly depleted as it turned into ES_{inact} or desorbed from the surface. The rate at which ES_{inact} is formed ($k_1 = 10.0 \text{ mM}^{-1} \text{ min}^{-1}$) is relatively slower than the rate of ES formation ($k_3 = 0.93 \text{ mM}^{-1} \text{ min}^{-1}$). However, while some of the ES_{inact} remains bound, only a very small fraction of ES remains on the surface. This prediction suggests the extent to which the effective hydrolysis rate was decreased by the presence of inactive enzyme on the cellulose surface.

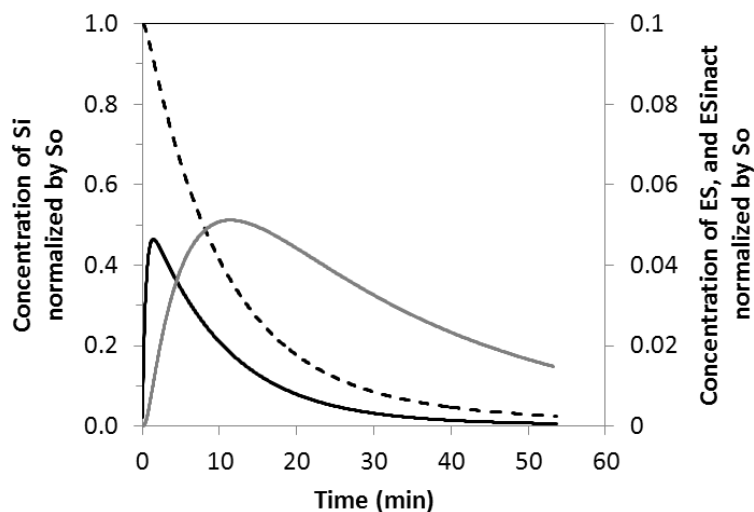


Figure 4-8 Model concentration profile of S_i (- - - black dashed line), ES (—black solid line), and ES_{inact} (— gray solid line) normalized by initial substrate concentration, S_o , during cellulose hydrolysis by cellulase (0.1 % v/v).

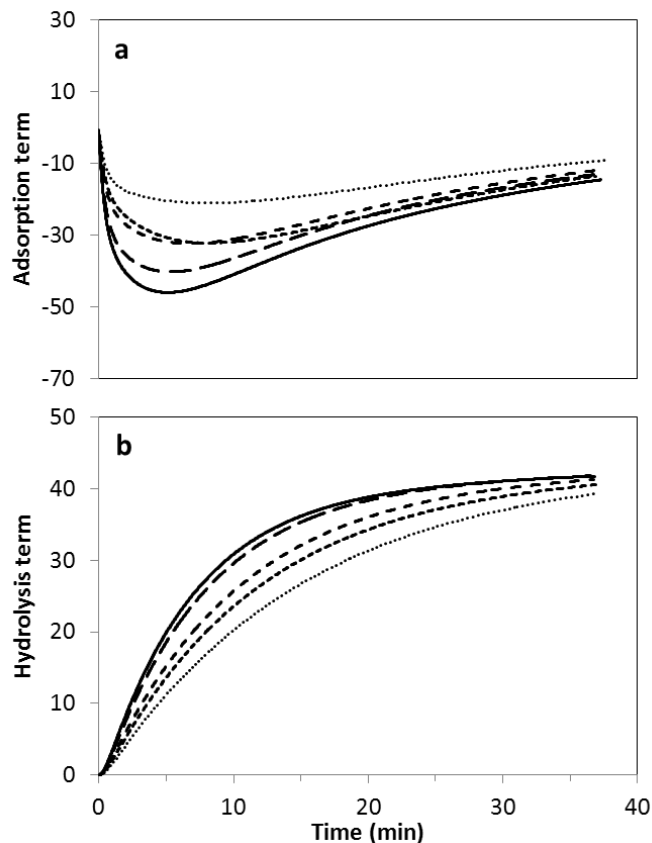


Figure 4-9 The adsorption term (a) and the hydrolysis term (b) of the model QCM frequency change for cellulose film hydrolysis at cellulase concentration of 0.01 % v/v (.... *small dotted line*), 0.05 % v/v (---- *short dash line*), 0.1 % v/v (- - - *medium dash line*), 0.5 % v/v (----- *long dash line*), 1 % v/v (— *solid line*). Figures shown are based on the parameters obtained from Table 4-2 with the surface coverage of $S_o = 1$.

The developed model can also be used to probe the apparent extent of enzyme adsorption and hydrolysis inferred from the raw QCM frequency response data and delineates the contribution of thin film mass increase due to adsorption and mass loss due to hydrolysis. The mass change due to the adsorption (of ES and ES_{inact}) and the hydrolysis events are described by the model frequency equation (eq 10). The adsorption term, $A \frac{ES}{S_o} + \frac{ES_{inact}}{S_o}$, and the hydrolysis term, $B \frac{S_o}{S_o} - \frac{S_i}{S_o}$, are plotted against time using the model parameters (Fig 4-9). The comparison is made at $S_o=1$, so it is not intended to describe the model data, which is dependent on surface

coverage, but a single surface. As time progresses, the adsorbed enzyme molecules slowly desorb from the surface as the substrate is turned into products. On the other hand, the frequency change due to hydrolysis increases as the cellulase concentration increased (Fig 4-9b). When the cellulase concentration reaches 0.5 and 1 % v/v, the extent of the frequency increase is minimal. This suggests that the maximum hydrolysis rate occurs at high enzyme concentrations and is consistent with a saturated surface. Thus, the model results suggest that the apparent maximum in the hydrolysis rate and extent in the QCM data at 0.05% v/v (Fig 4-2) is the result of differences in thin film thicknesses and not inherent to the hydrolysis kinetics of the thin films. However, the established model is capable of fitting and predicting hydrolysis data that do exhibit a maximum with respect to enzyme concentration, as suggested by some previous bulk experiments of cellulose hydrolysis (Sattler et al. 1989; Nidetzky et al. 1994).

Our initial analysis using the fractal, jammed and fractal jammed kinetics coupled with the first order adsorption model highlighted inconsistencies in the hydrolysis kinetics when describing the experimental QCM frequency responses as a function of enzyme concentration (Figure 4-3). Those inconsistencies are present when these kinetic models are coupled to an n -th order enzyme adsorption model and fit in the same manner as the surface enzyme inactivation model. The n -th order reaction constant (with respect to the enzyme concentration) was allowed to vary to obtain the best fit. The least squared fit using the fractal model showed an improved fit (from previous fit when $n = 1$), but the fractal exponent factors, f , became negligible. This suggested that the kinetic behavior was not governed by the fractal effect. When jammed model was applied to fit the experimental data, the fit also improved from the previous simulation (when $n = 1$) with the jamming factor, j , equaled 0.79. However, when the model was used to predict hydrolysis at increased enzyme concentration (3.8 % v/v), the

hydrolysis rate constant (k_2) became negative. This is a result of the limitation of the jammed formulism (Table 4-1) which requires the enzyme concentration to be lower than the product of jamming factor and the substrate concentration ($[E] \leq j[S]$). The fractal-jammed model, which combines the fractal and the jammed effect (Table 4-1) again demonstrates an improved fit from the previous simulation (when $n = 1$) with $j = 0.28$, and $f = 0.50$. However, this formulation is also limited by the jammed formulism, in which a negative hydrolysis rate is predicted at high enzyme concentrations. Although the semi-empirical approaches in general are consistent with the experimental observation, the overall mechanistic understanding and quantitative prediction are lacking. The ES-inactivation model provides the explicit mechanistic events with the kinetics parameters required to quantify the mode of decreased hydrolysis kinetics with time.

Conclusion

The effect of enzyme concentration on cellulose hydrolysis by cellulase was investigated using the QCM frequency change that reflects the mass change in cellulose thin film. The initial hydrolysis rates measured from the slope of the experimental QCM frequency curves are consistent with enzyme saturation on the surface, but potentially show a maximum rate at an intermediate enzyme concentration. Proposed kinetic models of cellulose hydrolysis intended to describe the effect of enzyme concentration (surface enzyme inactivation, fractal, jammed, fractal jammed) are fit to the QCM frequency response and compared to a model using a constant hydrolysis rate. A suitable description of enzyme adsorption is also required, where an n -th order model with respect to enzyme concentration significantly improves the experimentally observed enzyme adsorption relative to a traditional first-order Langmuir-based model. The modeling approach that employs surface enzyme inactivation and n -th order kinetics best captures the adsorption and hydrolysis trends with increasing enzyme concentration. The

resulting model suggests a mechanism by which enzyme hydrolysis rates are decreased with time and also predicts the extent of surface enzyme inactivation as a function of cellulose conversion. The model is also capable of predicting a maximum hydrolysis rate at an intermediate enzyme concentration, although it suggests that any observed maximum in the initial hydrolysis rates from our QCM response curves is an artifact of the cellulose film thickness. In general, hydrolysis kinetics is strongly dependent on the initial substrate accessibility. A more consistent measurement in initial hydrolysis rate can be performed with homogenous films where the surface coverage is uniformly distributed. However, heterogeneous films offer greater substrate surface area which promotes better enzyme adsorption and effective hydrolysis.

Chapter 5

Direct monitoring of the temperature dependence of cellulose hydrolysis by *Clostridium thermocellum* using Quartz Crystal Microbalance and liquid Atomic Force Microscopy

Summary

Increasing the activity and robustness of cellulases, the enzymes that break down cellulose into fermentable sugars, is key to realizing the next generation of lignocellulosic biofuels. The activity of cellulases is increasingly investigated using thin film techniques, such as QCM and AFM. Surface analysis techniques have the distinct advantage relative to bulk cellulose degradation experiments of the potential to observe and delineate cellulase adsorption and hydrolysis steps, where both enzymatic steps affect the observed hydrolysis rate. To date, the investigation of cellulase activity on cellulose thin films using surface techniques has been limited to naturally occurring fungal cellulase mixtures or purified enzymes. In contrast, bacterial cellulases are expressed as cellulosomes, a multi- complex protein that exhibits higher specific catalytic activity than fungal enzymes on cellulosic substrates. On the basis of their activity, bacterial cellulases from *Clostridium thermocellum* have been proposed as part of consolidated bioprocessing where the role of the bacterial cellulase is to liberate fermentable sugars for subsequent conversion to biofuels and solvents. Knowledge of cellulase activity as a function of temperature is needed to design processes that take advantage of the high activity of cellulosomes.

In this work, QCM and AFM are demonstrated for the first time for the monitoring of *C. thermocellum* cellulase binding and hydrolysis of cellulose thin films. The temperature-dependence of cellulose thin film hydrolysis by *C. thermocellum* is investigated. The adsorption

and the hydrolysis of cellulose thin film are monitored directly by QCM at different temperatures (30 °C, 40 °C, and 50 °C). In addition, the dynamic surface hydrolysis of cellulose is interpreted directly from the surface topography of the thin films, as measured by AFM in the presence of liquid cellulase from *Trichoderma reesei* and whole cell *C. thermocellum*. The hydrolytic activity of *C. thermocellum* observed by QCM is consistent with the AFM topography imaging data. QCM and AFM provide complementary information on cellulose surface changes during hydrolysis, which is particularly relevant to investigations employing whole cells in liquid media.

Introduction

Liquid biofuels, such as ethanol and butanol, derived from cellulosic biomass have a high energy content, low environmental impacts, and effectively use abundant, inexpensive substrates (Demain et al. 2005). The production of ethanol from native lignocellulosic biomass begins with a physicochemical pretreatment to increase cellulose accessibility followed by two subsequent processing steps: enzymatic conversion of cellulose into soluble sugars and ethanol fermentation by ethanologenic microbes. Cellulose hydrolysis is a limiting step in the production of commercially viable biofuels because of the recalcitrant nature of complex cellulose structures (Johnson et al. 1982). Long term efforts in developing an efficient saccharification process focus on understanding the mechanism and catalytic activity of cellulase (the enzyme responsible for the degradation of β -1,4-glucosidic bonds in polysaccharides to glucose monomers) and the structural change of the hydrolyzed substrate.

The proposed processes for commercial degradation of cellulose to fermentable sugars utilize cellulases from two types of microbial sources: aerobic fungi or bacteria (Wilson 2009). The cellulases produced by these organisms comprise the three types of cellulases that work

synergistically on the crystalline and amorphous region of the cellulose: endo-glucanases, exo-glucanases, and β -glucosidases. One distinct difference between the enzymes from the microbial sources is their connectivity with the cells. Fungal cellulases, most notably derived from *Trichoderma reesei*, are secreted independently and released freely into the fermentation broth. In contrast, bacterial cellulases are assembled in the form of a large extracellular surface-bound protein complex, known as a cellulosome. The first characterized cellulosome was that of *Clostridium thermocellum*, in which enzymes are bound to the noncatalytic scaffolding subunit attached to the cell surface via several anchoring proteins (Lamed et al. 1983; Bayer et al. 1994). Both microbial cellulase systems contain a cellulose-binding domain (CBD), which helps the cellulase complex binds effectively to the insoluble cellulose substrates and therefore promote efficient hydrolysis reaction (Bayer et al. 1998; Beguin and Alzari 1998). The arrangement of individual cellulases in the systematic order of a cellulosome is suggested to be advantageous over the free enzymes because of their ability to sequentially process soluble hydrolysis products to glucose (Shoham et al. 1999; la Grange et al. 2010).

Kinetic investigations of cellulases generally rely on measures of cellulose degradation to interpret the effects of environmental variables and enzyme perturbations on cellulase adsorption and hydrolysis (Woodward and Arnold 1981; Ghosh et al. 1982; Lynd et al. 2002; Gruno et al. 2004; Zhang and Lynd 2004; Bansal et al. 2009; Romsaiyud et al. 2009). More recently, innovations in surface analysis techniques have provided more direct measures of cellulase interactions and activity on model cellulose thin films. For example, the interaction of cellulases and cellulose is revealed by a piezoelectric quartz crystal microbalance (QCM) in which enzyme adsorption, inhibitor binding, and hydrolysis reaction are captured in real-time by the ultra-sensitive mass change deposited or leaving the crystal (Rodahl et al. 1997; Josefsson et al. 2007;

Ahola et al. 2008; Turon et al. 2008; Hu et al. 2009; Suchy et al. 2011). Cellulose morphology and the effect of enzyme action on the cellulose surface are characterized by atomic force microscopy (AFM) which offers direct visualization of the effect of cellulase activity on cellulose (Igarashi et al. 2009; Igarashi et al. 2011; Bubner et al. 2012); These surface analysis techniques have been applied exclusively to cellulose hydrolysis by fungal or purified cellulases. In extending these surface analysis techniques to cellulosomes, we have focused on temperature as a critical variable to maximize enzymatic productivity, recognizing that the temperature for optimum cell growth, cellulase adsorption, and cellulase hydrolysis may differ. In addition, if the cellulosome is used only for its catalytic activity, the optimal temperature for the subsequent fermentation of the soluble sugars is dictated by solventogenic microorganism. In the case of the thermophilic cellulolytic bacteria, *C. thermocellum*, the optimal growth temperature is around 60°C (Freier et al. 1988), but the cellulase activity is maximum at 60-64 °C (Ng et al. 1977). Cellulolytic activity of *C. thermocellum* has been reported at temperatures as high as 70 °C (Johnson et al. 1982). However, the cellulase system retains some activity in the mesophilic temperature range (Ng et al. 1977; Johnson et al. 1982; Saddler and Chan 1982).

The robustness of the cellulase system with respect to temperature provides the opportunities for *C. thermocellum* cellulase to be used at conditions outside from their ideal temperature. For example, *C. thermocellum* has been investigated in co-culture systems to produce other high-value products from cellulose, selected for use in co-cultures because most organisms do not produce the enzymes require to digest cellulose (Saddler et al. 1981; Yu et al. 1985; Nakayama et al. 2011). Recent co-culture with *Clostridium acetobutylicum* takes tadvantage of the hydrolytic ability of *C. thermocellum* to hydrolyze cellulose, and ferment the hydrolysis products to produce butanol (Nakayama et al. 2011). However, to accommodate the

growth of mesophilic *C. acetobutylicum*, fermentation temperature was lowered to 39 °C. The temperature of the co-culture is an important physical parameter to be optimized.

This study examines the effect of temperature on cellulose hydrolysis and applies the novel surface techniques to analyze the activity of whole cell cellulases (cellulosomes) for the first time on model cellulose thin films. The time-dependent adsorption and hydrolytic activity of *C. thermocellum* on spin-coated cellulose thin films are measured by the mass change of the model cellulose thin film using Quartz Crystal Microbalance (QCM) at 30 °C, 40 °C, and 50 °C. The QCM frequency response for hydrolysis by *C. thermocellum* is compared to that of cellulases from *T. reesei* at 30 °C. The change in surface topography during cellulose thin film hydrolysis by *C. thermocellum* is observed and quantified by imaging the cellulose surface using a liquid cell in atomic force microscopy (AFM) at 50 °C. The same imaging technique is applied to validate the hydrolysis of cellulose thin film by cellulase mixture (0.5 % v/v) from *T. reesei* at 30 °C. QCM and AFM are complementary tools to quantify the adsorption and hydrolytic performance of cellulase at different reaction temperatures and characterize the change in surface topography on model cellulose and other soluble substrate thin film.

Materials and Methods

Materials. Microcrystalline cellulose (MCC, 20 μ m) was purchased from Aldrich. N-methylmorpholine N-oxide (NMMO), dimethyl sulfoxide (DMSO, \geq 99.8%), and polyethyleneimine (PEI, 50 wt. % aqueous solution) were supplied by Acros Organics. Acetate buffer (0.1 M, pH 5) was prepared by diluting glacial acetic acid (Fisher Scientific) in Milli-Q de-ionized water (Millipore Corporation). Cellulase (an aqueous mixture consisting of *endo*-glucanases, *exo*-glucanases, cellobiohydrolases, and β -glucosidases) from *Trichoderma reesei*

26921 (Celluclast®) was purchased from Sigma Aldrich. Cellulase (0.5 % v/v) was diluted in acetate buffer (0.1 M, pH 5).

Strain and media composition. *C. thermocellum* ATCC 27405 was obtained from the culture collection of Herbert J. Strobel, University of Kentucky. *C. thermocellum* cells were grown anaerobically at 65°C. The basal medium contained (per liter): 30.6 g Na₂HPO₄, 30.0 g KH₂PO₄, 10.0 g NH₄Cl, 10.0 g (NH₄)₂SO₄, 1.8 g MgCl₂ 6-H₂O, 0.6 g CaCl₂, 2.0 g yeast extract, 10 ml standard vitamin mixture (Cotta and Russell 1982), 5.0 ml modified mineral mixture (Pfenning's Metals plus 10 mg Na₂WO₄·2 H₂O and 1 mg Na₂SeO₃ per liter) and 1 ml resazurin. The pH was adjusted to 6.7 with NaOH. The medium was autoclaved (121° C, 20 min) and cooled under O₂-free CO₂ sparge. The buffer, Na₂CO₃ (4 mg ml⁻¹) was added before the broth was at room temperature. Media for batch cultures were anaerobically dispensed into serum bottles and sealed with butyl rubber stoppers, and autoclaved for sterility. *C. thermocellum* was routinely transferred in the basal medium with cellulose (Whatman No.1 filter paper). *C. thermocellum* was transferred once with cellobiose (4 mg ml⁻¹) prior to QCM and AFM experiments to reduce the possibility of cellulose fragments from affecting the measurement. The cells used for the experiment were in resting state.

Preparation of Cellulose Thin Films. The procedures to make cellulose thin films were slightly modified from the previous investigations (Gunnars et al. 2002; Fält et al. 2004). Gold-coated QCM-D resonators (QSX 301, Q-Sense) were treated with ultraviolet cleaner (BioForce, Ames, IA) for 10 minutes to decompose and volatilize organic contaminants on the sensor surface. The UV-treated QCM-D sensors were immersed in diluted (0.2 % v/v) polyethyleneimine (PEI, 50 wt. % aqueous solution) for 15 minutes. PEI was used as an

anchoring polymer (Ahola et al. 2008; Aulin et al. 2009) to attach the cellulose to the QCM-D sensor (QSX 301 Gold, Q-Sense AB, Göteborg, Sweden). The QCM-D sensors were contacted with de-ionized water (pH adjusted with sodium hydroxide to that of the polymer solution, ~ pH 10) for an additional 10 minutes, during which time the polymer precipitated on the surface of the sensor. The PEI-coated sensors were dried in the oven (50° C, 30 min), then kept in a desiccator (room temperature) for storage. A solution of microcrystalline cellulose in N-methylmorpholine-N-Oxide (NMMO 50 wt. % aqueous solution in water) was prepared by adding cellulose (2 wt. %) to NMMO preheated to 110 °C and continuing to heat the mixture to 115 °C. The addition of cellulose at high temperature solution prevented the agglomeration of fine microcrystalline cellulose. A clear solution was obtained at 115 °C after approximately one hour. Dimethyl sulfoxide (DMSO, ≥99.8%) was slowly added to the mixture to make a final solution of 0.5 wt. % cellulose. The temperature of the cellulose solution was reduced to 70° C, prior to spin coating. Cellulose solution (0.1 ml) was spin-coated (4500 rpm, 40 sec, WS-400BZ-6NPP/Lite, Laurell Technologies) on the PEI-coated QCM-D sensors. After spin-coating, the sensors were immersed in deionized water (30 min), and then dried in the oven (50° C, 30 min). The cellulose-coated sensors were stored in a desiccator at room temperature prior to use.

Cellulose Thin Film Characterization by Atomic Force Microscopy (AFM). The surface topography of the cellulose on the QCM sensor (QSX301) was measured by AFM (Series 4500, Agilent Technologies) in air, liquid cellulase (0.5 % v/v Celluclast®, in pH 5, 0.1 M acetate buffer) or in *C. thermocellum* culture broth. The support base (QSX301) and the cellulose thin layer coating on the sensor (QSX301) were scanned in tapping mode using a silicon cantilever

(TAP 300AI-G, Budget Sensors) with a spring constant of 40 N/m and a driving frequency of 300 kHz. In liquid AFM, integral gain, proportional gain, and deflection set point were adjusted to increase the sensitivity and reduce the lateral friction and vertical force on the cellulose. Scanning speed (2 inch/sec) remained the same throughout the experiment. The temperature controlled plate (Hot MAC sample plate) was connected to the temperature controller (Model 332, Lake Shore Cryotronics, Inc, Westerville, OH). The acquired scan area ranged from 2×2 μm to 50×50 μm. At least three sensors were scanned to confirm reproducibility.

AFM topography images (5×5 μm) were processed by PicoView software. These images were loaded to Gwyddion software which is a modular program for scanning probe microscopy (SPM) data analysis. Height distribution (topography vs. distance) images were taken by measuring the same reference point of the 1-D topography image of the same cellulose sample at different times during the course of hydrolysis reaction.

Cellulose Thin Films/ Cellulase Interactions Measured by Quartz Microbalance with Dissipation (QCM-D). A quartz crystal microbalance (Q-Sense E4) equipped with four temperature controlled flow modules was used to measure changes in mass per unit area and in the viscoelasticity properties of the cellulose thin films from the change in frequency (Δf) and dissipation (D) of the cellulose-coated quartz crystal resonator. The oscillation frequency and dissipation energy were measured simultaneously from the application of an AC voltage across the electrode, causing the piezoelectric quartz crystal to vibrate (Rodahl et al. 1995). The resonance frequency change (Δf) can be used to calculate the proportional mass absorbed on the crystal surface by the Sauerbrey equation:

$$\Delta m = -\frac{c}{n} \Delta f \quad (1)$$

where c is the constant for mass sensitivity and n is the overtone number. “ c ” varies for different type of sensors. For the 4.95 MHz AT-cut sensor used in this study, c is equal to $17.8 \text{ ng cm}^{-2} \text{ Hz}^{-1}$. The QCM acquires frequency signal at the fundamental resonance (5 MHz) and at a multiple of resonance (overtone frequency). Third overtone frequency was used to avoid edge effect (unstable frequency signal at the edge of the sensor measured by the fundamental frequency). The Sauerbrey equation (Rodahl et al. 1995) is valid for the following conditions: 1) the surface film is flat and uniformly distributed, 2) the mass change of the crystal surface is much smaller than the mass of the quartz resonator, 3) the film is rigid, meaning that the mass absorbed on to the surface must be firmly attached with no oscillatory effect ($D < 10^{-6}$ per 10 Hz). In this study, the Sauerbrey equation is valid because the change in dissipation during cellulase treatment on ultrathin cellulose films prepared with the dissolved cellulose was relatively small ($2\text{-}6 \times 10^{-6}$ dissipation units).

The mass change of cellulase thin films in response to *T. reesei* cellulase (Celluclast, Sigma Aldrich) or whole cell *C. thermocellum* was measured by QCM. Prior to contacting the cellulose thin films with fungal cellulase or *C. thermocellum*, the cellulose-coated QCM sensors were incubated with the acetate buffer (0.1 M, pH 5) at a flow rate of 0.2 ml min^{-1} until a constant baseline in frequency measurement was reached ($< 2 \text{ Hz hr}^{-1}$), which was obtained in approximately 30 min. The temperature of the QCM chamber was controlled at $30 \text{ }^\circ\text{C}$ for fungal cellulase or $30 \text{ }^\circ\text{C}$, 40 and $50 \text{ }^\circ\text{C}$ for *C. thermocellum*. All liquid solutions were degassed for 30 min using an ultra-sonicator (Cole-Parmer 8890, IL) prior to injection in the flow cell. The change in mass of cellulose thin films was measured from *T. reesei* cellulase or *C. thermocellum* culture broth which was injected into the QCM chamber in continuous flow mode (0.2 ml min^{-1}). Both cellulase binding and cellulose hydrolysis were monitored simultaneously throughout the

experiment by the measurement of the change in oscillation frequency and dissipation energy in QCM. When the frequency signal and dissipation had no significant change ($< 2 \text{ Hz h}^{-1}$), the injection solution was switched to acetate buffer to rinse and remove any remaining hydrolysate on the sensor surface.

Results and Discussion

Cellulosome binding and hydrolysis as measured by QCM

QCM has been a versatile tool for analyzing molecular change in many biological or chemical processes. The use of piezoelectric quartz sensor allows the ultrasensitive mass change of the quartz crystal to be measured in real time, and therefore provide exceptional accurate analysis in characterizing wide range of immobilized surface and their interaction with low molecular-weighted compounds (ligands, metals, carbohydrates) or large, complex molecules (protein, nucleic acid, microbial cells). The applications of QCM to whole cells experimentation include biofilm, cell adhesion, attachment, growth, and substrate interactions (Becker and Cooper 2011). This work aims to extend the adsorption and hydrolytic measurement from simple and non-complex cellulases to whole cell *C. thermocellum*, which is demonstrated on the cellulose thin film for the first time.

In this study, QCM-D was employed to provide quantitative measurements on enzyme binding and hydrolysis on the cellulose thin film. The frequency profile of cellulose hydrolysis by 0.5 % v/v *T. reesei* cellulase and *C. thermocellum* was compared at 30 °C (Fig 5-1). When *T. reesei* cellulase solution (0.5 % v/v) replaced acetate buffer (0.1 M, pH 5) at 3 min, a rapid drop in frequency (to a minimum of -23 Hz) was observed due to the rapid adsorption/binding of cellulase onto the cellulose surface. This initial frequency drop corresponds to 136 ng cm⁻² of

adsorbed cellulase, as calculated by the Sauerbrey equation (Rodahl et al. 1995). After enzyme loading on the cellulose surface (approximately 6 min after the introduction of cellulase), the frequency increased with time due to the reduction of mass of the film. This reduction in mass is attributed to the loss of cellulose by enzymatic hydrolysis. Finally, the maximum frequency reached a plateau when the available substrate was hydrolyzed. Conversely, when *C. thermocellum* is introduced to the QCM chamber (3 min), a rapid decrease in the QCM frequency is observed, indicating the interaction of the whole cells with the cellulose thin film. However, there is not a subsequent increase in the frequency. This indicated that cellulose was not hydrolyzed by *C. thermocellum* at 30 °C.

The QCM frequency profile for cellular adsorption is greatly influenced by the type of cell and surface property that the cell is adhering to. Generally, the processes that can affect QCM frequency signal are: 1) physical contact with the surface, 2) secretion of proteins or products, 3) cell expanding on the surface, and 4) change in cellular shape, structure, or adhesion properties (Rodahl et al. 1997). In this study, we employed resting cells that were de-energized. The frequency response was most likely to be attributed to the initial physical contact of *C. thermocellum* with the cellulose surface.

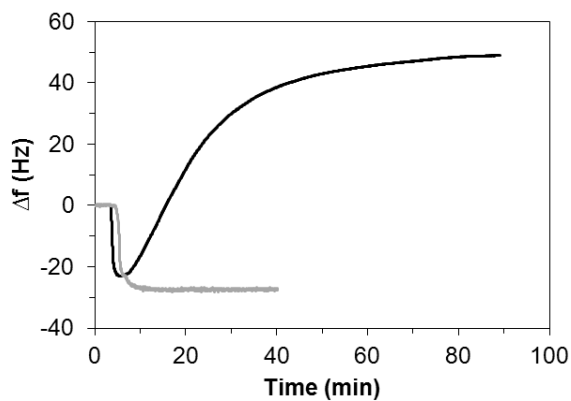


Figure 5-1 Frequency profile of cellulose hydrolysis by 0.5 % v/v *T. reesei* cellulase (*black*) and *C. thermocellum* (*gray*) at 30 °C.

When the temperature of the QCM chamber was increased to 40 °C and 50 °C, evidence of both cellulase adsorption/contact with the surface (initial decrease in frequency) and subsequent cellulose hydrolysis (increase in frequency) were observed after the introduction of *C. thermocellum* into the QCM chamber (Fig 5-2). A more pronounced rate of frequency increase, interpreted as an increased hydrolysis rate, was observed at 50 °C. This result is consistent with the observations that cellulase from commercial cellulase mixture obtained from *T. reesei* is active at lower temperature (20-40 °C), but *C. thermocellum* cellulase activity is reduced significantly in this temperature range (Peitersen et al. 1977; Josefsson et al. 2007; Ahola et al. 2008; Turon et al. 2008; Hu et al. 2009; Hu et al. 2009). Ng (1977) reported an optimal temperature of *C. thermocellum* cellulase activity from 60-64 °C, but the activity reduced nearly 70 % when the temperature dropped to 30 °C. Saddler et al (1982) found that the activity of *C. thermocellum* β -glucosidase enzyme alone decreased 80% after incubation at 37 °C for 24 h.

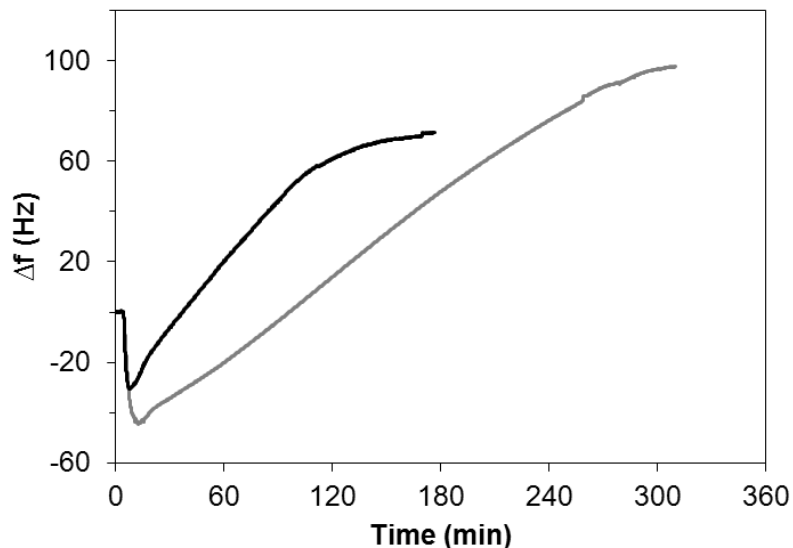


Figure 5-2 Frequency profile of cellulose hydrolysis by *C. thermocellum* at 40 °C (gray) and 50 °C (black).

AFM experimentation: cellulose degradation by *C. thermocellum*

Direct visualization of cellulose degradation process using AFM has been applied to purified or commercial cellulase system (Igarashi et al. 2009; Song et al. 2009; Igarashi et al. 2011; Bubner et al. 2012). Often, the surface imaging by cantilever was scanned in air. In this investigation, a liquid AFM cell was used to image the surface topography of cellulose thin film in liquid cellulase solutions at a controlled temperature. Figure 5-3 showed the comparison of AFM topography images of cellulose thin film in air and in liquid acetate buffer (0.1 M, pH 5) at 30 °C. The presence of cellulose was validated in both dry and liquid images. The area where the cellulose has higher altitude is reflected in white, and the area with lower altitude is reflected in dark brown. Ridge-like filaments of cellulose on the QCM sensor are clearly presented by the dry AFM image. The topographical image of the spin-coated cellulose film is comparable to that reported for microcrystalline cellulose thin films in previous work (Kontturi et al. 2006; Aulin et al. 2009). Surfaces of cellulose are also successfully scanned by AFM in the presence of liquid. Although the resolution is not as high as the dry AFM image due to disturbance of mechanism response from the film in liquid, the distribution and the physical shape and height of cellulose are still visible.

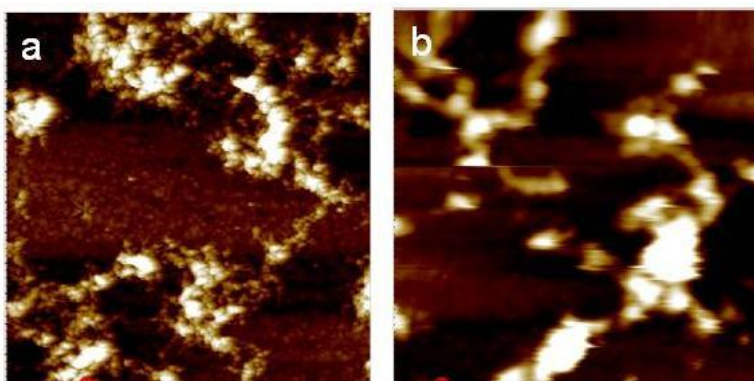


Figure 5-3 AFM topography image ($5 \times 5 \mu\text{m}^2$) of cellulose-coated quartz crystal resonator in a) air or in b) liquid acetate buffer (0.1 M, pH 5) at 30 °C.

The change in surface topography during cellulose thin film hydrolysis by cellulase is captured by AFM in liquid *C. thermocellum* at 50 °C (Fig 5-4). The fragments of cellulose (represented by the white spot) disappear as time progresses. After 70 min of incubation with *C. thermocellum*, the cellulose that originally appeared in white is not present on the surface. The surface texture of the QCM sensor after hydrolysis appeared globular, which is typical for colloidal gold particles of the gold QCM sensor (QSX301) surface.

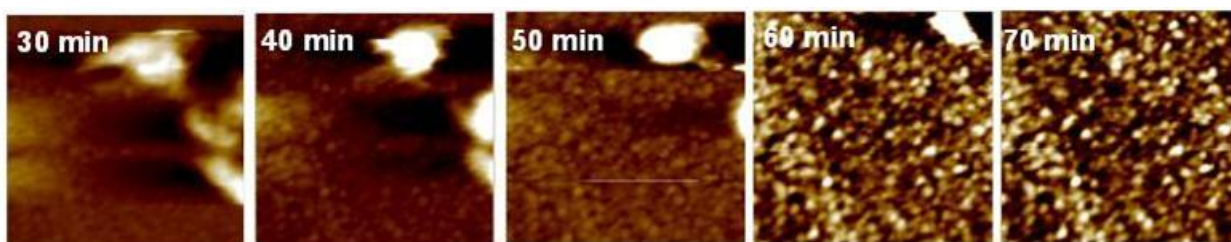


Figure 5-4 AFM Topography images (tapping mode, 5 x 5 μm^2) of cellulose-coated quartz crystal resonator incubated with *Clostridium thermocellum* at 50 °C

Similar topography changes are observed in liquid cellulase solution from *T. reesei*. The topography images accompanied by the cross-sectional height measurements are shown in Figure 5-5. The fibrous cellulose (represented by the white spot) disappears with time. The corresponding change in cellulose height decreases from 62 nm to approximately 5 nm in 1h. It is interesting to note that as cellulose was degraded by *T. reesei* cellulase, a scratch on the QCM sensor become visible, and the depth of the scratch was not affected by cellulase incubation.

The observation of hydrolysis using AFM is consistent with the results obtained from QCM in which cellulose hydrolysis occurred at 50 °C for *C. thermocellum* and 30 °C for *T. reesei* cellulase. No change in the cellulose topography or height is observed when cellulose is incubated in acetate buffer (0.1 M, pH 5) (Fig 5-6).

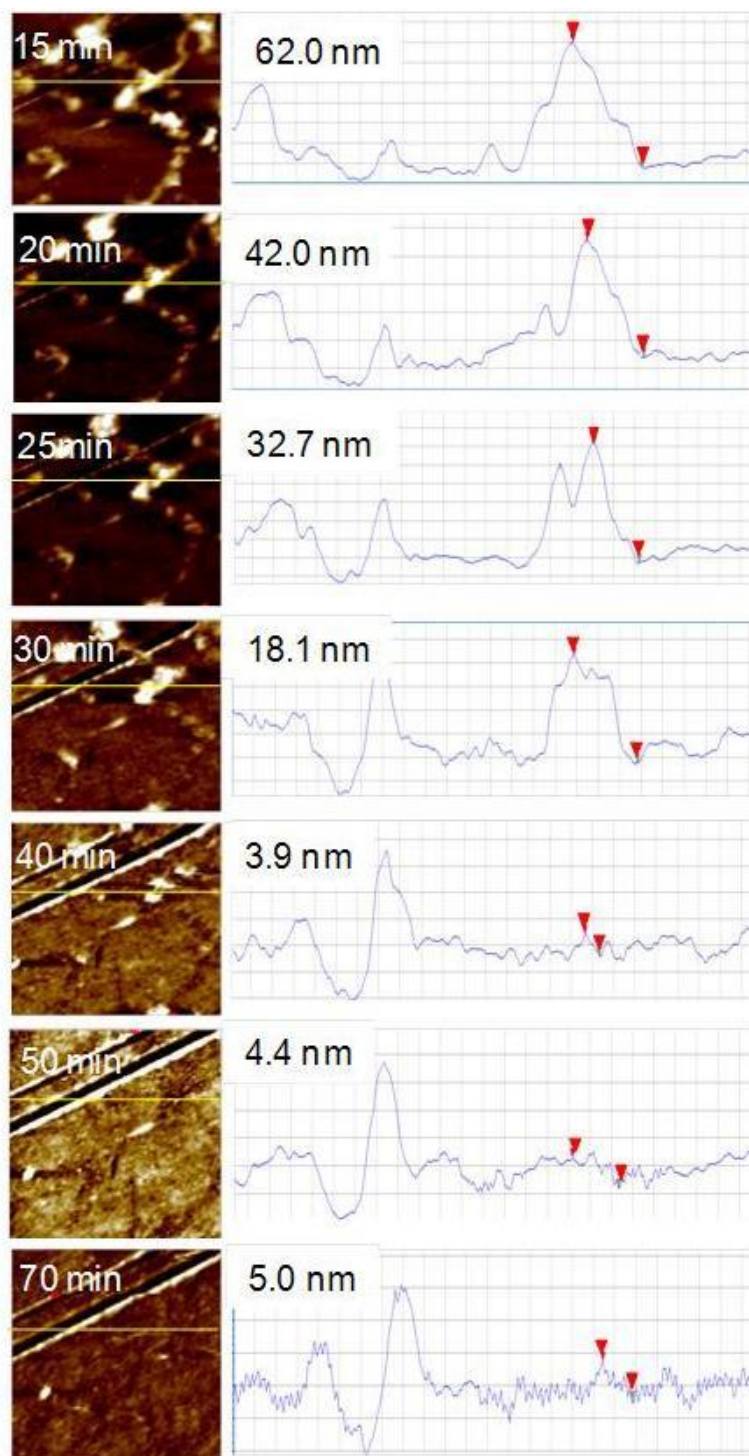


Figure 5-5 AFM topography images (left, $5 \times 5 \mu\text{m}^2$) and topography vs. distance (right) of cellulose-coated quartz crystal resonator incubated with cellulase from *Trichoderma reesei* (0.5% v/v, pH 5) at 30 °C. The vertical line indicated where the cross-sectional thickness measurement was made. The change in cellulose height (in nm) indicated by the red arrows was shown on the left upper corner of thickness profile image.

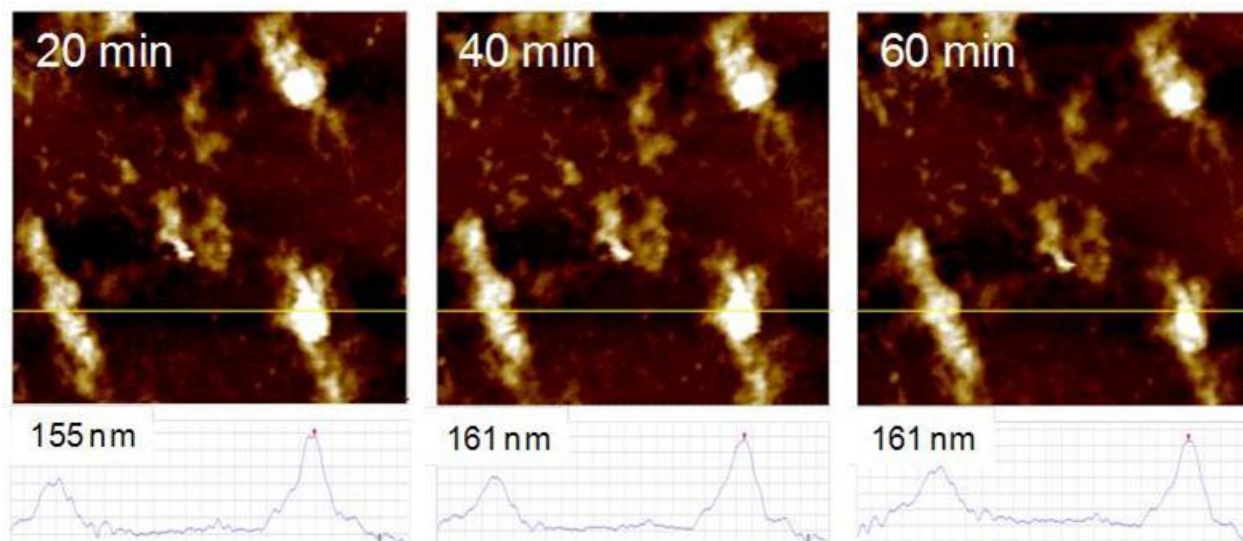


Figure 5-6 AFM Topography images (*top*, $5 \times 5 \mu\text{m}^2$) and the corresponding thickness (*bottom*) of cellulose-coated quartz crystal resonator incubated in liquid acetate buffer (0.1 M, pH 5) at 30 °C. The vertical line indicated where the cross-sectional thickness measurement was made. The change in cellulose height (in nm) indicated by the red arrows was shown on the left upper corner of the thickness profile image.

Recent studies demonstrated that the movement of purified cellulase on crystalline cellulose can be captured by high-speed liquid AFM (Igarashi et al. 2009; Igarashi et al. 2011; Bubner et al. 2012). The estimated velocity of cellobiohydrolases I from *T. reesei* was approximately 7.1 nm s^{-1} with nano-scale resolution captured up to 300 ms per frame. The speed of the enzyme movement in nanometer range cannot be captured by the micron-resolution AFM used in this study. However, the topography images of the deconstructed cellulose provide data on the rate at which cellulases from *T. reesei* or *C. thermocellum* degraded the cellulose thin film. The cellulases in solution are approximately 50 nm in size, meaning that they are not expected to be captured as features at the scale of the AFM images presented here ($5 \mu\text{m} \times 5 \mu\text{m}$). In contrast, *C. thermocellum* is typically rod shaped with 4-5 μm in length and 0.5 μm in thickness (Leschine and Canale-Parola 1983). The hydrolytic activity by *C. thermocellum* cellulosome is suggested to occur at a distance away from the cell surface, but connected by

several anchoring proteins. We did not image *C. thermocellum* or cellulosomes on the cellulose thin film surface, although we observed many disrupted images from AFM in the liquid cell that may be the result of the cantilever coming in contact with these larger size objects.

Conclusion

Surface analysis techniques such as QCM and AFM can provide quantitative measures of cellulase binding and hydrolytic activity on the surface of cellulose thin films. This investigation applies these surface techniques to cell-complexed cellulases, such as the cellulosome of *C. thermocellum*, for the first time. The temperature dependence of adsorption and cellulose hydrolysis by *C. thermocellum* is of significance to the design of efficient cellulose to biosolvent conversion processes. In this investigation, cellulose thin film hydrolysis by non-growing *C. thermocellum* is investigated at 30 °C, 40 °C, and 50 °C by QCM with *in-situ* monitoring of the changes in frequency due to changes in the mass of the cellulose thin film. The results are compared to cellulose hydrolysis by the non-cell complexed cellulases of fungal *T. reesei*, whose activity has been quantified previously using QCM and AFM. No hydrolysis activity is detected when the cellulose thin film was incubated with *C. thermocellum* at 30 °C. However, when the incubation temperature increased to 40 °C or 50 °C, cellulose hydrolysis was evident. A faster hydrolysis rate is observed at higher temperature, as indicated from the curve slope of the frequency profile. Complementary information on the hydrolytic activities of both *T. reesei* and *C. thermocellum* is obtained from AFM topography images using a liquid AFM cell, where the height of cellulose during deconstruction can be quantified by processing the image. The interactions of the whole cells with the cellulose thin films potentially result in less robust and accurate measurements of adsorbed mass on the QCM sensor and change in film height, as

measured by AFM in a liquid cell. However, the ability to simultaneously monitor thin film mass change and directly measure changes in surface thickness and topography during cellulose hydrolysis by commercially relevant cellulolytic microorganisms provides unique possibilities to quantify, screen, and design microorganisms and saccharification processes to enhance cellulose conversion.

Chapter 6

Metabolic Control of *Clostridium thermocellum* via Inhibition of Hydrogenase Activity and the Glucose Transport Rate

Summary

Clostridium thermocellum has the ability to catabolize cellulosic biomass into ethanol, but acetic acid, lactic acid, carbon dioxide, and hydrogen gas (H₂) are also produced. The effect of hydrogenase inhibitors (H₂, carbon monoxide (CO), and methyl viologen) on product selectivity was investigated. The anticipated effect of these hydrogenase inhibitors was to decrease acetate production. However, shifts to ethanol and lactate production are also observed as a function of cultivation conditions. When the sparge gas of cellobiose-limited chemostat cultures was switched from N₂ to H₂, acetate declined, and ethanol production increased 350%. In resting cell suspensions, lactate increased when H₂ or CO was the inhibitor or when the cells were held at elevated hyperbaric pressure (6.8 atm). In contrast, methyl viologen-treated resting cells produced twice as much ethanol as the other treatments. The relationship of chemostat physiology to methyl viologen inhibition was revealed by glucose transport experiments, in which methyl viologen decreased the rate of glucose transport by 90%. *C. thermocellum* produces NAD⁺ from NADH by H₂, lactate, and ethanol production. When the hydrogenases were inhibited, the latter two products increased. However, excess substrate availability causes fructose 1,6-diphosphate, the glycolytic intermediate that triggers lactate production, to increase. Compensatory ethanol production was observed when the chemostat fluid dilution rate or methyl viologen decreased substrate transport. This research highlights the complex effects of high concentrations of dissolved gases in fermentation, which are increasingly envisioned in microbial applications of H₂ production for the conversion of synthetic gases to chemicals.

Introduction

Ethanol is widely used as a renewable fuel, and it is typically produced by fermentation of cereal grains rich in soluble sugars. Unfortunately, demand from ethanol plants has increased the price of these important food crops (Pimentel and Patzek 2005; Mitchell 2008). Cellulose is the most abundant polymer in the world, and it is less expensive than many fermentation substrates (Zeikus 1980). However, the yeasts (*e.g. Saccharomyces cerevisiae*) typically used to ferment soluble sugars do not possess enzymes that allow them to catabolize cellulose. Some bacteria produce enzymes, which permit them to utilize cellulose and other recalcitrant fibers without prior saccharification. Previous researchers proposed direct fermentation of lignocellulosic biomass to ethanol with these latter organisms, and this technology has been termed consolidated bioprocessing (Hogsett et al. 1992).

Clostridium thermocellum is an anaerobic, thermophilic bacterium that catabolizes cellulose into soluble sugars, and produces ethanol (Gaughran 1947). Unfortunately, the ethanol yield is considerably lower than that of yeast (Shin et al. 2002). Glycolysis proceeds by the Embden-Meyerhof-Parnas pathway in *C. thermocellum* (Fig 6-1). This common scheme of fermentation couples the substrate-level production of ATP to the oxidation of glucose (Gottschalk 1986). The redox intermediate is NAD^+/NADH , which is converted to the oxidized form by lactate dehydrogenase, acetaldehyde-ethanol dehydrogenase, or hydrogenases. Because NAD^+ -producing and NAD^+ -consuming reactions must be balanced, factors that affect this cycle can also affect product formation (Gottschalk 1986). For example, when ferredoxin-dependent hydrogenases are inhibited, NADH can be co-produced with lactate and ethanol, but less pyruvate is available for acetate production.

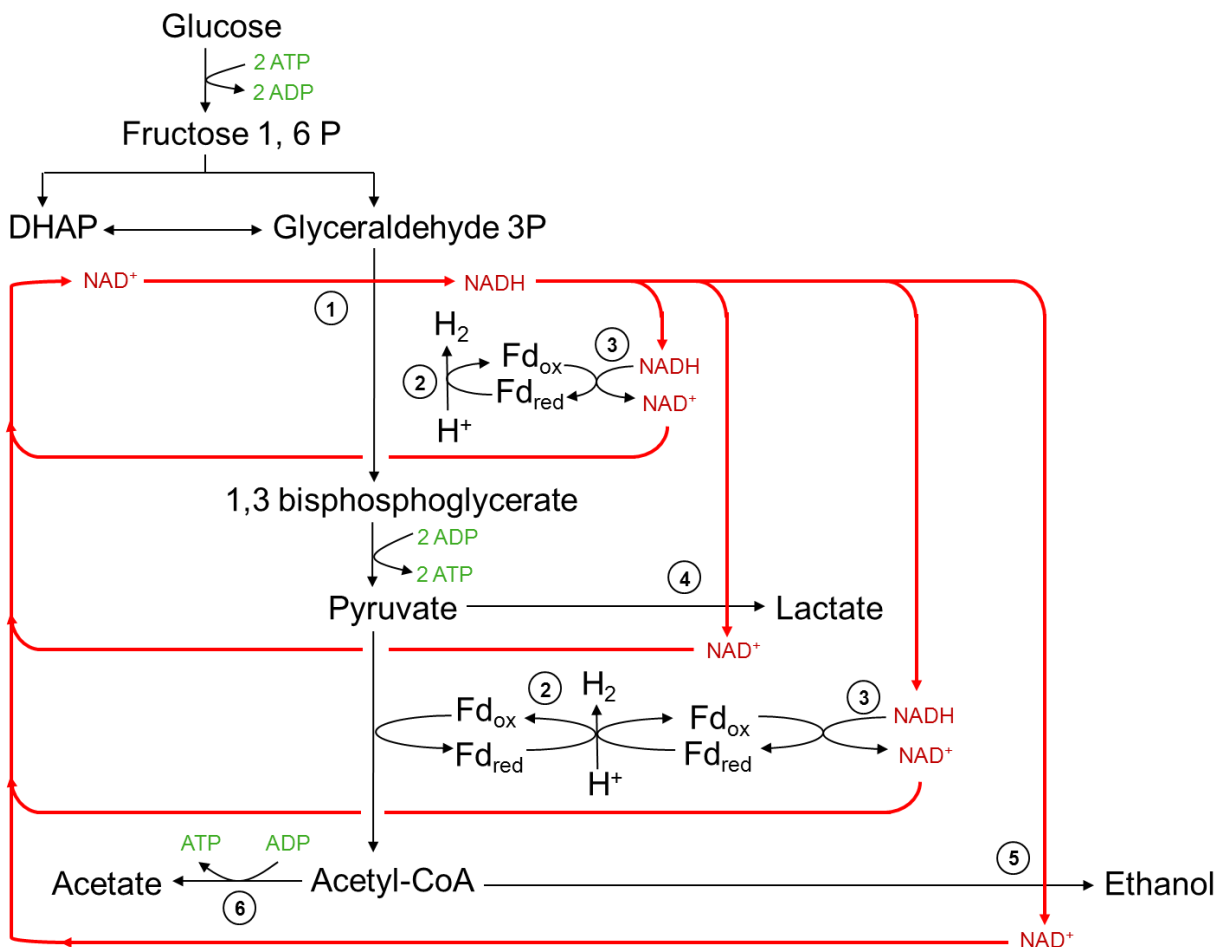


Figure 6-1 Simplified glycolytic scheme (Embden–Meyerhof–Parnas) of *C. thermocellum*. Adenosine phosphates are shown in green. Nicotinamide dinucleotides are shown in red. Numerals indicate enzymes: 1 glyceraldehyde 3-phosphate dehydrogenase, 2 ferredoxin-dependent hydrogenases, 3 NADH-ferredoxin oxidoreductase, 4 lactate dehydrogenase, 5 acetaldehyde–ethanol dehydrogenase, 6 acetate kinase.

The concentration of hydrogen gas in solution has been demonstrated to change the product yield and selectivity of *C. thermocellum*. When the H₂ concentration in the medium was decreased by either stirring (Lamed et al. 1988) or by the metabolism of a methanogen (Weimer and Zeikus 1977), acetate production increased. Conversely, when *C. thermocellum* was continuously cultured at elevated hydrostatic pressure, acetate production decreased (Bothun et al. 2004). Decreased acetate production was attributed to an increased concentration of H₂ in the fermentation broth, which caused more pyruvate to be catabolized for NAD⁺ recovery rather

than acetate production. However, the reason for the dramatic increase in ethanol production (>10 fold), and corresponding increase in the ethanol/acetate ratio (>30 fold) under certain cultivation conditions was unclear.

The purpose of the following experiments was to further delineate the influence of hydrogenase inhibition on the product selectivity of *C. thermocellum*, and to describe the dramatic shifts in product yield and selectivity when acetogenesis is inhibited.

Materials and Methods

Strain and media composition. *Clostridium thermocellum* ATCC 27405 was obtained from the culture collection of Herbert J. Strobel, University of Kentucky. The basal medium contained (per liter): 0.61 g Na₂HPO₄, 19.6 g KH₂PO₄, 0.5 g (NH₄)₂SO₄, 0.5 g NH₄Cl, 0.09 g MgCl₂ 6-H₂O, 0.03 g CaCl₂, 0.001 g resazurin, 0.5 g cysteine, 2 g yeast extract, 10 ml vitamin mixture (Cotta and Russell 1982) and 5 ml mineral mixture (Cotta and Russell 1982). The pH was adjusted to 7.1 with NaOH, and pH was not affected by sterilization or sparge gas (N₂ or H₂). The medium was autoclaved (121° C, 20 min) to drive off dissolved gasses, and cooled under O₂-free N₂. Media for batch cultures were anaerobically dispensed into Hungate tubes, sealed with butyl rubber stoppers, and autoclaved. Media for continuous cultures were maintained in Erlenmeyer flasks (4 l), and continuously sparged with O₂-free N₂. Cellobiose was prepared separately and added aseptically to a final concentration of 4 mg ml⁻¹.

Batch culture conditions. The culture was routinely transferred in the basal medium with cellobiose (4 mg ml⁻¹, unless otherwise indicated). All experiments were conducted in Hungate tubes at 65° C. Growth was monitored by optical density (abs 600 nm) using a Biowave II

spectrophotometer (Biochrom, Cambridge, UK). Inhibitors were added either as solutions via a tuberculin syringe or as gasses via a gas manifold. Methyl viologen was prepared as aqueous solutions and was added to freshly inoculated (10% v/v) cultures to $30 \mu\text{g ml}^{-1}$. Methyl viologen is stable under these conditions at temperatures up to $300 \text{ }^{\circ}\text{C}$ (Lin et al. 2004). In the case of gases, basal medium (10 ml in Hungate tubes) was sparged with carbon monoxide or hydrogen gas in a fume hood for 1 min prior to inoculation, and the tubes were stoppered with a headspace of the gas.

Continuous culture conditions. Continuous culture was conducted in a stainless steel culture vessel (Fig 6-2). The medium reservoir (4 l Erlenmeyer flask) was continuously sparged with N_2 , and it was connected to a syringe pump (ISCO 500D, 500 ml, max. pressure 25.8 MPa, max. flow rate 204 ml min^{-1}). The pump was connected to the culture vessel via 304 stainless steel tubing. This line was equipped with a unidirectional valve (Nupro SS-53F2) to prevent backflow, and an inline filter (Nupro SS-2F-7, pore size $0.5 \mu\text{m}$) to remove particles. The culture vessel (Parr mini-bioreactor 100 ml, rated to 623 K and 20.7 MPa) was equipped with a steel impeller (no. 822HC4, 300 rpm), and a pressure gauge (Ashcroft). A Teflon effluent line connected the culture vessel to the effluent flask (500 ml Erlenmeyer).

The syringe pump was filled with 70% ethanol and incubated (14.7 psi, 24 h; 1500 psi, 24 h) to sterilize. The ethanol was drained, and the pump was rinsed with sterile water. The pump was cooled ($2 \text{ }^{\circ}\text{C}$) and filled with CO_2 . When the pump and the CO_2 tank were equilibrated (800 psi, $\sim 30 \text{ min}$), the pump was permitted to warm to ambient temperature, which caused the pressure to increase ($\sim 1500 \text{ psi}$, 24 h). The gas was vented prior to the experiment. Basal medium was transferred to the syringe pump by positive displacement in the medium

reservoir. When the syringe pump was filled, the medium was delivered to the culture vessel. Nitrogen (N_2) was introduced via one of the culture vessel's ports to maintain anaerobic conditions. The culture vessel was inoculated (24h batch culture, 10% v/v), and permitted to incubate ($65^\circ C$). When optical density increased (24h), the syringe pump was engaged to initiate continuous culture. The flow rate (F) was set at 5.0 ml h^{-1} to maintain a dilution rate (D) of 0.05 h^{-1} . A 97% turnover was permitted between each sample. Samples (1 ml) were collected from one of the culture vessel ports for optical density and product analysis. These latter samples were immediately clarified by centrifugation ($14,800 \times g$, 3 min), and frozen ($-20^\circ C$).

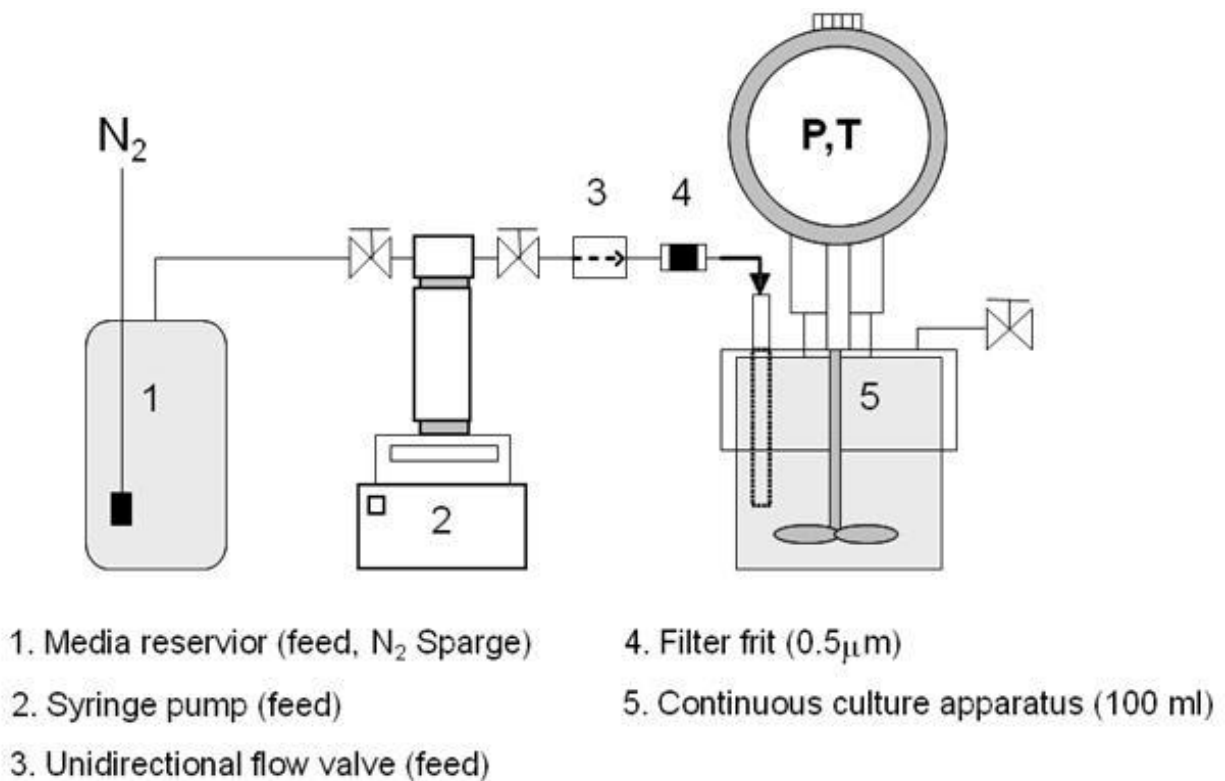


Figure 6-2 Culture vessel. *Shaded components* contain media. P pressure gauge, T temperature control. The vessel was operated as a chemostat or a batch-culture device, at either ambient or elevated hyperbaric pressure.

High Density Washed Cell Conditions. Stationary phase cells (24 h) were harvested by centrifugation ($10,000 \times g$, 10 min), washed in sodium phosphate buffer (50 mM, pH 7.5), and harvested again. The cells were resuspended in basal medium (~ 15 OD). The suspensions were pooled into serum bottles with a N_2 headspace, and transferred to the culture vessel by syringe. Cellobiose was added to obtain a concentration of 4 mg ml^{-1} . Inhibitors were added as indicated above. Washed cell experiments were performed at 65°C . Under ambient pressure conditions, gasses were introduced via one of the culture vessel's ports. A submersed tube was used to sparge the suspension when indicated. The ports were closed for elevated pressure experiments, and the syringe pump was engaged to achieve the pressure indicated. Samples were obtained with syringes, clarified by centrifugation ($14,800 \times g$, 3 min), and frozen for later analysis.

Glucose transport assays. *C. thermocellum* was transferred at least three times with glucose (4 mg ml^{-1}) as the sole substrate prior to glucose transport experiments. Stationary phase cells (24 h) were harvested by centrifugation ($10,000 \times g$, 10 min), and resuspended in basal medium (~ 4.9 OD). The cell suspensions (0.2 ml) were transferred anaerobically to N_2 -gassed culture tubes. Cellobiose (1 mg ml^{-1}) was added to energize the cells when indicated. De-energized and cellobiose-energized cell suspensions were incubated with methyl viologen (0, 3 or $30 \text{ } \mu\text{g ml}^{-1}$) for 1 h at 65°C . Glucose transport assays were performed as described by Strobel et al (1995). Briefly, the cell suspensions were stirred at 65°C under a N_2 headspace. [^{14}C]-glucose ($1 \text{ } \mu\text{Ci}$, $2 \text{ } \mu\text{l}$) was added to initiate the assay. Transport was terminated by the addition of LiCl (100 mM , 2 ml). Assays with de-energized cells were terminated at 0, 5, 30, and 60 s. Assays with energized cells were not linear beyond 5 s. The cells were collected on a filter ($0.45 \text{ } \mu\text{m}$ pore size, nitrocellulose) via a Buchner funnel. The filters were dried (85°C , 20 min) before mixing

with liquid scintillation cocktail (Research Products International Corp., Mount Prospect, IL). Radioactivity was determined by liquid scintillation (Packard Tri-Carb 1500 TR liquid scintillation analyzer, PerkinElmer, Waltham, MA). The transport rate was determined from five replications.

Product analysis (HPLC). Cellobiose, acetate, lactate, and ethanol were quantified by HPLC (Dionex). The anion exchange column (Aminex 87H; BioRad) was operated at 50° C, flow rate 0.4 ml min⁻¹. Eluting compounds were detected by refractive index (Shodex/Showa).

Bioenergetic calculations. The NAD⁺ from lactate and ethanol production (NAD⁺_{LE}) was calculated from the substrate and product concentrations (Gottschalk 1986, Lamed et al. 1988). Lactate and ethanol co-produced NAD⁺_{LE} = 2 (ethanol) + lactate – 4 (Δ cellobiose). ATP production was calculated from acetate and catabolized glucose (2 moles ATP per mole). ATP = acetate + 2 (glucose consumed). The product yield was calculated from the substrate and product concentrations (YP/S=ΔP/ΔS, mmol product formed mmol⁻¹ substrate consumed).

Results

When *C. thermocellum* steady state continuous cultures were sparged with N₂, 30 mM acetate, negligible lactate, and 4 mM ethanol were formed, and no residual cellobiose was detected (Fig 6-3a). When the sparge gas of the same culture was switched to H₂, culture pH and cell density remained unchanged, but acetate production decreased 35% and ethanol production increased by 350%. Lactate production remained low. The product yield was not affected by H₂, but the ethanol to acetate ratio increased from approximately 0.12 to 0.75 (Fig 6-3b).

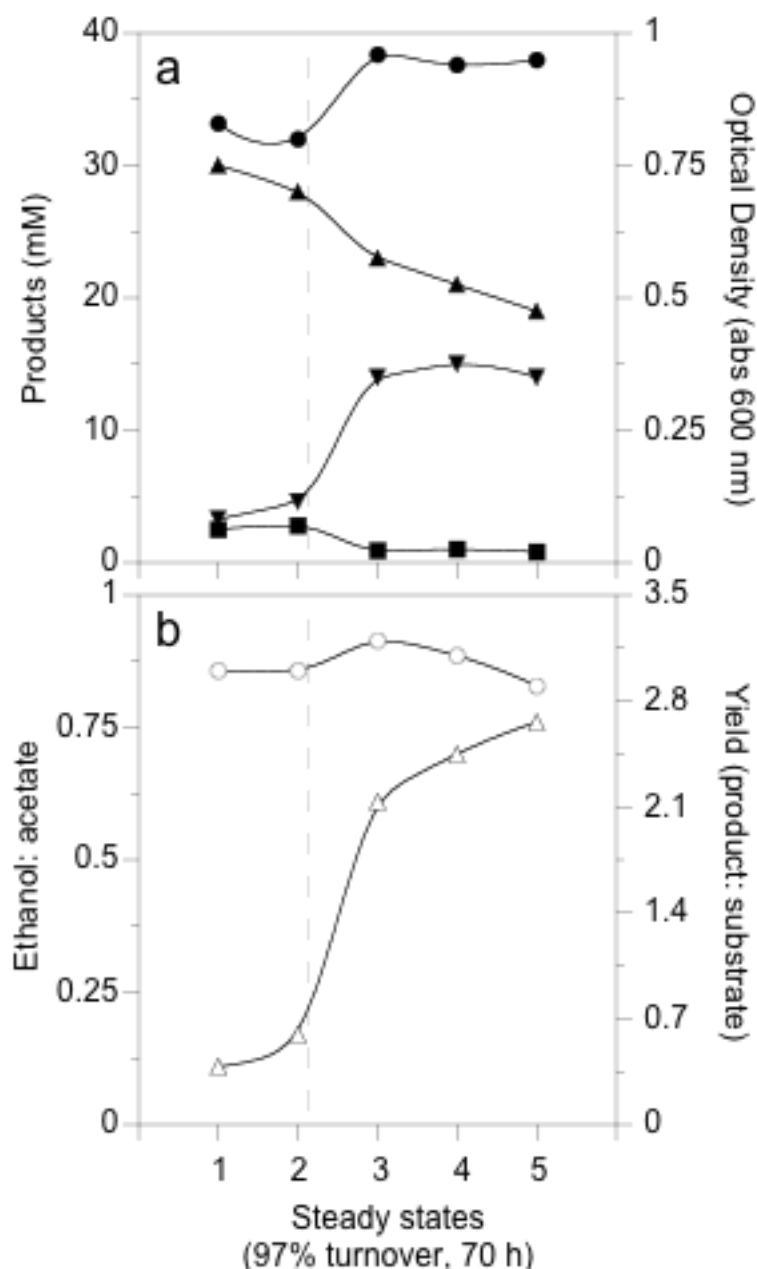


Figure 6-3 The effect of sparge gas on cellobiose-limited *C. thermocellum* continuous culture. Steady-state data are shown (97% turnover, 70 h). Cultivation was initiated under N₂, and the sparge gas was switched to H₂ (*dashed line*). Part a includes the optical density (*black circles*) and the concentrations of acetate (*black triangles*), ethanol (*black inverted triangles*), and lactate (*black squares*). Part b includes the ethanol-to-acetate ratio (*open triangles*) and yield (*open circles*). Representative data are shown.

High-density washed cell experiments were conducted to decouple hydrogen and pressure effects from exponential cell growth effects. These experiments were performed under

N₂ (1.0 or 6.8 atm) or H₂ (1.0 atm) (Table 1). The low-pressure cell suspensions under N₂ fermented cellobiose (10 mM). The final lactate, acetate and ethanol concentrations were approximately 19.4, 16.9, and 10.9 mM, respectively. Preliminary experiments indicated that changing the gas phase did not significantly alter broth pH (data not shown). When the headspace gas was switched to H₂, acetate production decreased from 16.9 to 14.6 mM. The addition of the hydrogenase inhibitor, methyl viologen (30 µg ml⁻¹), caused the acetate concentration to decrease to 7.2 mM. In this latter treatment, lactate production was half that of the N₂ treatment, but ethanol production nearly doubled. Consequently, the ethanol to acetate ratio under hydrogen and methyl viologen added was more than 400 % greater than that of the N₂ treatment. When the cell suspensions under N₂ were incubated at 6.8 atm, acetate production was reduced by approximately 40%, but ethanol did not increase.

Table 6-1 Products of high-density washed *C. thermocellum* cell suspensions with the addition of H₂, H₂+MV (methyl viologen, 30 µg ml⁻¹), or N₂ under 1 or 6.8 atm. The product concentrations were sampled at 48 h.

Treatments	Lactate (mM)	Acetate (mM)	Ethanol (mM)	C product (mM)	E:A ratio -
N ₂	19.4 (1.2)	16.9 (0.3)	10.9 (0.1)	113.8 (0.4)	0.6 (0.02)
H ₂	22.5 (0.1)	14.6 (0.1)	10.4 (0.1)	117.5 (0.8)	0.7 (0.003)
H ₂ + MV	8.8 (0.2)	7.2 (0.01)	19.1 (0.1)	79 (3.1)	2.7 (0.01)
6.8 atm N ₂	21.4 (2.3)	10.0 (2.5)	11.4 (0.8)	107 (9.8)	1.3 (0.4)

Glucose-grown, cellobiose-energized cell suspensions transported [¹⁴C]-glucose across the cell membrane at a rate of approximately 0.0075 nmol mg cell protein⁻¹ s⁻¹ (Fig 6-4). The addition of methyl viologen (30 or 300 µg ml⁻¹) 1 h prior to the assay decreased the transport rate to less than 0.001 nmol mg cell protein⁻¹ s⁻¹, which was similar to the transport rates of de-

energized cells (i.e., cellobiose was not added). Methyl viologen had no effect on transport by de-energized cells.

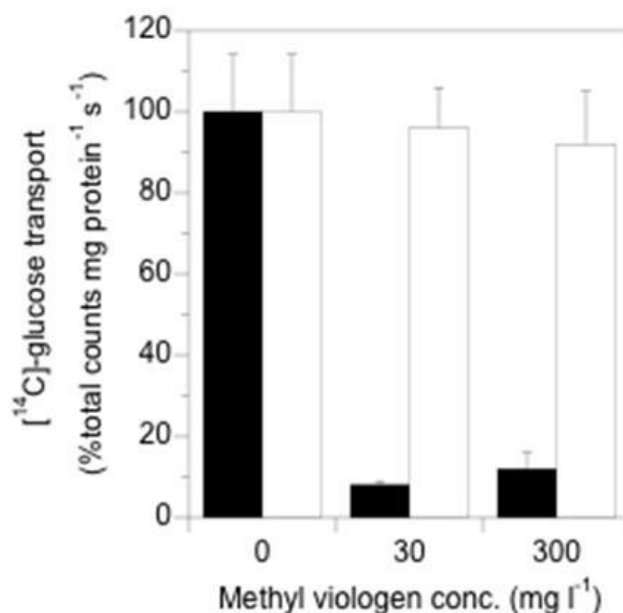


Figure 6-4 Glucose transport by *C. thermocellum* cell suspensions. Cellobiose-energized (*black bars*) or de-energized (*open bars*) cell suspensions were incubated with methyl viologen in the concentrations indicated. Means (n=5) of the 5-s assays are shown. Error bars represent standard error.

Batch cultures grown under a N₂ headspace with cellobiose (6 mM) as the substrate achieved maximum optical density within 10 h (Fig 6-5a). Methyl viologen did not alter growth rate when the concentration was 30 µg ml⁻¹, but there was a significant (P<0.05) decrease in final optical density. The results were similar when the headspace gas was switched to carbon monoxide (CO), another hydrogenase inhibitor. The N₂ culture produced acetate, lactate and ethanol (data not shown). Acetate production was inhibited in the methyl viologen and CO cultures. Ethanol production was approximately twice as great in the methyl viologen culture, which resulted in an ethanol to acetate ratio 2 times that of the CO culture and 4 times that of the

N₂ culture (Fig 6-5b). Methyl viologen concentrations as great as 200 μg ml⁻¹ did not completely inhibit growth, but total product yields were very low in this case (data not shown).

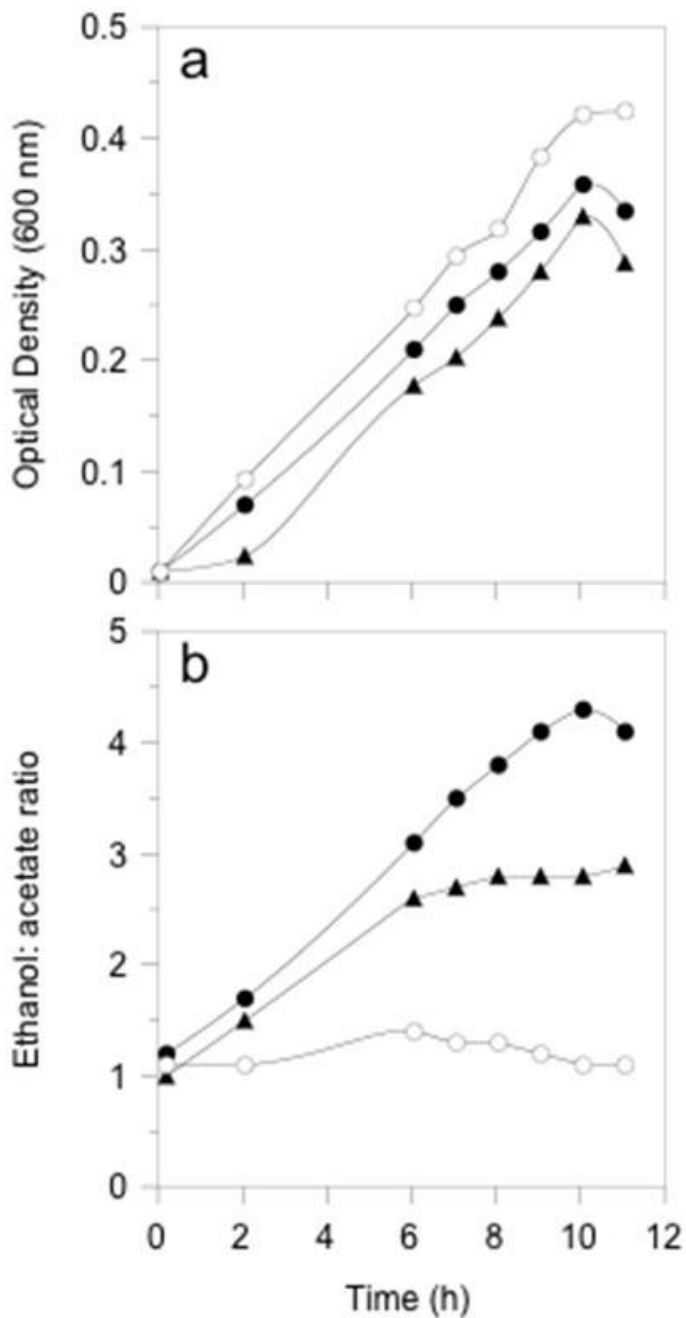


Figure 6-5 The growth (a) and ethanol: acetate ratios (b) of *C. thermocellum* under N₂ (open circles), N₂ with 30-μg ml⁻¹ methyl viologen (black circles), or under CO (triangles). Representative data are shown.

Discussion

Metabolism is defined as the ability of an organism to obtain and utilize energy (Gottschalk 1986). In the case of anaerobic bacteria, metabolism is often fermentative; i.e., all ATP is generated via substrate level phosphorylation. The energetic value of a metabolic scheme is directly related to the redox difference between the substrate and the product. Electron transfer is facilitated by reducing equivalents, such as NAD^+ . The oxidation of the substrate is coupled to the reduction of NAD^+ , which must be recovered for fermentation to continue.

C. thermocellum's primary enzymatic mechanisms of NAD^+ production are lactate dehydrogenase, acetaldehyde-ethanol dehydrogenase, and ferredoxin-dependent hydrogenases (Lamed and Zeikus 1980). H_2 production is favorable because NAD^+ is produced without the utilization of pyruvate for lactate or ethanol production. When reducing equivalents are recovered via the hydrogenases more carbon is available for ATP production and biosynthesis. However, the change in Gibb's free energy ($4.3 \text{ kcal mol}^{-1}$) of H_2 production is unfavorable when H_2 accumulates (Lamad et al. 1988; Bothun et al. 2004). When H_2 production is inhibited, lactate or ethanol must be produced to recover NAD^+ at the expense of acetate and ATP.

Exogenous H_2 , elevated hydrostatic pressure, methyl viologen, and carbon monoxide (CO) were used to manipulate metabolism in this study. In our study, dissolved H_2 in the fermentation broth was used to inhibit the hydrogenases. Elevated pressure can also be used to inhibit *C. thermocellum*'s hydrogenases. Bothun and colleagues (2004) increased the pressure on continuous cultures to increase the solubility of H_2 , and they saw a dramatic increase in the ethanol: acetate ratio. The effect of methyl viologen on hydrogen production was not determined in this study. However, other researchers determined that it inhibits the hydrogenases of clostridia through competitive inhibition by competing with reduced ferredoxin (FdH_2) to accept

the electrons from pyruvateferredoxin oxidoreductase (Reimann et al. 1996). CO deactivates hydrogenases by binding reversibly to the iron cluster of the active site (Rao and Mutharasan 1987).

The effect of elevated pressure on metabolic selectivity is not specific to continuous culture. Previous (Berberich et al. 2000) and current (Table 1) results demonstrated that elevated pressure decreased acetate production in high-density cell suspensions. Acetogenesis was inhibited even at near atmospheric pressure when the cell suspensions were incubated under H₂. The addition of methyl viologen caused an even greater decrease in acetate. To explore the possibility that the decrease in acetate could be due to a general effect on growth inhibition, experiments were conducted with the protein synthesis inhibitor, lincomycin. No effects on product ratios were observed (data not shown). These results were consistent with the hypothesis of metabolic selectivity through hydrogenase inhibition.

The notable effects of methyl viologen on product formation were a sharp decrease in lactate and a corresponding increase in ethanol (Table 1). This was not seen in the H₂ or pressure treatments presented here. The question then became, why did methyl viologen change these latter two product concentrations, but H₂ and pressure did not? It appeared that ethanol production was favored only when methyl viologen was present or in continuous culture under H₂. A principle difference between chemostats and batch culture experiments is substrate availability. A continuous culture is a chemostat only when the substrate is limiting. *C. thermocellum*'s lactate dehydrogenase is activated by the accumulation of fructose 1,6-diphosphate (Özkan et al. 2004). When excess substrate is available, ATP production from glycolysis is adequate, and NAD⁺ is readily recovered via lactate dehydrogenase. In the chemostat, lactate production is minimal because the fructose diphosphate-dependent lactate

dehydrogenase is not activated by excess substrate (Özkan et al. 2004; Strobel et al. 1995; Desvaux et al. 2005; Rydzak et al. 2009). Fructose diphosphate-dependent lactate production has been linked to non-growth energy dissipation in other bacteria (Russell et al. 1996).

Strobel et al (1995) determined that *C. thermocellum* employs separate transporters for glucose and cellobiose. Glucose transporter expression is induced in glucose-grown cells, but cellobiose transporters are constitutively expressed. These characteristics permitted the measurement of glucose transport in glucose-grown cells when the cells were energized by cellobiose. Methyl viologen decreased the rate of glucose transport, but because CO did not impact glucose transport, it did not appear that the effect was due to hydrogenase inhibition. Methyl viologen, also known as paraquat, is also toxic to animals and plants. Superoxide formation is the presumed mechanism of toxicity in animals (Bus et al. 1976). Recent research revealed the presence of a methyl viologen efflux pump in *Streptococcus mutans* (Biswas and Biswas 2011), and radical oxygen species (ROS) also occurs in bacteria (Gonzalez-Flecha and Demple 1997). ROS formation generally occurs during aerobic growth, which makes this mechanism of toxicity seem unlikely in this case (MacMichael 1988; Gonzalez-Flecha and Demple 1997).

Our hypothesis is that *C. thermocellum* recovered NAD^+ via H_2 production when possible. However, when the hydrogenases were inhibited, lactate was produced unless lactate dehydrogenase was not stimulated by fructose diphosphate accumulation. When substrate transport was limited by either methyl viologen or the fluid dilution rate of the chemostat, acetaldehyde-ethanol dehydrogenase was activated to compensate. Lamed and colleagues pointed out that electron transfer can be estimated from product concentrations (Lamed et al. 1988). This is because the production of NAD^+ is stoichiometrically correlated with lactate and

ethanol (one and two, respectively). Likewise, NAD^+ coproduction with lactate and ethanol can be calculated. A comparison of lactate and ethanol co-produced NAD^+ and ATP production in chemostat cultures is shown in Fig 6-6. This analysis shows that a greater proportion of substrate carbon was utilized for NAD^+ recovery when the ambient-pressure culture was sparged with H_2 (Fig 6-6). A similar trend is also apparent in previously reported high-pressure chemostat data, which is consistent with the hypothesis that hydrogenase inhibition occurs under these circumstances (Bothun et al. 2004).

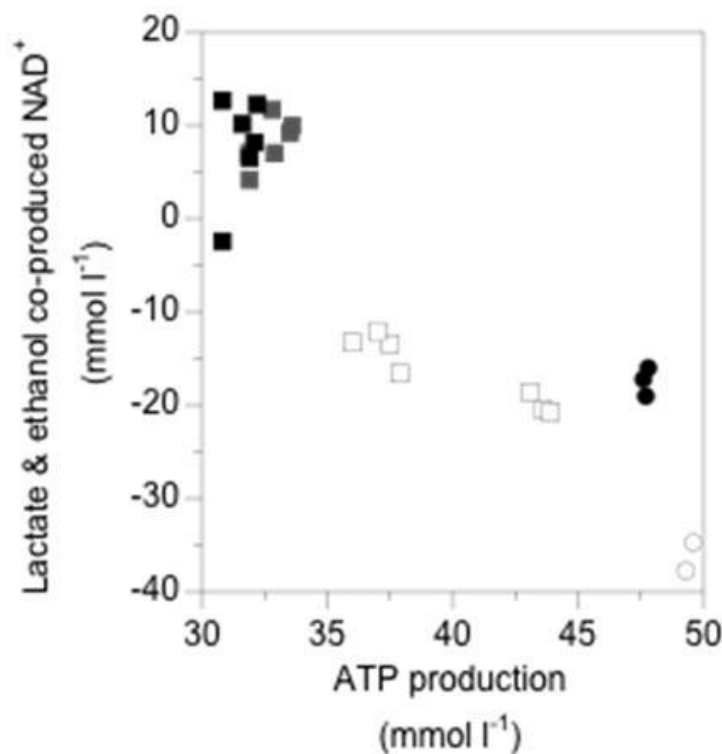


Figure 6-6 An analysis of metabolism *C. thermocellum* chemostat cultures (Fig 6-3). Data from N_2 -sparged (*open circles*) and H_2 -sparged (*black circles*) cultures are shown alongside data from Bothun et al. 2004 (*squares*). These latter cultures were in CO_2 -based media. The hydrostatic pressure is indicated: 0.1 MPa (*open squares*), 7.0 MPa (*gray squares*), and 17.3 MPa (*black squares*). These NAD^+ and ATP values were calculated from the concentrations of cellobiose, acetate, ethanol, and lactate.

Conclusion

Metabolic engineering takes advantage of a microorganism's ability to change product patterns in response to environmental stimuli (Bailey et al. 1996). In this case, the product ratios were improved by hydrogenase inhibition and limitations on substrate transport. This was achieved by end product inhibition (i.e. hydrogen gas), or by inhibitors. One advantage of metabolic engineering is that no permanent change in the genome is required. A gaseous inhibitor can be added or removed at any point during the fermentation. Thus, the fermentation can be directed without decreasing the physiological plasticity of the organism. This study demonstrates compensatory product formation, which is an example of this plasticity. Furthermore, controlling the product selectivity with dissolved gases could be a convenient way to manipulate many fermentative organisms. Methyl viologen may not be ideal because its broad toxicity could pose environmental and safety concerns. However, limiting the rate of substrate transport is feasible in chemostats, which could be a useful metabolic engineering strategy.

The interest in fermentation in the presence of high concentrations of dissolved gases, particularly H₂, is not limited to designing for conditions of high ethanol yield by *C. thermocellum*. Other clostridia have been cultivated in high-H₂ environments to achieve higher product yields. For example, *Clostridium saccharolyticum* increased ethanol production by more than 10% through the addition of exogenous H₂ (Murray and Khan, 1983). *Clostridium ljungdahlii* and *Clostridium carboxidivorans* were investigated to utilize synthetic gas (mixture of H₂ and CO) into ethanol (Datar et al, 2004; Henstra et al, 2007). High partial pressures of substrate gases are envisioned in future technologies and applications such as microbial fuel cells, and microbial reduction of CO₂ for organic fuels production.

Chapter 7

Conclusion and Recommendations for Future Work

With proper processing strategy to increase production yield and efficiency, lignocellulose-derived ethanol can potentially replace heavily polluted and non-sustainable petroleum, and provide a sustainable energy supply. Consolidated bioprocessing offers a potentially economically feasible process alternative to directly convert lignocellulosic biomass to fermentation products such as ethanol. The conversion process, however, heavily relies on the ability of biological catalysts and microorganisms to effectively hydrolyze cellulose to soluble sugars and maximize ethanol yield. The purpose of this work is to develop approaches to enhance the efficiency of cellulose saccharification by cellulase and cellulosic ethanol production. The technical barriers that limit the efficiency of enzymatic hydrolysis and the production of ethanol from biocatalysts are 1) low cellulase activity in the saccharification process and 2) low ethanol yield due to the production of other metabolic products. Novel surface analysis techniques were used to quantify and model the saccharification process on cellulose thin films. The selectivity of the fermentation to the desired products was probed and interpreted using novel environmental perturbations.

Advanced surface techniques were developed to characterize and quantify cellulose thin film and hydrolysis by cellulase at the interfacial level (Chapters 3, 4 and 5). This work first addressed the effect of a potential inhibitor (cellobiose) from hydrolysis products that inhibit cellulase activity (Chapter 3). The cellulose thin film was successfully synthesized from thermochemically dissolved cellulose and was coated on a quartz crystal resonator. Detailed surface reactions involving enzyme adsorption, cellulose hydrolysis, and product inhibition were captured in real-time by the piezoelectric quartz crystal microbalance (QCM). The cellulose

surface coverage and topography change before and after the hydrolysis experiment was observed by atomic force microscopy (AFM). The formation of multi-enzyme, substrate, and inhibitor complexes were modeled from the kinetics of a mechanistic, reaction pathway. Kinetic parameters such as adsorption/desorption rate constant, rate constants, and equilibrium constants were determined and compared with values from literature for bulk cellulose hydrolysis. The concentration dependence of inhibition of cellulase by cellobiose was captured by the QCM frequency profile and translated into a predictive model, an approach which can be used to screen and design more efficient saccharification process.

The mechanistic model of cellulase reaction pathways on cellulose thin films was further developed to describe the effect of enzyme concentration on cellulose hydrolysis, including the phenomena of reduced hydrolytic activity due to jamming or overcrowding effects (Chapter 4). The dynamic events of enzyme adsorption and cellulose hydrolysis were examined as a function of cellulase concentrations. While bulk models of cellulose degradation have employed fractal and jammed kinetics to describe the effect of enzyme concentration on hydrolysis rate, concentration-dependent enzyme deactivation on the cellulose surface best described the frequency response of the QCM during adsorption and hydrolysis of cellulose thin films. The developed mechanistic model presents the capability to predict hydrolysis performance at different enzyme concentrations.

The surface techniques were further applied to examine the temperature effect on cellulose thin film hydrolysis using liquid *Clostridium thermocellum* as an enzyme system (Chapter 5). The use of whole cell bacterial suspensions to observe the hydrolytic activity on cellulose thin film was demonstrated for the first time using QCM and AFM. The results showed no hydrolytic activity from *C. thermocellum* at 30 °C, but an increased hydrolysis rate

was evident at 40 °C and 50 °C. The mass reduction of cellulose during hydrolysis was quantified by QCM, and this result is complemented by the direct visualization of enzymatic hydrolysis on the cellulose surface using AFM. The real-time topography images and surface thickness changes were successfully captured in liquid, which suggests the opportunity to examine hydrolysis and immobilization on other lignocellulosic substrates.

Commercially viable ethanol fermentation from saccharified cellulose using cellulolytic microorganisms requires an improved ethanol yield. The influence of environmental perturbations on microbial product selectivity was examined through the metabolic study of *Clostridium thermocellum* (a model thermophilic bacterium). The effect of dissolved H₂ on ethanol production was investigated through the perturbation of exogenous hydrogenase inhibitors (Chapter 6). The addition of both H₂ and a hydrogenase inhibitor (methyl viologen) caused approximately 60% decrease in acetate production in batch fermentations. Likewise, *C. thermocellum* grown in the presence of the carbon monoxide (CO) produced less than 10% acetate. In addition, the introduction of exogenous hydrogen to a continuous fermentation decreased acetate production approximately 35 % and increased ethanol production more than 350 %. The product selectivity toward ethanol yield can be altered through the inhibition of hydrogenase coupled with substrate limited condition. The conversion of NADH to NAD⁺ which is coupled to the production of H₂, lactic acid, or ethanol can be metabolically directed toward ethanol production through the inhibition of hydrogenase and deactivation of lactate dehydrogenase. This was a result of compensatory product formation, which is a demonstration of the microorganism's ability to change product pattern in response to environmental stimuli.

Future Work

The developed surface techniques including synthesis of substrate thin films, mass change measurement by QCM and surface characterization can be further extended to more representative cellulosic substrate. The regenerated cellulose obtained from N-methylmorpholine-N-oxide (NMMO) dissolution is generally amorphous (cellulose type II), but highly crystalline films can be obtained from nanofibrillar cellulose, which displays similar morphology and crystallinity as the native type I cellulose (Edgar and Gray 2003; Lefebvre and Gray 2005; Ahola et al. 2008). The difference in cellulose properties (i.e. crystallinity, morphology, composition, surface area, and crystal plane orientation) can greatly influence cellulase adsorption and enzymatic hydrolysis. Additional characterization techniques such as X-ray diffraction would be required to determine the crystallinity index of the cellulose substrate. In addition, thin film thickness measurement can be developed in QCM to allow simultaneous monitoring of surface change. The calculation of the film thickness is a function of viscoelastic properties, which may not obey the Sauerbrey equation (Rodahl et al. 1995). Therefore, multiple overtones frequency measurements are required to model particular film properties. The thickness analysis in AFM can be used to support the thickness measurement by QCM. Direct visualization of cellulose hydrolysis in liquid AFM can be used to evaluate the surface change of lignocellulosic substrate composed of cellulose, lignin and hemicelluloses which may ideal for studying non-productive binding and inhibition of catalytic activity.

The developed reaction pathway model can be used to describe other physical parameters, such as temperature or pH, to accommodate the condition of fermentation environment. It was well known that cellulase activity is greatly influenced by the incubation temperature and pH (Ng et al. 1977; Johnson et al. 1982; Golovchenko et al. 1992). Cellulase from *C. thermocellum*

has maximum catalytic activity at 70 °C and pH 6.5 (Johnson et al. 1982). However, the actual operating temperature and pH may vary depending whether the fermentation system consists of pure or mixed microbial cultures. Recent developments in butanol production using the co-culture of *Clostridium acetobutylicum* and *C. thermocellum* is an example where the fermentation temperature is lowered to 39 °C to accommodate the growth of co-fermenting cultures (Nakayama et al. 2011). The culture broth pH can also decrease over the fermentation, as Clostridia are known to produce other acids such as lactate or acetate in addition to solvents. The pH of the mixed-acid fermentation reduces the productivity of cellulases and therefore decreases the hydrolysis rate. A mechanistic model combining the effect of these environmental parameters would allow the enzyme productivity to be predicted and therefore, help better control and design ethanol production process.

Significant increases in ethanol to acetate ratio were successfully obtained using exogenous hydrogen in single-phase continuous chemostat operation. Dissolved gas at elevated pressure can potentially achieve the same purpose. The formation of H₂ in continuous fermentation based on metabolic flux analysis calculation was previously estimated 15.6-38.3 mM at atmospheric pressure (Bothun et al. 2004). However, the observed hydrogen concentration in the culture was only 0.7 mM at atmospheric pressure, indicating that hydrogen formed in continuous culture evolved into the headspace (Bothun et al. 2004). Pressurizing the contents of the fermentation vessel will force more product gas into the fermentation broth resulting in higher aqueous solubility of H₂ (50.9 mM and 130.4 mM at 7.0 MPa and 17.3 MPa, respectively) at 333K (Harvey 1996).

A continuous high-pressure biphasic system (fermentation broth and controlled gas headspace) was previously developed by Bothun et al (2004). This high pressure chemostat

system was used to investigate the toxicity effect of nitrogen (N₂), ethane and propane on *C. thermocellum* at elevated pressures. This experimental set up with the change of hydrogen headspace can be used to investigate the ability of *C. thermocellum* to alter its metabolic products and selectivity. An additional syringe pump located before the reactor can be used to mix and deliver the desired partial pressure of the gas, and control the pressure of gas supplied to the reactor. In addition, a second syringe pump, as well as a back-pressure regulator, will be required to maintain a constant pressure of gas environment for two-phase system. A third syringe pump will receive the effluent from the bioreactor. Chemostat samples can be collected from cultures grown at different partial-pressure gases under controlled gas environments. Samples can be collected by rapidly depressurizing the sample loop and flushing with sterile air. Dissolved H₂ is believed to act upon the regulation of reduced and oxidized electron carriers in the metabolic pathway of thermophilic bacteria (Jones and Greenfield 1982; Lamed et al. 1988). Membrane fluidity, permeability as well as the cellular transport may be altered by the presence of dissolved gas at elevated pressures (Chin et al. 1976; Jones and Greenfield 1982) and should be taken into consideration when interpreting the results.

The suggested gas treatments are: atmospheric pressure in the presence of nitrogen headspace gas (0.1 MPa), atmospheric pressure in the presence of hydrogen headspace gas (0.1 MPa), and pressurized system with hydrogen below 1.0 MPa. Our previous chemostat results showed that the optical density of the cells dropped from 1.7 to 1.3 when nitrogen was replaced by hydrogen at atmospheric pressure (0.1 MPa). The growth of the organism may be inhibited by the presence of hydrogen (0.7 mM at 333K and atmospheric pressure). Based on this result, we anticipated that the organism may be unlikely to grow at concentration of dissolved hydrogen greater than 7 mM (10 folds of dissolved hydrogen concentration at atmospheric pressure),

which corresponds to hydrostatic pressure of 1.0 MPa. Therefore, hydrostatic pressures below 1.0 MPa are best range to elicit the effect of partial pressure of hydrogen on growth, substrate utilization and product formation and selectivity. These experiments will provide measurable differences in product selectivity. The total pressure (corresponding to the operating pressures of the hydrostatic chemostat) can be investigated at the intermediate constant p_{H_2} , which will provide insight into the pure pressure effect of the perturbation.

Environmental perturbation in chemostat has been shown to alter an organism's phenotype. This technique presents a potential tool for microorganisms to naturally adapt to their fermentation environment to address the low tolerance of a desired product. The H_2 adaptation of *C. thermocellum* has been demonstrated in a controlled-gas environment in a chemostat (See Appendix A). The results of natural adaptation of *C. thermocellum* were interpreted from end product concentrations. A significant increase in ethanol yield was observed as *C. thermocellum* was repeatedly exposed to H_2 after several steady state conditions. Natural adaptation of microorganisms to high concentrations of dissolved gas, particularly H_2 , is highly envisioned in future technologies such as microbial fuel cells and syngas conversion for biofuel production. Important findings of this research suggested greater utility of chemostat to manipulate/probe metabolic phenotypes for enhanced biofuel production.

Appendix A

Hydrogen-adapted *Clostridium thermocellum*

The effect of hydrogen (H₂) on ethanol production in substrate-limited chemostat has been demonstrated in this dissertation (Chapter 6). Ethanol production increased as a result of hydrogenase inhibition and low substrate transport rate. The observed effect of H₂ on ethanol production can be achieved by performing the fermentation in a chemostat, where the fluid dilution rate controls the introduction of substrate to the culture and also the growth rate of fermentation). Product selectivity of *Clostridium thermocellum* has been shown to depend on the dilution rate (Lynd et al. 1989; Strobel 1995; Bothun et al. 2004; Stevenson and Weimer 2005; Magnusson et al. 2009). Fluid dilution rate of a continuous flow bioreactor is defined as:

$$D = \frac{F}{V} \quad (1)$$

where F is the flow of medium (ml h⁻¹), and V is the volume of culture in the bioreactor (ml).

The relationship between the fluid dilution rate and the growth rate is described by the mass balance equation of the continuous flow bio-reactor:

$$DX_o - DX + \mu X - k_d X = \frac{dX}{dt} \quad (2)$$

where X is the concentration of biomass, μ is the specific growth rate (h⁻¹), and k_d is the specific death rate (h⁻¹). When the growth reaches a constant rate under steady state condition ($\frac{dX}{dt} = 0$), and the death rate is negligible (during growth phase), the growth rate is equal to the fluid dilution rate. Therefore growth rate of *C. thermocellum* can be easily controlled by manipulating the dilution rate. This work aims to investigate the effect of H₂ at different fluid dilution rates on product formation by *C. themrocellum* for the purpose of achieving higher ethanol yield.

The chemostat continuous culture system consisted of a bioreactor (a 100 ml stainless steel Parr Pressure reactor) to which medium is fed using a high pressure syringe pump (ISCO 500D) and discharged in 500 ml effluent Erlenmeyer flask. The schematic diagram of general assembly is shown in Figure A-1. The medium obtained in a 5000 mL flask was continuously spurge with deoxygenated N₂ to maintain the required anaerobic condition for *C. thermocellum*. The medium reservoir was then connected to the ISCO 500D pump with a quick connect metal tubing to allow the transfer of medium from the flask to the pump. With a controlled flow rate, the syringe pump fed the medium to the stirred reactor at a constant flow rate through a unidirectional needle valve. Samples were collected at a sample port of the reactor using a Luer lock syringe. The spent medium and the culture broth were then collected from the reactor outlet in the effluent flask.

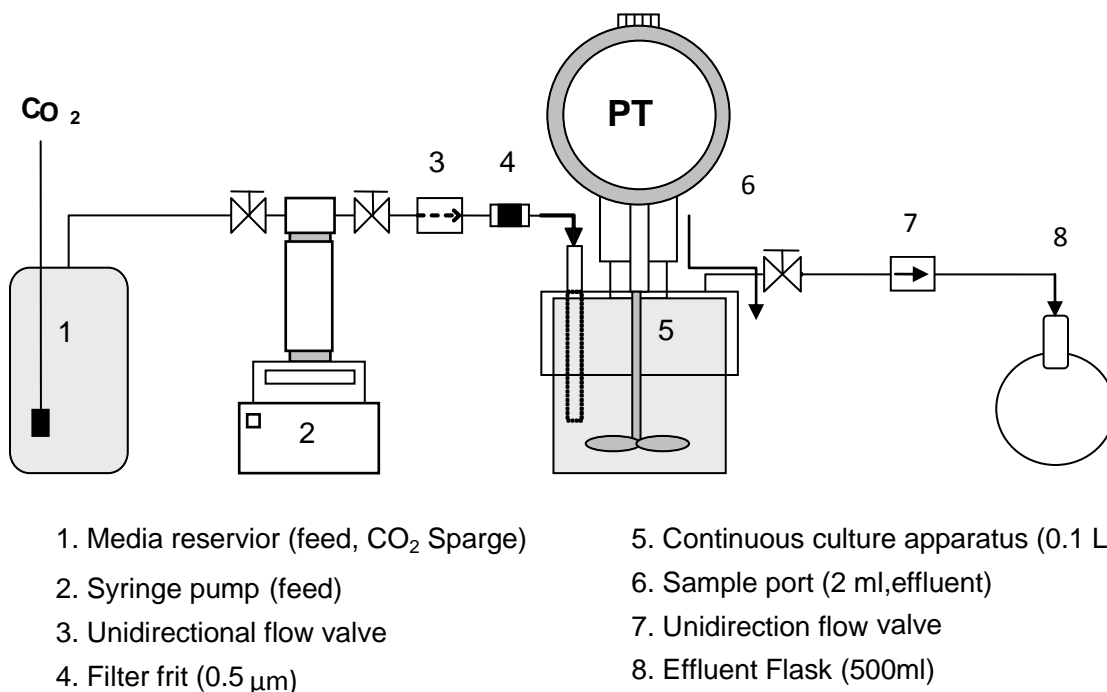


Figure A-1 Schematic diagram of continuous fermentation set up.

C. thermocellum was cultured with cellobiose (4 g l^{-1}) in a chemostat at dilution rates ranging from 0.05 to 0.32 h^{-1} . These dilution rates are selected based on the organism's maximum growth rate of up to 0.35 h^{-1} at atmospheric pressure (Fig A-2). 10 ml of the overnight cultures grown on 4 g l^{-1} cellobiose were inoculated in the sterilized chemostat system through the sample port of the reactor. After inoculation, the reactor was first operated at batch mode at 55°C at atmospheric pressure. After the cell growth reached stationary phase, the reactor was switched to continuous mode under nitrogen (N_2) at a dilution rate of 0.05 h^{-1} (at 5 ml h^{-1}). The time required to achieve 98% turnover in the reactor (approximately 391 ml) was approximately 78 hr . Samples were taken for product analysis at steady state before the sparged gas switched to H_2 . When 98% turnover was reached, samples were taken again under steady state H_2 -sparged condition. The sparged gas was then switched back to N_2 to confirm the reproducibility of the original N_2 gas effect at the same dilution rate. The procedures to switch gases from $\text{N}_2 \rightarrow \text{H}_2 \rightarrow \text{N}_2$ were repeated for different fluid dilution rates ($0.05, 0.08, 0.12, 0.16, 0.21, 0.26, 0.32 \text{ h}^{-1}$).

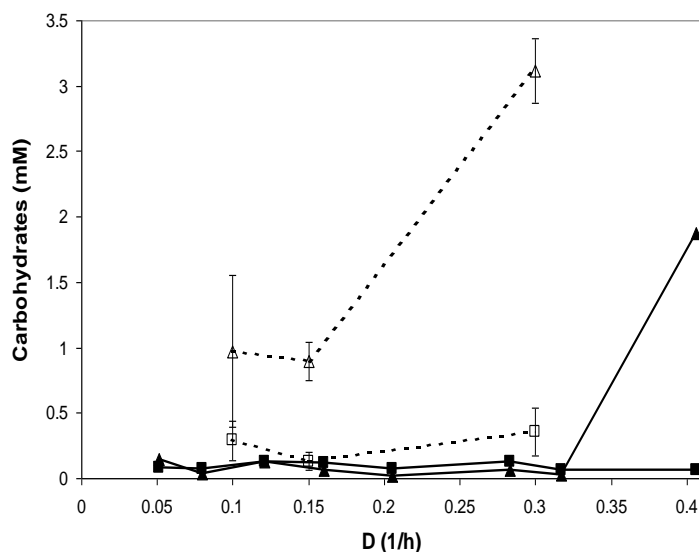


Figure A-2: Residual glucose (*square*) and cellobiose (*triangle*) during continuous fermentation of *C. thermocellum* JW20 at different fluid dilution rates under 0.1 MPa (*filled symbols*) or 7.0 MPa (*open symbols*). Figures adapted from Bothun et al 2004.

End-products (acetate, ethanol, and lactate) of *C. thermocellum* grown on 4 g/L cellobiose were analyzed in cell-free cultures supernatants as a function of seven dilution rates ranging from 0.05 to 0.32 h⁻¹. No residual cellobiose was detected at each dilution rate. Figure A-3 showed the production of ethanol, acetate and the respective ratios at different dilution rates.

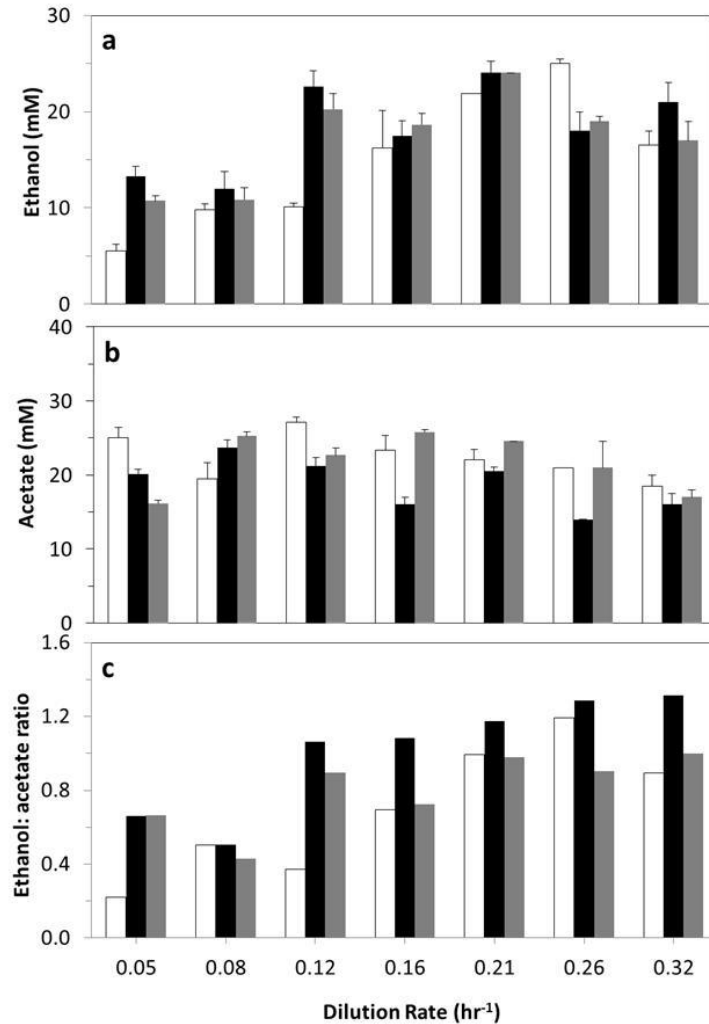


Figure A-3 Production of *a)* ethanol, *b)* acetate and *c)* ethanol to acetate ratio of *C. thermocellum* continuous culture grown on cellobiose (4 g l⁻¹) at different dilution rates. The cultures were first gassed under nitrogen (*white*). When steady state (98% turnover) was reached, the headspace was switched to hydrogen (*black*), and the products were sampled at steady states. The headspace gas was switched back to nitrogen (*gray*) using the same cultures. The treatment of exogenous gas was repeated for each dilution rates. The same culture was used throughout the experiment. Dilution rates are given within ± 0.01 h⁻¹ and the standard deviation of duplicate runs are shown as error bars.

When the cultures were gassed under N₂ at the lowest dilution rate (0.05 h⁻¹), approximately 6 mM of ethanol and 25 mM of acetate was produced. When the sparged gas switched to H₂, ethanol concentration increased to 13 mM, and acetate concentration decreased to 20 mM. This result was consistent with our previous investigations that observed an increase in ethanol and decrease in acetate with exogenous hydrogen in a chemostat system (Chapter 6 and Bothun et al 2004). However, when the sparged gas was switched back to N₂, ethanol and acetate production did not return to the level in which they were originally produced under the same cultivation condition (N₂, 0.05 h⁻¹). Instead, ethanol and acetate production only dropped slightly, but their corresponding ethanol to acetate ratio stayed the same. Similar observation persisted for most of the N₂ → H₂ → N₂ fluid dilution rate series when ethanol or acetate produced relatively similar concentrations after the H₂ treatment. These results suggested that *C. thermocellum* may be adapted to hydrogen. Although acetate production did not change significantly with fluid dilution rate, an increasing trend of ethanol production was observed with increasing dilution rate starting from 0.05 to 0.21 h⁻¹. As a result, ethanol to acetate ratio increased, and the maximum ethanol to acetate ratio was observed at the highest dilution rate (0.32 h⁻¹) under H₂.

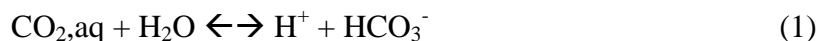
Micro-organisms have great adaptive ability to non-ideal cultivation environment. For example, *C. thermocellum* has been shown to adapt to increasing concentration of ethanol by a serial transfer (Williams et al. 2007; Timmons et al. 2009). The increased ethanol adaption was reported to be a result of increased membrane rigidity with longer fatty acid chains in ethanol-adapted cells (Timmons et al. 2009). Hydrogen adaptation has not been demonstrated before in *C. thermocellum*. A possible mechanism for persistent ethanol production may be a result of protein regulation in the adapted strain. For example, enzymatic uptake of hydrogen by hydrogenase may be down-regulated in the presence of H₂ which is the case for hydrogen-

adapted algae including *Scenedesmus obliquus* and *Ankistrodesmus braunii* (Kessler 1968; Stuart and Gaffron 1972). Chemostat environment is a demonstration of a simultaneous selective and adaptive process in which a perturbation promotes mutational and persistent change in fermentation cultures (Ferenci 2008). The characteristic of chemostat cultures to respond quickly in a nutrient-limited condition makes the chemostat an ideal tool for directing a desired phenotype in microbials over many generations.

Appendix B

Use of a new buffer in *Clostridium thermocellum* culture medium

The culture medium for *C. thermocellum* is slightly modified with the change of a new buffer (potassium phosphate) that is used in this dissertation to maintain better buffering capacity. The original culture medium for was prepared using the method adopted from culturing ammonia-limited ruminant bacteria *Bacteroides ruminicola* under anaerobic condition (Russell 1992). The medium pH was adjusted to 6.7, and the medium was kept anaerobic by deoxygenated CO₂. The pH was maintained by 80 g l⁻¹ sodium carbonate buffer. Under atmospheric pressure, the relative concentrations of aqueous carbon dioxide and carbonic acid are well buffered inside the cell (eq 1).



However, the presence of the exogenous CO₂ in the media limits the measurement of CO₂ produced by the organism. Therefore, we have conducted experiments to examine the effect of different sparge gas (H₂ or CO₂) with a goal of establishing a baseline for the effects of dissolved product gases on growth and pH of fermentation broth.

This experiment first begins with the investigation of exogenous gas effect (H₂ or CO₂) on the growth of *C. thermocellum* in sodium carbonate buffer medium. Two test tubes containing sodium carbonate buffer medium were prepared with 2 g l⁻¹ cellobiose. The tubes were inoculated with 1 ml of *C. thermocellum* and gassed with H₂ or CO₂. Growth curve of *C. thermocellum* under H₂ or CO₂ was shown in Figure B-1. Cells gassed under H₂ grew much faster than cells grew under CO₂. Also, longer lag phase was observed in CO₂-gassed cultures,

and the growth did not initiate after 24 h. The final optical density of H₂-gased cells was 60% greater than that in CO₂-gased cells. This indicates a faster and better cell growth with H₂.

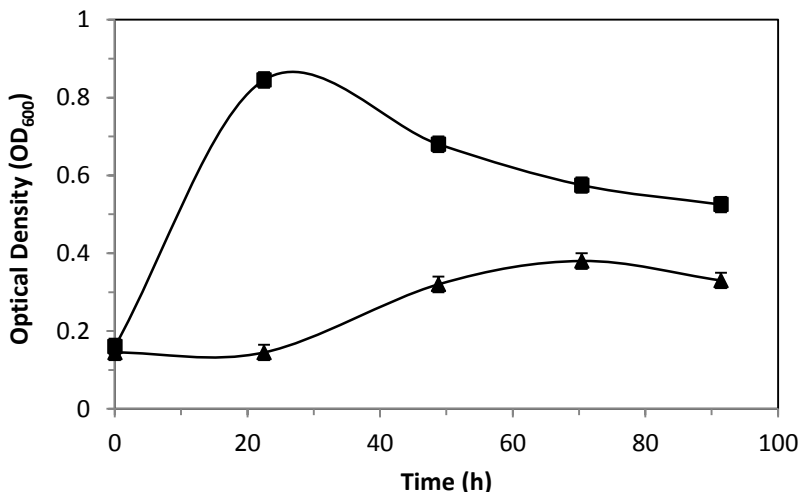
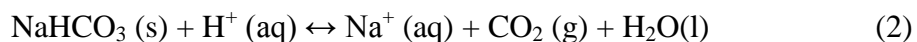


Figure B-1 Growth curve of *C. thermocellum* gassed with H₂ (square) or CO₂ (triangle).

In addition to the growth measurement, pH of each culture broth was also measured at the end of the batch experiment. Result showed that the test tube gassed with H₂ had overall higher final pH values (approximately 5.72 ± 0.08) than the test tubes gassed with CO₂ (approximately 5.53 ± 0.08). A further test was conducted to measure initial pH without inoculation. The result showed that by changing the headspace gas of the test tube to CO₂, the pH of the carbonate buffer medium immediately decreased from 6.7 to 6.55, whereas the pH of the test tube gassed with N₂ and H₂ increased from 6.7 to 6.86 and 6.96, respectively (Table B-1). This decrease in pH value coincided with a decline in cell growth rate (Fig B-1). This indicated that *C. thermocellum* had slower growth in an acidic pH medium. Russell (1992) suggested that anion accumulation as a result of organic acids production is responsible for the toxic effect of fermentation acids at low pH. Essentially, the transport of protonated species across the cell

membrane in response to the pH gradient ceased when the presence of large concentration of end-product acids exceeds the buffering capacity of the medium (Dharmagadda et al. 2010).

The observation of less microbial growth in CO₂ gassed test tube might be a result of lowered pH in the presence of CO₂ gas in sodium carbonate buffer medium. The addition of CO₂ pushes the dissociative reaction of sodium carbonate (eq 2) in the reverse direction, resulting in more acidic pH in the solution (McMurry and Fay, 1995).



Several studies have reported detrimental effect of non-optimum acidic pH on microbial growth (Weimer and Zeikus 1977; Islam et al. 2006). Further experiments were conducted to test the effect of pH on *C. thermocellum* growth on 4 g/L cellobiose in batch fermentation using the initial buffered medium, as described later in this study.

Correct buffering of the medium in the presence of dissolved gases is critical to the interpretation of our results. Unintended changes in pH of the medium corresponding to dissolved gas perturbations would introduce an additional treatment variable. Although dissolved CO₂ is not a perturbation variable, it is a product gas and will therefore be present in the aqueous fermentation broth. Thus, an alternative buffer medium was tested and validated for these dissolved gas experiments. Specifically, batch growth of *C. thermocellum* in the presence of CO₂ and H₂ was performed using potassium phosphate monobasic buffer medium. Monopotassium phosphate is a common buffer used in most basal medium with pKa (negative logarithm of the acid dissociation constant, Ka) equal to 6.82. The buffering capacity of a weak acid reaches its maximum when its pH value matches pKa. Since the targeting pH of the original

buffer is initially adjusted to 6.7, monopotassium phosphate is a better buffering agent than sodium carbonate which only has pKa value around 6.37 (Sigma-Aldrich).

With potassium phosphate (4 g l^{-1}) as the new buffer, we observe that the pH of the medium changes in the presence of different deoxygenated gases. Originally, the medium was prepared at pH of 6.7. After gassing the medium with CO_2 , the pH of the medium was reduced to 5.99, which was significantly lower than that of the test tubes gassing with N_2 or H_2 (Table B-1). However, pH of the media was well maintained when we increase the concentration of potassium phosphate to 100 mM (54.4 g l^{-1}).

Table B-1 Effect of sparged gas on pH in different buffer medium (Initial pH=6.7).

Headspace Gas	Buffer Medium Type		
	Sodium Carbonate (80 g/L)	Potassium Phosphate (3 g/L)	Potassium Phosphate (54.4 g/L)
	pH	pH	pH
Carbon dioxide	6.55 (0.09)	5.99 (0.05)	6.30 (0.06)
Nitrogen	6.86 (0.04)	6.56 (0.06)	6.69 (0.06)
Hydrogen	6.96 (0.05)	6.54 (0.04)	6.64 (0.04)

Appendix C

Effect of pH and dissolved gas on cell growth and product formation

The decrease in pH (< 6.0) due to the accumulation of acetate or other organic acids can limit the growth of *C. thermocellum* (Herrero et al. 1985). Elevated levels of pH and pervasive effects of dissolved gasses can have positive impacts on cell growth, product yield, and product selectivity, although there appears to be an optimum pH with respect to individual gases. We initiated experiment to investigate the effect of initial medium pH on the product formation of *C. thermocellum*.

The growth of *C. thermocellum* in potassium phosphate buffered medium was examined at different initial pH values. The final optical density (24 h after inoculation) is shown in Figure C-1. When *C. thermocellum* was grown under CO₂ headspace gas, the final optical density was highest at the initial pH of 7.3. When the pH of the medium decreased, the optical density reduced approximately 30% with every 0.2 decrease in pH until pH 6.5. A similar trend was observed in N₂-gassed cultures except that the final optical density was highest when the initial pH was 7.1. In general, when the initial pH of the medium was adjusted between 6.7 and 7.1, cells sparged with N₂ and H₂ had higher final optical density than cells sparged with CO₂. H₂-gassed cultures were not affected by the initial pH of the medium unless it was below 6.7. At initial pH of 6.5, the growth of all three gassed cultures had minimal growth. Lowe et al (1993) also reported the optimum growth pH for *C. thermocellum* is at 7.0.

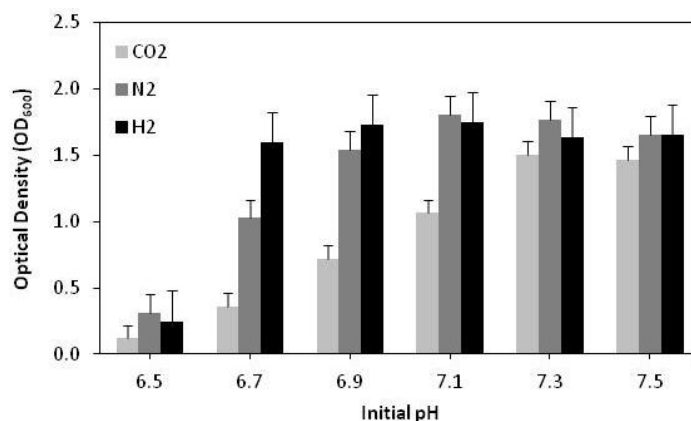


Figure C-1 The effect of initial pH on the batch growth of *C. thermocellum* in phosphate buffer medium sparged with CO₂ (light gray), N₂ (gray) and H₂ (black). The cells were incubated at 65 °C. The optical densities were taken 24 h after inoculation.

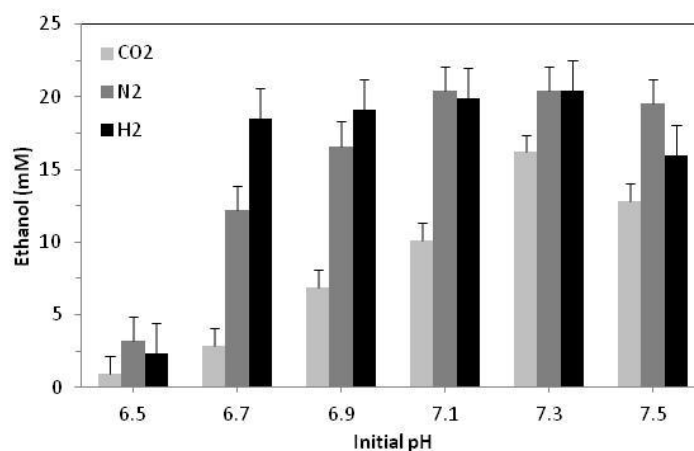


Figure C-2 The effect of initial pH on ethanol production by *C. thermocellum* in phosphate buffer medium sparged with CO₂ (light gray), N₂ (gray) and H₂ (black). The cells were incubated at 65 °C (24 h).

In addition to cell growth, ethanol concentrations were measured after 24 h of incubation at 65 °C (Fig C-2). The amount of ethanol produced by *C. thermocellum* followed closely with growth (Fig C-1). The maximum ethanol yield was observed when the cultures was gassed with N₂ or H₂ at initial pH of 7.1 or 7.3, whereas the maximum ethanol yield from the culture broth in the presence of CO₂ was observed when the initial pH was 7.3. No previous investigations report

the effect of pH on the ethanol production of *C. thermocellum*; however, the positive relationship between the microbial growth and product formation is well recognized. Ethanol production was generally greater in H₂-gassed cultures but acetate production was slightly less compared to the N₂-gassed cultures (Fig C-3). The result of enhanced ethanol production and reduced acetate production demonstrated the positive effect of exogenous hydrogen on the ethanol to acetate ratio (E/A). The increased E/A ratio in batch cultures are mainly due to the decreased acetate formation as a result of end product inhibition (Bothun et al. 2004). E/A ratios were reported to increase by nearly 6 folds when the operating pressure increased from atmospheric pressure to 7.0 MPa in continuous fermentation (Bothun et al. 2004). The study showed the best growth condition and ethanol production under N₂ at pH 7.1. Therefore, the original medium buffer (sodium carbonate) prepared with deoxygenated carbon dioxide was replaced by monobasic potassium phosphate with nitrogen to increase buffer capacity.

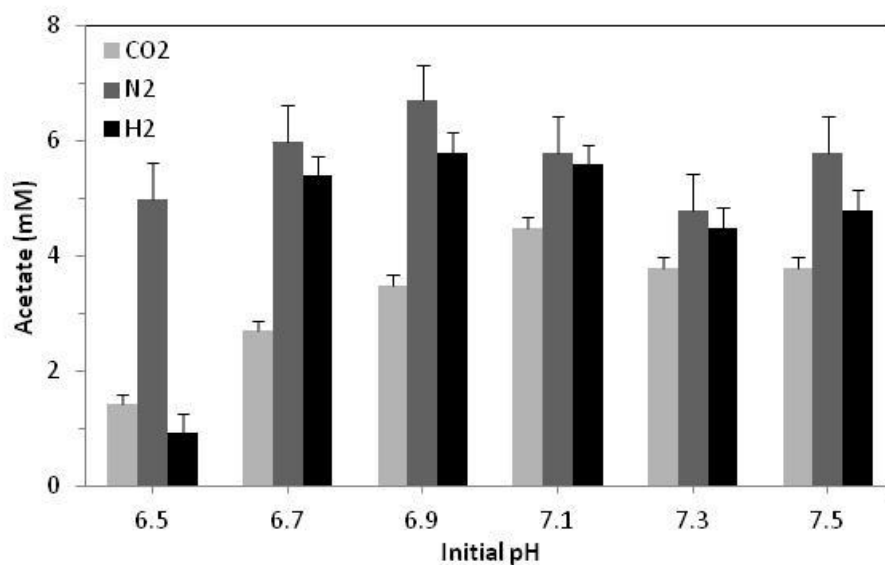


Figure C-3 The effect of initial pH on acetate production by *C. thermocellum* in phosphate buffer medium sparged with CO₂ (light gray), N₂ (gray) and H₂ (black). The cells were incubated at 65 °C (24 h).

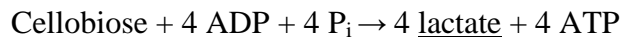
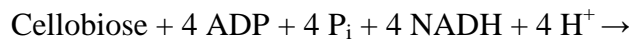
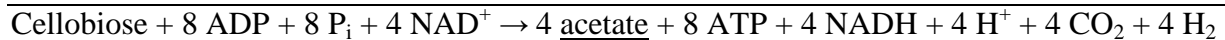
Appendix D

Bioenergetic calculations

Bioenergetic calculations of NAD^+ and ATP are presented in Chapter 6. Appendix D is a supplement to the calculation. A simplified biochemical scheme of a typical catabolism of glucose to end products in *Clostridium thermocellum* is shown in Figure D-1. Based on this metabolic scheme, products can be calculated based on their stoichiometric relations. For example, 1 mole of CO_2 and 2 moles of H_2 are produced with 1 mole of acetate formed; 1 mole of CO_2 is produced with 1 mole of ethanol formed. This metabolic reaction scheme leads to the generalized equations that describe the oxidation of cellobiose to end products (Table D-1).

Table D-1 Overall equation for cellobiose oxidation by *C. thermocellum*

Generalized reactions



The calculated for NAD^+ and ATP in Chapter 6 is therefore based on this stoichiometric relationship where 2 moles NAD^+ are produced with 1 mole of ethanol; 1 mole of NAD^+ is produced with 1 mole of lactate, and 4 moles of NAD^+ are consumed with 1 moles of cellobiose utilized. ATP is calculated from produced acetate and catabolized glucose (which produced 2 moles of ATP for every glucose catabolized).

Table D-2 Bioenergetic equations for NAD⁺ and ATP

Bioenergetics relations

NAD⁺ = 2 ethanol + lactate – 4 cellobiose (consumed)

ATP = acetate + 2 glucose (consumed)

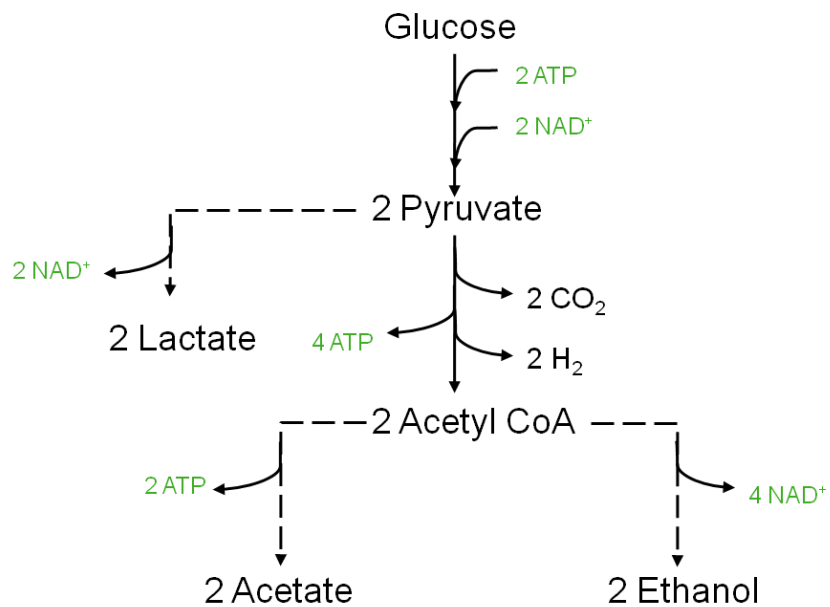


Figure D-1 Metabolic scheme of glucose conversion to lactate, acetate and ethanol in *C. thermocellum*.

References

- Adams, M. W. W. (1990). "The Structure and Mechanism of Iron-hydrogenases." *Biochimica Et Biophysica Acta* **1020**(2): 115-145.
- Adams, M. W. W., L. F. Mortenson, and J. S. Chen. (1981). "Hydrogenase." *Biochim. Biophys. Acta* **594**:105-176.
- Adelwoehrer, C., Y. Yoneda, T. Takano, F. Nakatsubo and T. Rosenau (2009). " Synthesis of the Perdeuterated Cellulose Solvents N-methylmorpholine N-oxide (NMMO-d(11) and NMMO-(15)N-d(11), N,N-dimethylacetamide (DMAc-d(9) and DMAc-(15)N-d(9), 1-ethyl-3-methylimidazolium acetate (EMIM-OAc-d(14) and 1-butyl-3-methylimidazolium acetate (BMIM-OAc-d(18))." *Cellulose* **16**(1): 139-150.
- Ahola, S., X. Turon, M. Osterberg, J. Laine and O. J. Rojas (2008). "Enzymatic Hydrolysis of Native Cellulose Nanofibrils and Other Cellulose Model Films: Effect of Surface Structure." *Langmuir* **24**(20): 11592-11599.
- Aulin, C., S. Ahola, P. Josefsson, T. Nishino, Y. Hirose, M. Osterberg, et al. (2009). "Nanoscale Cellulose Films with Different Crystallinities and Mesostuctures-Their Surface Properties and Interaction with Water." *Langmuir* **25**(13): 7675-7685.
- Bailey, J. E., A. Shurlati, V. Hatzimanikatis, K. Lee, W. A. Renner and P. S. Tsai (1996). "Inverse metabolic engineering: A Strategy for Directed Genetic Engineering of Useful Phenotypes." *Biotechnol. Bioeng.* **52**(1): 109-121.
- Bansal, P., M. Hall, M. J. Realff, J. H. Lee and A. S. Bommarius (2009). "Modeling Cellulase Kinetics on Lignocellulosic Substrates." *Biotechnology Advances* **27**(6): 833-848.
- Bayer, E. A., E. Morag and R. Lamed (1994). "The Cellulosome - A Treasure-trove for Biotechnology." *Trends in Biotechnology* **12**(9): 379-386.
- Bayer, E. A., H. Chanzy, R. Lamed and Y. Shoham (1998). "Cellulose, Cellulases and Cellulosomes." *Curr. Opin. Struct. Biol.* **8**(5): 548-557.
- Bayer, E. A., J. P. Belaich, Y. Shoham and R. Lamed (2004). "The Cellulosomes: Multienzyme Machines for Degradation of Plant Cell Wall Polysaccharides." *Annu. Rev. Microbiol.* **58**: 521-554.
- Bayer, E. A., R. Kenig and R. Lamed (1983). "Adherence of *Clostridium thermocellum* to Cellulose." *Journal of Bacteriology* **156**(2): 818-827.
- Beauchemin, K. A., D. Colombatto, D. P. Morgavi and W. Z. Yang (2003). "Use of Exogenous Fibrolytic Enzymes to Improve Feed Utilization by Ruminants." *Journal of Animal Science* **81**(14 suppl 2): E37-E47.
- Becker, B. and M. A. Cooper (2011). "A Survey of the 2006-2009 Quartz Crystal Microbalance Biosensor Literature." *Journal of Molecular Recognition* **24**(5): 754-787.

- Beguin, P. and P. M. Alzari (1998). "The Cellulosome of *Clostridium thermocellum*." *Biochem. Soc. Trans.* **26**(2): 178-185.
- Bender, J., Y. Vatcharapijarn and T. W. Jeffries (1985). "Characteristics and Adaptability of Some New Isolates of *Clostridium thermocellum*." *Appl. Environ. Microbiol.* **49**(3): 475-477.
- Beran, M. and V. Paulicek (1992). "Flow-microcalorimetric Determination of Enzymatic-activities of the Trichoderma Viridae-cellulase Complex." *J. Therm. Anal.* **38**(9): 1979-1988.
- Berberich JA, Knutson BL, Strobel HJ, Tarhan S, Nokes SE, Dawson KA (2000) Product selectivity shifts in *Clostridium thermocellum* in the presence of compressed solvents. *Ind Eng Chem Res* 39 (12):4500-4505. doi:10.1021/ie0001265
- Berger, W., M. Keck and B. Philipp (1988). "On the Mechanism of Cellulose Dissolution in Non-aqueous Solvents, Especially in O-basic Systems." *Cell Chem. Technol.* **22**(4): 387-397.
- Berghem, E. R. and Petterss.Lg (1973). "Mechanism of Enzymatic Cellulose Degradation - Purification of a Cellulolytic Enzyme from *Trichoderma viride* Active on Highly Ordered Cellulose." *Eur. J. Biochem.* **37**(1): 21-30.
- Berlin, A., V. Maximenko, N. Gilkes and J. Saddler (2007). "Optimization of Enzyme Complexes for Lignocellulose Hydrolysis." *Biotechnol. Bioeng.* **97**(2): 287-296.
- Bernardez, T. D., K. A. Lyford and L. R. Lynd (1994). "Kinetics of the Extracellular Cellulases of *Clostridium thermocellum* Acting on Pretreated Mixed Hardwood and Avicel." *Appl. Microbiol. Biotechnol.* **41**(5): 620-625.
- Bidlack, J., M. Malone and R. Benson (1992). "Molecular Structure and Component Integration of Secondary Cell Walls in Plants." *Proceedings of the Oklahoma Academy of Science* **72**(0): 51-56.
- Biganska, O. and P. Navard (2005). "Kinetics of Precipitation of Cellulose from Cellulose-NMMO-water Solutions." *Biomacromolecules* **6**(4): 1948-1953.
- Biswas S, Biswas I (2011) Role of VltAB, an ABC transporter complex, in viologen tolerance in *Streptococcus mutans*. *Antimicrob Agents Chemother* 55(4):1460–1469
- Bochek, A. M. (2003). "Effect of Hydrogen Bonding on Cellulose Solubility in Aqueous and Nonaqueous Solvents." *Russian Journal of Applied Chemistry* **76**(11): 1711-1719.
- Bommarius, A. S., A. Katona, S. E. Cheben, A. S. Patel, A. J. Ragauskas, K. Knudson, et al. (2008). "Cellulase Kinetics as a Function of Cellulose Pretreatment." *Metab. Eng.* **10**(6): 370-381.

- Bothun, G. D., B. L. Knutson, H. J. Strobel and S. E. Nokes (2005). "Molecular and Phase Toxicity of Compressed and Supercritical Fluids in Biphasic Continuous Cultures of *Clostridium thermocellum*." *Biotechnol. Bioeng.* **89**(1): 32-41.
- Bothun, G. D., B. L. Knutson, J. A. Berberich, H. J. Strobel and S. E. Nokes (2004). "Metabolic Selectivity and Growth of *Clostridium thermocellum* in Continuous Culture under Elevated Hydrostatic Pressure." *Appl. Microbiol. Biotechnol.* **65**(2): 149-157.
- Bravo, V., M. P. Páez, M. A. El-Hadj, A. Reyes and A. I. García (2002). "Hydrolysis of Carboxymethylcellulose with Mixtures of Cellulase and β -1,4-glucosidase." *Journal of Chemical Technology & Biotechnology* **77**(1): 15-20.
- Briggs, G. E. (1925). "A Further Note on the Kinetics of Enzyme Action." *Biochem. J.* **19**(6): 1037-1038.
- Brown, R. M., I. M. Saxena and K. Kudlicka (1996). "Cellulose Biosynthesis in Higher Plants." *Trends in Plant Science* **1**(5): 149-156.
- Bubner, P., J. Dohr, H. Plank, C. Mayrhofer and B. Nidetzky (2012). "Cellulases Dig Deep." *Journal of Biological Chemistry* **287**(4): 2759-2765.
- Buijtenhuijs, F. A., M. Abbas and A. J. Witteveen (1986). "The Degradation and Stabilization of Cellulose Dissolved in N-methylmorpholine-n-oxide (NMMO)." *Papier* **40**(12): 615-619.
- Bus JS, Aust SD, Gibson JE (1976) Paraquat toxicity: proposed mechanism of action involving lipid peroxidation. *Environ Health Perspect* 16:139–146
- Cantarella, M., L. Cantarella, A. Gallifuoco, A. Spera and F. Alfani (2004). "Effect of Inhibitors Released during Steam-Explosion Treatment of Poplar Wood on Subsequent Enzymatic Hydrolysis and SSF." *Biotechnology Progress* **20**(1): 200-206.
- Carere, C. R., R. Sparling, N. Cicek and D. B. Levin (2008). "Third Generation Biofuels via Direct Cellulose Fermentation." *International Journal of Molecular Sciences* **9**(7): 1342-1360.
- Carpita, N. C. and D. M. Gibeaut (1993). "Structural Models of Primary-cell Walls in Flowering Plants - Consistency of Molecular-structure with the Physical-properties of the Walls during Growth." *Plant Journal* **3**(1): 1-30.
- Chandra, R. P., K. Au-Yeung, C. Chanis, A. A. Roos, W. Mabee, P. A. Chung, et al. (2011). "The Influence of Pretreatment and Enzyme Loading on the Effectiveness of Batch and Fed-Batch Hydrolysis of Corn Stover." *Biotechnology Progress* **27**(1): 77-85.
- Chanzy, H., M. Dubé and R. H. Marchessault (1979). "Crystallization of Cellulose with N-methylmorpholine N-oxide: A New Method of Texturing Cellulose." *Journal of Polymer Science: Polymer Letters Edition* **17**(4): 219-226.

- Chanzy, H., S. Nawrot, A. Peguy, P. Smith and J. Chevalier (1982). "Phase Behavior of the Quasiternary System N-methylmorpholine-N-oxide, Water, and Cellulose." *Journal of Polymer Science: Polymer Physics Edition* **20**(10): 1909-1924.
- Chin, J. H., J. R. Trudell and E. N. Cohen (1976). "The Compression-ordering and Solubility-disordering Effects of High Pressure Gases on Phospholipid Bilayers." *Life Sciences* **18**(5): 489-497.
- Clark, D. and R. Kelly (1990). "Hot Bacteria." *Chemtech* **20**(11): 654-662.
- Collet, C., O. Gaudard, P. Peringer and J. P. Schwitzguebel (2005). "Acetate Production from Lactose by *Clostridium Thermolacticum* and Hydrogen-scavenging Microorganisms in Continuous Culture - Effect of Hydrogen Partial Pressure." *Journal of Biotechnology* **118**(3): 328-338.
- Converse, A. O. and J. D. Optekar (1993). "A Synergistic Kinetics Model for Enzymatic Cellulose Hydrolysis Compared to Degree-of-synergism Experimental Results." *Biotechnology and Bioengineering* **42**(1): 145-148.
- Converse, A. O., R. Matsuno, M. Tanaka and M. Taniguchi (1988). "A Model of Enzyme Adsorption and Hydrolysis of Microcrystalline Cellulose with Slow Deactivation of the Adsorbed Enzyme." *Biotechnology and Bioengineering* **32**(1): 38-45.
- Cornish-Bowden, A. (1995). "Fundamentals of Enzyme Kinetics." *Portland Press, London*.
- Cotta MA, Russell JB (1982) Effect of peptides and amino acids on efficiency of rumen bacterial protein synthesis in continuous culture. *J Dairy Sci* 65 (2):226-234
- Cotta, M. A. and J. B. Russell (1982). "Effect of Peptides and Amino Acids on Efficiency of Rumen Bacterial Protein Synthesis in Continuous Culture." *Journal of Dairy Science* **65**(2): 226-234.
- Datar RP, Shenkman, RM, Cateni BG, Huhnke RL, Lewis RS (2004) Fermentation of biomass-generated producer gas to ethanol. *Biotechnol Bioeng* 86(5):587-594
- Datta, R. and J. G. Zeikus (1985). "Modulation of Acetone-butanol-ethanol Fermentation by Carbon-monoxide and Organic-acids." *Appl. Environ. Microbiol.* **49**(3): 522-529.
- Demain, A. L., M. Newcomb and J. H. D. Wu (2005). "Cellulase, Clostridia, and Ethanol." *Microbiology and Molecular Biology Reviews* **69**(1): 124-+.
- Desvaux M (2005) *Clostridium cellulolyticum*: model organism of mesophilic cellulolytic clostridia. *FEMS Microbiol Rev* 29 (4):741-764. doi:10.1016/j.femsre.2004.11.003
- Dharmagadda, V. S. S., S. E. Nokes, H. J. Strobel and M. D. Flythe (2010). "Investigation of the Metabolic Inhibition Observed in Solid-substrate Cultivation of *Clostridium thermocellum* on Cellulose." *Bioresource Technology* **101**(15): 6039-6044.

- Dube, M., Y. Deslandes and R. H. Marchessault (1984). "Spherulitic Precipitation of Cellulose from Amine-oxide Solutions." *Journal of Polymer Science Part C-Polymer Letters* **22**(3): 163-171.
- Dubé, R.H. Blackwell. "Precipitation and Crystallization of Cellulose from Amine Oxide Solutions." Proceedings of the International Dissolving and Speciality Pulps Conference Tappi Press, Boston, USA (1983) p. 111–9
- Dwivedi, C. P. and T. K. Ghose (1979). "Model on Hydrolysis of Bagasse Cellulose by Enzyme from *Trichoderma reesei* QM-9414." *Journal of Fermentation Technology* **57**(1): 15-24.
- Edgar, C. D. and D. G. Gray (2003). "Smooth Model Cellulose I Surfaces from Nanocrystal Suspensions." *Cellulose* **10**(4): 299-306.
- El-Wakil, N. A. and M. L. Hassan (2008). "Structural Changes of Regenerated Cellulose Dissolved in FeTNa, NaOH/thiourea, and NMMO Systems." *J. Appl. Polym. Sci.* **109**(5): 2862-2871.
- Eriksson, M., S. M. Notley and L. Wågberg (2007). "Cellulose Thin Films: Degree of Cellulose Ordering and Its Influence on Adhesion." *Biomacromolecules* **8**(3): 912-919.
- Fägerstam, L.G. Pettersson. "The 1,4- β -glucan Cellobiohydrolases of *Trichoderma Reesei* QM 9414. A New Type of Cellulolytic Synergism." *FEBS Lett.*, 119 (1980), pp. 97–100
- Fält, S., L. Wågberg, E. L. Vesterlind and P. T. Larsson (2004). "Model Films of Cellulose ID - Improved Preparation Method and Characterization of the Cellulose Film." *Cellulose* **11**(2): 151-162.
- Fink, H. P., P. Weigel, H. J. Purz and J. Ganster (2001). "Structure Formation of Regenerated Cellulose Materials from NMMO-solutions." *Progress in Polymer Science* **26**(9): 1473-1524.
- Freier, D., C. P. Mothershed and J. Wiegel (1988). "Characterization of *Clostridium thermocellum* JW20." *Appl. Environ. Microbiol.* **54**(1): 204-211.
- Freudenberg, U., S. Zschoche, F. Simon, A. Janke, K. Schmidt, S. H. Behrens, et al. (2005). "Covalent Immobilization of Cellulose Layers onto Maleic Anhydride Copolymer Thin Films." *Biomacromolecules* **6**(3): 1628-1634.
- Gan, Q., S. J. Allen and G. Taylor (2003). "Kinetic Dynamics in Heterogeneous Enzymatic Hydrolysis of Cellulose: An Overview, an Experimental Study and Mathematical Modelling." *Process Biochem.* **38**(7): 1003-1018.
- García-Aparicio, M. A. P., I. Ballesteros, A. González, J. M. Oliva, M. Ballesteros and M. A. J. Negro (2006). "Effect of Inhibitors Released During Steam-Explosion Pretreatment of Barley Straw on Enzymatic Hydrolysis" Twenty-Seventh Symposium on Biotechnology for Fuels and Chemicals. J. D. McMillan, W. S. Adney, J. R. Mielenz and K. T. Klasson, Humana Press: 278-288.

- Gaughran ERL (1947) The thermophilic microorganisms. *Microbiol Mol Biol Rev* 11(3):189–225
- Ghose, T. and K. Das (1971). "A Simplified Kinetic Approach to Cellulose-cellulase System." *Advances in Biochemical Engineering*, Volume 1, Springer Berlin / Heidelberg. **1**: 55-76.
- Ghosh, P., N. B. Pamment and W. R. B. Martin (1982). "Simultaneous Saccharification and Fermentation of Cellulose: Effect of B-d-glucosidase Activity and Ethanol Inhibition of Cellulases." *Enzyme and Microbial Technology* **4**(6): 425-430.
- Ghosh, P., N. B. Pamment and W. R. B. Martin (2002). "Simultaneous Saccharification and Fermentation of Cellulose: Effect of β -D-glucosidase Activity and Ethanol Inhibition of Cellulases." *Enzyme and Microbial Technology* **4**(6): 425-430.
- Golovchenko, N. P., I. A. Kataeva and V. K. Akimenko (1992). "Analysis of PH-dependent Adsorption of *Clostridium thermocellum* Endoglucanase on Cellulose." *Biokhimiya* **57**(7): 1031-1038.
- Gonzalez-Flecha B, Demple B (1997) Homeostatic regulation of intracellular hydrogen peroxide concentration in aerobically growing *Escherichia coli*. *J Bacteriol* 179(2):382–388
- Gottschalk G (1979) *Bacterial Metabolism*. 2nd Ed., Springer-Verlag, New York
- Gray, C. T. and H. Gest (1965). "Biological Formation of Molecular Hydrogen." *Science* **148**(3667): 186-&.
- Gruno, M., P. Valjamae, G. Pettersson and G. Johansson (2004). "Inhibition of the *Trichoderma reesei* Cellulases by Cellobiose Is Strongly Dependent on the Nature of the Substrate." *Biotechnol. Bioeng.* **86**(5): 503-511.
- Gunnars, S., L. Wagberg and M. A. C. Stuart (2002). "Model Films of Cellulose: I. Method Development and Initial Results." *Cellulose* **9**(3-4): 239-249.
- Gusakov, A. V., A. P. Sinitsyn and A. A. Klyosov (1985). "Kinetics of the Enzymatic Hydrolysis of Cellulose: 1. A Mathematical Model for a Batch Reactor Process." *Enzyme and Microbial Technology* **7**(7): 346-352.
- Gusakov, A., A. Sinitsyn, J. Manenkova and O. Protas (1992). "Enzymatic Saccharification of Industrial and Agricultural Lignocellulosic Wastes." *Applied Biochemistry and Biotechnology* **34-35**(1): 625-637.
- Harvey, A. H. (1996). "Semiempirical Correlation for Henry's Constants over Large Temperature Ranges." *Aiche Journal* **42**(5): 1491-1494.
- Hendriks, A. T. W. M. and G. Zeeman (2009). "Pretreatments to Enhance the Digestibility of Lignocellulosic Biomass." *Bioresource Technology* **100**(1): 10-18.

- Henrissat, B., T. T. Teeri and R. A. J. Warren (1998). "A Scheme for Designating Enzymes That Hydrolyse the Polysaccharides in the Cell Walls of Plants." *Febs Letters* **425**(2): 352-354.
- Henstra AM, Sipma J, Rinzema A, Stams AJM (2007) Microbiology of synthesis gas fermentation for biofuel production. *Curr Opin Biotechnol* 18(3):200-6
- Herrero, A. A. and R. F. Gomez (1980). "Development of Ethanol Tolerance in *Clostridium thermocellum* - Effect of Growth Temperature." *Appl. Environ. Microbiol.* **40**(3): 571-577.
- Herrero, A. A., R. F. Gomez, B. Snedecor, C. J. Tolman and M. F. Roberts (1985). "Growth Inhibition of *Clostridium Thermocellum* by Carboxylic Acids: A Mechanism Based on Uncoupling by Weak Acids." *Appl. Microbiol. Biotechnol.* **22**(1): 53-62.
- Herrero, A.A., R.F. Gomez, and M.F. Roberts, "Ethanol Induced Changes in the Membrane Lipid Composition of *Clostridium thermocellum*." *Biochim. Biophys. Acta*, 1982. 693:195-204.
- Hianik, T., V. Ostatná, Z. Zajacová, E. Stoikova and G. Evtugyn (2005). "Detection of Aptamer-protein Interactions Using QCM and Electrochemical Indicator Methods." *Bioorganic & Medicinal Chemistry Letters* **15**(2): 291-295.
- Hildén, L. and G. Johansson (2004). "Recent Developments on Cellulases and Carbohydrate-binding Modules with Cellulose Affinity." *Biotechnology Letters* **26**(22): 1683-1693.
- Himmel, M. E., M. F. Ruth and C. E. Wyman (1999). "Cellulase for Commodity Products from Cellulosic Biomass." *Curr. Opin. Biotechnol.* **10**(4): 358-364.
- Hodge, D. B., M. N. Karim, D. J. Schell and J. D. McMillan (2009). "Model-Based Fed-Batch for High-Solids Enzymatic Cellulose Hydrolysis." *Applied Biochemistry and Biotechnology* **152**(1): 88-107.
- Hogan, C., M. Mes-Hartree, J. Saddler and D. Kushner (1990). "Assessment of Methods to Determine Minimal Cellulase Concentrations for Efficient Hydrolysis of Cellulose." *Appl. Microbiol. Biotechnol.* **32**(5): 614-620.
- Hogsett DA, Ahn HJ, Bernardez TD, South CR, Lynd LR (1992) Direct microbial conversion - prospects, progress, and obstacles. *Appl Biochem Biotechnol* 34-5:527-541
- Holtzapple, M., M. Cognata, Y. Shu and C. Hendrickson (1990). "Inhibition of *Trichoderma reesei* Cellulase by Sugars and Solvents." *Biotechnol. Bioeng.* **36**(3): 275-287.
- Hong, J., X. Ye and Y. H. P. Zhang (2007). "Quantitative Determination of Cellulose Accessibility to Cellulase Based on Adsorption of a Nonhydrolytic Fusion Protein Containing CBM and GFP with Its Applications." *Langmuir* **23**(25): 12535-12540.

- Hou, Y., J. Chen, P. Sun, Z. Gan and G. Zhang (2007). "In Situ Investigations on Enzymatic Degradation of Poly(-caprolactone)." *Polymer* **48**(21): 6348-6353.
- Howard, R. L., E. Abotsi, E. L. Jansen van Rensburg and S. Howard (2003). "Review - Lignocellulose Biotechnology: Issues of Bioconversion and Enzyme Production." Academic Journals.
- Howell, J. A. and J. D. Stuck (1975). "Kinetics of Solka Floc Cellulose Hydrolysis by *Trichoderma viride* Cellulase." *Biotechnol. Bioeng.* **17**(6): 873-893.
- Howell, J. A. and M. Mangat (1978). "Enzyme Deactivation during Cellulose Hydrolysis." *Biotechnology and Bioengineering* **20**(6): 847-863.
- Hu, G., J. A. Heitmann and O. J. Rojas (2009). "In Situ Monitoring of Cellulase Activity by Microgravimetry with a Quartz Crystal Microbalance." *J. Phys. Chem. B* **113**(44): 14761-14768.
- Hu, G., J. A. Heitmann and O. J. Rojas (2009). "Quantification of Cellulase Activity Using the Quartz Crystal Microbalance Technique." *Analytical Chemistry* **81**(5): 1872-1880.
- Huang, A. A. (1975). "Kinetic Studies on Insoluble Cellulose-cellulase System." *Biotechnol. Bioeng.* **17**(10): 1421-1433.
- Igarashi, K., A. Koivula, M. Wada, S. Kimura, M. Penttilä and M. Samejima (2009). "High Speed Atomic Force Microscopy Visualizes Processive Movement of *Trichoderma reesei* Cellobiohydrolase I on Crystalline Cellulose." *Journal of Biological Chemistry* **284**(52): 36186-36190.
- Islam, R., N. Cicek, R. Sparling and D. Levin (2006). "Effect of Substrate Loading on Hydrogen Production during Anaerobic Fermentation by *Clostridium thermocellum* 27405." *Appl. Microbiol. Biotechnol.* **72**(3): 576-583.
- Jie, X., Y. Cao, J.-J. Qin, J. Liu and Q. Yuan (2005). "Influence of Drying Method on Morphology and Properties of Asymmetric Cellulose Hollow Fiber Membrane." *Journal of Membrane Science* **246**(2): 157-165.
- Johnson, E. A., M. Sakajoh, G. Halliwell, A. Madia and A. L. Demain (1982). "Saccharification of Complex Cellulosic Substrates by the Cellulase System from *Clostridium thermocellum*." *Appl. Environ. Microbiol.* **43**(5): 1125-1132.
- Jones, R. P. and P. F. Greenfield (1982). "Effect of Carbon-dioxide on Yeast Growth and Fermentation." *Enzyme and Microbial Technology* **4**(4): 210-222.
- Jorgensen, H., J. B. Kristensen and C. Felby (2007). "Enzymatic Conversion of Lignocellulose into Fermentable Sugars: Challenges and Opportunities." *Biofuels Bioproducts & Biorefining-Biofpr* **1**(2): 119-134.

- Josefsson, P., G. Henriksson and L. Wågberg (2007). "The Physical Action of Cellulases Revealed by a Quartz Crystal Microbalance Study Using Ultrathin Cellulose Films and Pure Cellulases." *Biomacromolecules* **9**(1): 249-254.
- Josefsson, P., G. Henriksson and L. Wågberg (2007). "The Physical Action of Cellulases Revealed by a Quartz Crystal Microbalance Study Using Ultrathin Cellulose Films and Pure Cellulases." *Biomacromolecules* **9**(1): 249-254.
- Josefsson, P., L. Wågberg and G. Henriksson (2007). "Cell 114-mode of Action of Fungal Cellulases Studied Using Model Cellulose Films and a Quartz Crystal Microbalance." *Abstracts of Papers of the American Chemical Society* **233**: 773-773.
- Kadam, K. L., E. C. Rydholm and J. D. McMillan (2004). "Development and Validation of a Kinetic Model for Enzymatic Saccharification of Lignocellulosic Biomass." *Biotechnology Progress* **20**(3): 698-705.
- Kempner, W. and F. Kubowitz (1933). "The Effect of Light on the Carbon-dioxide Inhibition of Butyric Acid Fermentation." *Biochemische Zeitschrift* **265**: 245-252.
- Kim, B. H., P. Bellows, R. Datta and J. G. Zeikus (1984). "Control of Carbon and Electron Flow in *Clostridium-acetobutylicum* Fermentations - Utilization of Carbon-monoxide to Inhibit Hydrogen-production and to Enhance Butanol Yields." *Appl. Environ. Microbiol.* **48**(4): 764-770.
- Kim, J. H., B. C. Campbell, N. Mahoney, K. L. Chan and G. S. May (2006). "Targeting Antioxidative Signal Transduction and Stress Response System: Control of Pathogenic *Aspergillus* with Phenolics That Inhibit Mitochondrial Function." *J. Appl. Microbiol.* **101**(1): 181-189.
- Kim, J. K., B. R. Oh, H.-J. Shin, C.-Y. Eom and S. W. Kim (2008). "Statistical Optimization of Enzymatic Saccharification and Ethanol Fermentation Using Food Waste." *Process Biochem.* **43**(11): 1308-1312.
- Klein, G. L. and Snodgrass, W. R. (1993). Cellulose. In: Macrae R, Robinson RK, Saddler MJ, (eds.) *Encyclopedia of food science, food technology and nutrition*. London: Academic Press. Pp 758–767.
- Klemm, D., B. Heublein, H. P. Fink and A. Bohn (2005). "Cellulose: Fascinating Biopolymer and Sustainable Raw Material." *Angewandte Chemie-International Edition* **44**(22): 3358-3393.
- Knutson, B. L., H. J. Strobel, S. E. Nokes, K. A. Dawson, J. A. Berberich and C. R. Jones (1999). "Effect of Pressurized Solvents on Ethanol Production by the Thermophilic Bacterium *Clostridium thermocellum*." *Journal of Supercritical Fluids* **16**(2): 149-156.
- Kontturi, E., P. C. Thune and J. W. Niemantsverdriet (2003). "Cellulose Model Surfaces-simplified Preparation by Spin Coating and Characterization by X-ray Photoelectron

- Spectroscopy, Infrared Spectroscopy, and Atomic Force Microscopy." *Langmuir* **19**(14): 5735-5741.
- Kontturi, E., T. Tammelin and M. Osterberg (2006). "Cellulose - Model Films and the Fundamental Approach." *Chemical Society Reviews* **35**(12): 1287-1304.
- Kontturi, E., T. Tammelin and M. Osterberg (2006). "Cellulose-model Films and the Fundamental Approach." *Chemical Society Reviews* **35**(12).
- Kopelman, R. (1986). "Rate-processes on Fractals - Theory, Simulations, and Experiments." *Journal of Statistical Physics* **42**(1-2): 185-200.
- Krassig HA. 1993. Cellulose: Structure, Accessibility and Reactivity. Yverdon, Switzerland: Gordon & Breach.
- Kruus, K., A. Andreacchi, W. K. Wang and J. H. D. Wu (1995). "Product Inhibition of the Recombinant CelS, an Exoglucanase Component of the *Clostridium thermocellum* Cellulosome." *Appl. Microbiol. Biotechnol.* **44**(3-4): 399-404.
- Kurakake, M., T. Shirasawa, H. Ooshima, A. Converse and J. Kato (1995). "An Extension of the Harano-Ooshima Rate Expression for Enzymatic Hydrolysis of Cellulose to Account for Changes in the Amount of Adsorbed Cellulase." *Applied Biochemistry and Biotechnology* **50**(3): 231-241.
- la Grange, D. C., R. den Haan and W. H. van Zyl (2010). "Engineering Cellulolytic Ability into Bioprocessing Organisms." *Appl. Microbiol. Biotechnol.* **87**(4): 1195-1208.
- Lamed R, Zeikus JG (1980) Ethanol production by thermophilic bacteria - relationship between fermentation product yields of and catabolic enzyme activities in *Clostridium thermocellum* and *Thermoanaerobium brockii*. *J Bacteriol* 144 (2):569-578
- Lamed, R. and E. A. Bayer (1988). The Cellulosome of *Clostridium thermocellum*. Advances in Applied Microbiology. I. L. Allen, Academic Press. **Volume 33**: 1-46.
- Lamed, R. J., J. H. Lobos and T. M. Su (1988). "Effects of Stirring and Hydrogen on Fermentation Products of *Clostridium thermocellum*." *Appl. Environ. Microbiol.* **54**(5): 1216-1221.
- Lamed, R., E. Setter and E. A. Bayer (1983). "Characterization of a Cellulose-binding, Cellulase-containing Complex in *Clostridium thermocellum*." *Journal of Bacteriology* **156**(2): 828-836.
- Lee, J. (1997). "Biological Conversion of Lignocellulosic Biomass to Ethanol." *Journal of Biotechnology* **56**(1): 1-24.
- Lee, Y.-H. and L. T. Fan (1982). "Kinetic Studies of Enzymatic Hydrolysis of Insoluble Cellulose: Analysis of the Initial Rates." *Biotechnology and Bioengineering* **24**(11): 2383-2406.

- Lee, Y.-H., L. Fan and L.-S. Fan (1980). "Kinetics of Hydrolysis of Insoluble Cellulose by Cellulase." *Advances in Biochemical Engineering*, Volume 17, Springer Berlin / Heidelberg. **17**: 131-168.
- Lefebvre, J. and D. G. Gray (2005). "AFM of Adsorbed Polyelectrolytes on Cellulose I Surfaces Spin-coated on Silicon Wafers." *Cellulose* **12**(2): 127-134.
- Lemon, B. J. and J. W. Peters (1999). "Binding of Exogenously Added Carbon Monoxide at the Active Site of the Iron-only Hydrogenase (CpI) From *Clostridium pasteurianum*." *Biochemistry* **38**(40): 12969-12973.
- Leschine, S. B. and E. Canale-Parola (1983). "Mesophilic Cellulolytic Clostridia from Freshwater Environments." *Appl. Environ. Microbiol.* **46**(3): 728-737.
- Levine, S. E., J. M. Fox, H. W. Blanch and D. S. Clark (2010). "A Mechanistic Model of the Enzymatic Hydrolysis of Cellulose." *Biotechnology and Bioengineering* **107**(1): 37-51.
- Li, H.-F., B. L. Knutson, S. E. Nokes, B. C. Lynn and M. D. Flythe (2012). "Metabolic Control of *Clostridium thermocellum* via Inhibition of Hydrogenase Activity and the Glucose Transport Rate." *Appl. Microbiol. Biotechnol.* **93**(4): 1777-1784.
- Li, L. H., R. M. Flora and K. W. King (1965). "Individual Roles of Cellulase Components Derived from *Trichoderma viride*." *Archives of Biochemistry and Biophysics* **111**(2): 439-&.
- Lin M, Katsumura Y, Muroya Y, He H, Wu G, Han Z, Miyazaki T, Kudo H (2004) Pulse radiolysis study on the estimation of radiolytic yields of water decomposition products in high-temperature and supercritical water: use of methyl viologen as a scavenger. *J Phys Chem A* 108(40):8287–8295
- Lin, J. Q., S. M. Lee and Y. M. Koo (2005). "Modeling and Simulation of Simultaneous Saccharification and Fermentation of Paper Mill Sludge to Lactic Acid." *J. Microbiol. Biotechnol.* **15**(1): 40-47.
- Lovitt, R. W., G. J. Shen and J. G. Zeikus (1988). "Ethanol-production by Thermophilic Bacteria - Biochemical Basis for Ethanol and Hydrogen Tolerance in *Clostridium thermohydrosulfuricum*." *Journal of Bacteriology* **170**(6): 2809-2815.
- Lowe, S. E., M. K. Jain and J. G. Zeikus (1993). "Biology, Ecology, and Biotechnological Applications of Anaerobic Bacteria Adapted to Environmental Stresses in Temperature, PH, Salinity, or Substrates." *Microbiological Reviews* **57**(2): 451-509.
- Luterbacher, J. S., L. P. Walker and J. M. Moran-Mirabal (2012). "Observing and Modeling BMCC Degradation by Commercial Cellulase Cocktails with Fluorescently Labeled *Trichoderma reesei* Cel7A through Confocal Microscopy." *Biotechnol. Bioeng.:* n/a-n/a.

- Lynd, L. R., H. E. Grethlein and R. H. Wolkin (1989). "Fermentation of Cellulosic Substrates in Batch and Continuous Culture by *Clostridium thermocellum*." *Appl. Environ. Microbiol.* **55**(12): 3131-3139.
- Lynd, L. R., P. J. Weimer, W. H. van Zyl and I. S. Pretorius (2002). "Microbial Cellulose Utilization: Fundamentals and Biotechnology." *Microbiology and Molecular Biology Reviews* **66**(3): 506-+.
- MacMichael GJ (1988) Effects of oxygen and methyl viologen on *Thermus aquaticus*. *J Bacteriol* 170(10):4995–4998
- Maia, E., A. Peguy and S. Perez (1981). "Cellulose Organic Solvents. I. The Structures of Anhydrous N-methylmorpholine N-oxide and N-methylmorpholine N-oxide Monohydrate." *Acta Crystallographica Section B* **37**(10): 1858-1862.
- Mandels, M. and E. T. Reese (1965). "Inhibition of Cellulases." *Annual Review of Phytopathology* **3**: 85-&.
- McCormick, C. L., P. A. Callais and B. H. Hutchinson (1985). "Solution Studies of Cellulose in Lithium-chloride and N,n-dimethylacetamide." *Macromolecules* **18**(12): 2394-2401.
- McMurry and Fay (1995). "Chemistry." Prentice Hall; 2 Sub edition
- McCormick. C. L., Shen, T. C. In "Macromolecular Solutions"; Seymour. R. B.; Stahl, G. S., Eds.; Peqamon P m : New York. 1982; pp 101-107.
- Meyer, C. L., J. W. Roos and E. T. Papoutsakis (1986). "Carbon Monoxide Gasing Leads to Alcohol Production and Butyrate Uptake without Acetone Formation in Continuous Cultures of *Clostridium acetobutylicum*." *Appl. Microbiol. Biotechnol.* **24**(2): 159-167.
- Michaelis, L., and M. I. Menten (1913). "Die Kinetik der Invertinwirkung." *Biochem. Z.*, 49:333–369.
- Mitchell D (2008) A note on rising food prices. World Bank Development Prospects Group, World Bank, Washington, DC
- Mitchell, R., K. P. Vogel and G. Sarath (2008). "Managing and Enhancing Switchgrass as a Bioenergy Feedstock." *Biofuels Bioproducts & Biorefining-Biofpr* **2**(6): 530-539.
- Mohan, T., S. Spirk, R. Kargl, A. Doliska, H. M. A. Ehmman, S. Koestler, et al. (2012). "Watching Cellulose Grow - Kinetic Investigations on Cellulose Thin Film Formation at the Gas-solid Interface Using a Quartz Crystal Microbalance with Dissipation (Qcm-d)." *Colloids and Surfaces a-Physicochemical and Engineering Aspects* **400**: 67-72.
- Moldes, A. B., J. L. Alonso and J. C. Parajó (1999). "Cogeneration of Cellobiose and Glucose from Pretreated Wood and Bioconversion to Lactic Acid: A Kinetic Study." *Journal of Bioscience and Bioengineering* **87**(6): 787-792.

- Monserrate, E., S. B. Leschine and E. Canale-Parola (2001). "*Clostridium hungatei* Sp Nov., a Mesophilic, N₂-fixing Cellulolytic Bacterium Isolated from Soil." *International Journal of Systematic and Evolutionary Microbiology* **51**: 123-132.
- Mori, Y. (1990). "Isolation of Mutants of *Clostridium-thermocellum* with Enhanced Cellulase Production." *Agricultural and Biological Chemistry* **54**(3): 825-826.
- Mosier, N. S., P. Hall, C. M. Ladisch and M. R. Ladisch (1999). "Reaction Kinetics, Molecular Action, and Mechanisms of Cellulolytic Proteins." *Advances in Biochemical Engineering/Biotechnology* **65**: 23-40.
- Movagarnejad, K., M. Sohrabi, T. Kaghazchi and F. Vahabzadeh (2000). "A Model for the Rate of Enzymatic Hydrolysis of Cellulose in Heterogeneous Solid-liquid Systems." *Biochemical Engineering Journal* **4**(3): 197-206.
- Munasinghe, P. C. and S. K. Khanal (2010). "Biomass-derived syngas fermentation into biofuels: Opportunities and challenges." *Bioresource Technology* **101**(13): 5013-5022.
- Murray WD, Khan AW (1983) Ethanol production by a newly isolated anaerobe, *Clostridium saccharolyticum*: effects of culture medium and growth conditions. *Can J Microbiol* **29**(3): 342-347
- Mussatto, S. I., G. Dragone, M. Fernandes, A. M. F. Milagres and I. C. Roberto (2008). "The Effect of Agitation Speed, Enzyme Loading and Substrate Concentration on Enzymatic Hydrolysis of Cellulose from Brewer's Spent Grain." *Cellulose* **15**(5): 711-721.
- Nakayama, S., K. Kiyoshi, T. Kadokura and A. Nakazato (2011). "Butanol Production from Crystalline Cellulose by Cocultured *Clostridium thermocellum* and *Clostridium saccharoperbutylacetonicum* N1-4." *Appl. Environ. Microbiol.* **77**(18): 6470-6475.
- Ng, T. K. and J. G. Zeikus (1981). "Comparison of Extracellular Cellulase Activities of *Clostridium-thermocellum*-lqri and *Trichoderma reesei* QM 9414." *Appl. Environ. Microbiol.* **42**(2): 231-240.
- Ng, T. K., P. J. Weimer and J. G. Zeikus (1977). "Cellulolytic and Physiological Properties of *Clostridium thermocellum*." *Archives of Microbiology* **114**(1): 1-7.
- Nidetzky, B., W. Steiner, M. Hayn and M. Claeysens (1994). "Cellulose Hydrolysis by the Cellulases from *Trichoderma reesei* - A New Model for Synergistic Interaction." *Biochem. J.* **298**: 705-710.
- Nivens, D. E., J. Q. Chambers, T. R. Anderson and D. C. White (1993). "Long-term, Online Monitoring of Microbial Biofilms Using a Quartz Crystal Microbalance." *Anal. Chem.* **65**(1): 65-69.
- Notley, S. M., M. Eriksson, L. Wågberg, S. Beck and D. G. Gray (2006). "Surface Forces Measurements of Spin-Coated Cellulose Thin Films with Different Crystallinity." *Langmuir* **22**(7): 3154-3160.

- Nyfors, L., M. Suchy, J. Laine and E. Kontturi (2009). "Ultrathin Cellulose Films of Tunable Nanostructured Morphology with a Hydrophobic Component." *Biomacromolecules* **10**(5): 1276-1281.
- Ohmine, K., H. Ooshima and Y. Harano (1983). "Kinetic-study on Enzymatic-hydrolysis of Cellulose by Cellulase from *Trichoderma viride*." *Biotechnol. Bioeng.* **25**(8): 2041-2053.
- Ooshima, H., M. Kurakake, J. Kato and Y. Harano (1991). "Enzymatic Activity of Cellulase Adsorbed on Cellulose and Its Change during Hydrolysis." *Applied Biochemistry and Biotechnology* **31**(3): 253-266.
- Osullivan, A. C. (1997). "Cellulose: The Structure Slowly Unravels." *Cellulose* **4**(3): 173-207.
- Özkan M, Yilmaz EI, Lynd LR, Özcengiz G (2004) Cloning and expression of the *Clostridium thermocellum* L-lactate dehydrogenase gene in *Escherichia coli* and enzyme characterization. *Can J Microbiol* 50 (10):845-851
- Parajó, J., J. Alonso and V. Santos (1996). "Development of a Generalized Phenomenological Model Describing the Kinetics of the Enzymatic Hydrolysis of NaOH-treated Pine Wood." *Applied Biochemistry and Biotechnology* **56**(3): 289-299.
- Park, E., Y. Ikeda and N. Okuda (2002). "Empirical Evaluation of Cellulase on Enzymatic Hydrolysis of Waste Office Paper." *Biotechnology and Bioprocess Engineering* **7**(5): 268-274.
- Payton, M. A. (1984). "Production of Ethanol by Thermophilic Bacteria." *Trends in Biotechnology* **2**(6): 153-158.
- Peguín, S. and P. Soucaille (1996). "Modulation of Metabolism of *Clostridium acetobutylicum* Grown in Chemostat Culture in a Three-electrode Potentiostatic System with Methyl Viologen as Electron Carrier." *Biotechnol. Bioeng.* **51**(3): 342-348.
- Peitersen, N., J. Medeiros and M. Mandels (1977). "Adsorption of *Trichoderma* Cellulase on Cellulose." *Biotechnol. Bioeng.* **19**(7): 1091-1094.
- Pereira, A. N., M. Mobedshahi and M. R. Ladisch (1988). "Preparation of Cellodextrins." *Methods in Enzymology* **160**: 26-38.
- Peterson, G. L. (1977). "A Simplification of the Protein Assay Method of Lowry Et Al. Which Is More Generally Applicable." *Analytical Biochemistry* **83**(2): 346-356.
- Philippidis, G. P., T. K. Smith and C. E. Wyman (1993). "Study of the Enzymatic Hydrolysis of Cellulose for Production of Fuel Ethanol by the Simultaneous Saccharification and Fermentation Process." *Biotechnology and Bioengineering* **41**(9): 846-853.
- Pienkos, P. and M. Zhang (2009). "Role of Pretreatment and Conditioning Processes on Toxicity of Lignocellulosic Biomass Hydrolysates." *Cellulose* **16**(4): 743-762.

- Pimentel, D. and T. W. Patzek (2005). "Ethanol Production Using Corn, Switchgrass, and Wood; Biodiesel Production Using Soybean and Sunflower." *Natural Resources Research* **14**(1): 65-76.
- Przybyla, A. E., J. Robbins, N. Menon and H. D. Peck (1992). "Structure-function-relationships among the Nickel-containing Hydrogenases." *Fems Microbiology Reviews* **88**(2): 109-135.
- Rabinovich, M. L., M. S. Melnik and A. V. Boloboba (2002). "Microbial Cellulases (Review)." *Applied Biochemistry and Microbiology* **38**(4): 305-321.
- Rao, G. and R. Mutharasan (1987). "Altered Electron Flow in Continuous Cultures of *Clostridium acetobutylicum* Induced by Viologen Dyes." *Appl. Environ. Microbiol.* **53**(6): 1232-1235.
- Raynolds, R. G. H. and G. D. Johnson (1985). "Structural Control on Molasse Sedimentation - Example of Siwalik Group of Northern Pakistan." *Aapg Bulletin-American Association of Petroleum Geologists* **69**(2): 299-299.
- Reese, E. T. , Mandels, M. "Cellulose and Cellulose Derivatives." N. M. Bikales, L. Segal (Eds.), "Series on High Polyme r" , Vol. 5, Pa r t 5, p. 1079. New Yo r k : John Wiley 1971
- Reimann A, Biebl H, Deckwer WD (1996) Influence of iron, phosphate and methyl viologen on glycerol fermentation of *Clostridium butyricum*. *Appl Microbiol Biotechnol* 45 (1-2):47-50
- Richardson, S., T. Andersson, G. Brinkmalm and B. Wittgren (2003). "Analytical Approaches to mproved Characterization of Substitution in Hydroxypropyl Cellulose." *Analytical Chemistry* **75**(22): 6077-6083.
- Rodahl, M., F. Hook, A. Krozer, P. Brzezinski and B. Kasemo (1995). "Quartz-crystal Microbalance Setup for Frequency and Q-factor Measurements in Gaseous and Liquid Environmet." *Rev. Sci. Instrum.* **66**(7): 3924-3930.
- Rodahl, M., F. Hook, C. Fredriksson, C. A. Keller, A. Krozer, P. Brzezinski, et al. (1997). "Simultaneous Frequency and Dissipation Factor QCM Measurements of Biomolecular Adsorption and Cell Adhesion." *Faraday Discussions* **107**: 229-246.
- Rojas Orlando, J., C. Jeong, X. Turon and S. Argyropoulos Dimitris (2007). "Measurement of Cellulase Activity with Piezoelectric Resonators." *Materials, Chemicals, and Energy from Forest Biomass*, American Chemical Society. **954**: 478-494.
- Rojas Rejon, O. A., M. T. Ponce Noyola, H. M. P. Varaldo and M. de la Torre Martinez (2007). "Saccharification of Cellulosic Biomass: Regulation of Cellulase and Xylanase Activities under Catabolic Repression Conditions." *Journal of Biotechnology* **131**(2): S28-S28.

- Romsaiyud, A., W. Songkasiri, A. Nopharatana and P. Chaiprasert (2009). "Combination Effect of PH and Acetate on Enzymatic Cellulose Hydrolysis." *Journal of Environmental Sciences-China* **21**(7): 965-970.
- Russell JB, Bond DR, Cook GM (1996) The fructose diphosphate/phosphate regulation of carbohydrate metabolism in low G+C Gram-positive anaerobes. *Res Microbiol* 147(6-7):528-535
- Russell, J. B. (1992). "Another Explanation for the Toxicity of Fermentation Acids at Low PH: Anion Accumulation versus Uncoupling." *Journal of Applied Microbiology* **73**(5): 363-370.
- Rydzak T, Levin DB, Cicek N, Sparling R (2009) Growth phase-dependant enzyme profile of pyruvate catabolism and end-product formation in *Clostridium thermocellum* ATCC 27405. *J Bacteriol* 140 (3-4):169-175
- Ryu, D. D. Y. and M. Mandels (1980). "Cellulases - Biosynthesis and Applications." *Enzyme and Microbial Technology* **2**(2): 91-102.
- Ryu, D. D. Y. and S. B. Lee (1986). "Enzymatic Hydrolysis of Cellulose: Determination of Kinetic Parameters." *Chemical Engineering Communications* **45**(1-6): 119-134.
- Saarinen, T., M. Osterberg and J. Laine (2008). "Adsorption of Polyelectrolyte Multilayers and Complexes on Silica and Cellulose Surfaces Studied by QCM-D." *Colloids and Surfaces a-Physicochemical and Engineering Aspects* **330**(2-3): 134-142.
- Saddler, J. N. and M. K. H. Chan (1982). "Optimization of *Clostridium thermocellum* Growth on Cellulose and Pretreated Wood Substrates." *Appl. Microbiol. Biotechnol.* **16**(2): 99-104.
- Saddler, J. N., M. K. H. Chan and G. Louis-Seize (1981). "A One Step Process for the Conversion of Cellulose to Ethanol Using Anaerobic Microorganisms in Mono- and Co-culture." *Biotechnology Letters* **3**(6): 321-326.
- Sai Ram, M. and G. Seenayya (1989). "Ethanol Production by *Clostridium thermocellum* SS8 a Newly Isolated Thermophilic Bacterium." *Biotechnology Letters* **11**(8): 589-592.
- Sato, K. J., S. G. Goto, S. T. Yonemura, K. J. Sekine, E. K. Okuma, Y. S. Takagi, et al. (1992). "Effect of Yeast Extract and Vitamin-b12 on Ethanol Production from Cellulose by *Clostridium thermocellum* I-1-B." *Appl. Environ. Microbiol.* **58**(2): 734-736.
- Sattler, W., H. Esterbauer, O. Glatter and W. Steiner (1989). "The Effect of Enzyme Concentration on the Rate of the Hydrolysis of Cellulose." *Biotechnol. Bioeng.* **33**(10): 1221-1234.
- Scheiding, W., M. Thoma, A. Ross and K. Schügerl (1984). "Modelling of the Enzymatic Hydrolysis of Cellobiose and Cellulose by a Complex Enzyme Mixture of *Trichoderma reesei* QM 9414." *Applied Microbiology and Biotechnology* **20**(3): 176-182.

- Schurz, J. (1994). "Cellulose Chemists Round-table Discussion, Dusseldorf 1994 - Functional-groups in Celluloses for Chemical-processing and Cellulose Products - Analysis, Properties and Effects - Introduction." *Papier* **48**(12): 737-738.
- Schwarz, W. H. (2001). "The Cellulosome and Cellulose Degradation by Anaerobic Bacteria." *Appl. Microbiol. Biotechnol.* **56**(5-6): 634-649.
- Shao, X., L. Lynd and C. Wyman (2009). "Kinetic Modeling of Cellulosic Biomass to Ethanol Via Simultaneous Saccharification and Fermentation: Part II. Experimental Validation Using Waste Paper Sludge and Anticipation of CFD Analysis." *Biotechnol. Bioeng.* **102**(1): 66-72.
- Shin HS, Zeikus JG, Jain MK (2002) Electrically enhanced ethanol fermentation by *Clostridium thermocellum* and *Saccharomyces cerevisiae*. *Appl Microbiol Biotechnol* 58 (4):476-481. doi:10.1007/s00253-001-0923-2
- Shoham, Y., R. Lamed and E. A. Bayer (1999). " The Cellulosome Concept as an Efficient Microbial Strategy for the Degradation of Insoluble Polysaccharides." *Trends Microbiol.* **7**(7): 275-281.
- Slapack GE, Russell I, Stewart GG. Project Report submitted to division of Energy, NRCC No. 2441, Ottawa, ON 1985, p. 1-404.
- Song, J., J. Liang, X. Liu, W. E. Krause, J. P. Hinestroza and O. J. Rojas (2009). "Development and Characterization of Thin Polymer Films Relevant to Fiber Processing." *Thin Solid Films* **517**(15): 4348-4354.
- Spindler, D., C. Wyman and K. Grohmann (1991). "The Simultaneous Saccharification and Fermentation of Pretreated Woody Crops to Ethanol." *Applied Biochemistry and Biotechnology* **28-29**(1): 773-786.
- Strobel HJ, Caldwell FC, Dawson KA (1995) Carbohydrate transport by the anaerobic thermophile *Clostridium thermocellum* LQRI. *Appl Environ Microbiol* 61 (11):4012-4015
- Suchy, M., M. B. Linder, T. Tammelin, J. M. Campbell, T. Vuorinen and E. Kontturi (2011). "Quantitative Assessment of the Enzymatic Degradation of Amorphous Cellulose by Using a Quartz Crystal Microbalance with Dissipation Monitoring." *Langmuir* **27**(14): 8819-8828.
- Sudha Rani, K., M. V. Swamy and G. Seenayya (1996). "High Ethanol Production by New Isolates of *Clostridium thermocellum*." *Biotechnology Letters* **18**(8): 957-962.
- Sukumaran, R. K., R. R. Singhanian, G. M. Mathew and A. Pandey (2009). "Cellulase Production Using Biomass Feed Stock and Its Application in Lignocellulose Saccharification for Bio-ethanol Production." *Renewable Energy* **34**(2): 421-424.

- Sun, R., X. Song, R. Sun and J. Jiang (2011). "Effect of Lignin Content on Enzymatic Hydrolysis of Furfural Residues." *BioResources* **6**(1): 317-328.
- Sun, Y. and J. Y. Cheng (2002). "Hydrolysis of Lignocellulosic Materials for Ethanol Production: A Review." *Bioresource Technology* **83**(1): 1-11.
- Swatloski, R. P., S. K. Spear, J. D. Holbrey and R. D. Rogers (2002). "Dissolution of Cellulose with Ionic Liquids." *Journal of the American Chemical Society* **124**(18): 4974-4975.
- Tailliez, P., H. Girard, J. Millet and P. Beguin (1989). "Enhanced Cellulose Fermentation by an Asporogenous and Ethanol-Tolerant Mutant of *Clostridium thermocellum*." *Appl. Environ. Microbiol.* **55**(1): 207-211.
- Tammelin, T., T. Saarinen, M. Osterberg and J. Laine (2006). "Preparation of Langmuir/blodgett-cellulose Surfaces by Using Horizontal Dipping Procedure. Application for Polyelectrolyte Adsorption Studies Performed with QCM-D." *Cellulose* **13**(5): 519-535.
- Tarantili, P. A., D. P. Koullas, P. Christakopoulos, D. Kekos, E. G. Koukios and B. J. Macris (1996). "Cross-synergism in Enzymatic Hydrolysis of Lignocellulosics: Mathematical Correlations according to a Hyperbolic Model." *Biomass and Bioenergy* **10**(4): 213-219.
- Teeri, T. T. (1997). "Crystalline Cellulose Degradation: New Insight into the Function of Cellobiohydrolases." *Trends in Biotechnology* **15**(5): 160-167.
- Tengborg, C., M. Galbe and G. Zacchi (2001). "Influence of Enzyme Loading and Physical Parameters on the Enzymatic Hydrolysis of Steam-pretreated Softwood." *Biotechnology Progress* **17**(1): 110-117.
- Thauer, R. K., A. R. Klein and G. C. Hartmann (1996). "Reactions with Molecular Hydrogen in Microorganisms: Evidence for a Purely Organic Hydrogenation Catalyst." *Chemical Reviews* **96**(7): 3031-3042.
- Thauer, R. K., B. Käfer, K. Jungermann and M. Zähringer (1974). "The Reaction of the Iron-Sulfur Protein Hydrogenase with Carbon Monoxide." *Eur. J. Biochem.* **42**(2): 447-452.
- Toda, S., H. Suzuki and K. Nisizawa (1968). "Mode of Action of Trichoderma Cellulases toward Normal and Reduces Cello-oligosaccharides." *Journal of Fermentation Technology* **46**(9): 711-&.
- Turon, X., O. J. Rojas and R. S. Deinhammer (2008). "Enzymatic Kinetics of Cellulose Hydrolysis: A Qcm-d Study." *Langmuir* **24**(8): 3880-3887.
- Valjamae, P., K. Kipper, G. Pettersson and G. Johansson (2003). "Synergistic Cellulose Hydrolysis Can Be Described in Terms of Fractal-like Kinetics." *Biotechnol. Bioeng.* **84**(2): 254-257.

- Wald, S., C. R. Wilke and H. W. Blanch (1984). "Kinetics of the Enzymatic Hydrolysis of Cellulose." *Biotechnology and Bioengineering* **26**(3): 221-230.
- Warden, A., B. Little and V. Haritos (2011). "A Cellular Automaton Model of Crystalline Cellulose Hydrolysis by Cellulases." *Biotechnology for Biofuels* **4**(1): 39.
- Weimer, P. J. and J. G. Zeikus (1977). "Fermentation of Cellulose and Cellobiose by *Clostridium thermocellum* in the Absence of *Methanobacterium thermoautotrophicum*." *Appl. Environ. Microbiol.* **33**(2): 289-297.
- Wesseler J (2007) Opportunities ('costs) matter: A comment on Pimentel and Patzek "Ethanol production using corn, switchgrass, and wood; biodiesel production using soybean and sunflower". *Energ policy* 35 (2):1414-1416. doi:10.1016/j.enpol.2006.02.007
- Whitaker, D. R. (1956). "The Steric Factor in the Hydrolysis of Beta-1,4'-oligoglucosides by Myrothecium Cellulase." *Canadian Journal of Biochemistry and Physiology* **34**(1): 102-115.
- Wiegel, J. (1980). "Formation of Ethanol by Bacteria - A Pledge for the Use of Extreme Thermophilic Anaerobic-bacteria in Industrial Ethanol Fermentation Processes." *Experientia* **36**(12): 1434-1446.
- Wilson, D. B. (2009). "Cellulases and Biofuels." *Curr. Opin. Biotechnol.* **20**(3): 295-299.
- Wood, T. M. (1992). "Fungal Cellulases." *Biochem. Soc. Trans.* **20**(1): 46-53.
- Wood, T. M. and K. M. Bhat (1988). "Methods for Measuring Cellulase Activities." *Methods in Enzymology* **160**: 87-112.
- Woodward, J. and S. L. Arnold (1981). "The Inhibition of B-glucosidase Activity in *Trichoderma Reesei* C30 Cellulase by Derivatives and Isomers of Glucose." *Biotechnol. Bioeng.* **23**(7): 1553-1562.
- Woodward, J., M. Lima and N. E. Lee (1988). "The Role of Cellulase Concentration in Determining the Degree of Synergism in the Hydrolysis of Microcrystalline Cellulose." *Biochem. J.* **255**(3): 895-899.
- Xiao, Z., X. Zhang, D. Gregg and J. Saddler (2004). "Effects of Sugar Inhibition on Cellulases and B-glucosidase during Enzymatic Hydrolysis of Softwood Substrates." *Applied Biochemistry and Biotechnology* **115**(1): 1115-1126.
- Xu, F. and H. Ding (2007). "A New Kinetic Model for Heterogeneous (Or Spatially Confined) Enzymatic Catalysis: Contributions from the Fractal and Jamming (Overcrowding) Effects." *Applied Catalysis a-General* **317**(1): 70-81.
- Xu, Q., A. Singh and M. E. Himmel (2009). "Perspectives and New Directions for the Production of Bioethanol Using Consolidated Bioprocessing of Lignocellulose." *Current Opinion in Biotechnology* **20**(3): 364-371.

- Yamashita, K., Y. Kikkawa, K. Kurokawa and Y. Doi (2005). "Enzymatic Degradation of Poly(l-lactide) Film by Proteinase Quartz Crystal Microbalance and Atomic Force Microscopy Study." *Biomacromolecules* **6**(2): 850-857.
- Yu, E. K. C., M. K. H. Chan and J. N. Saddler (1985). "Butanol Production from Cellulosic Substrates by Sequential Co-culture *Clostridium thermocellum* and *Clostridium acetobutylicum*." *Biotechnology Letters* **7**(7): 509-514.
- Yu, L. and M. J. Wolin (1969). "Hydrogenase Measurement with Photochemically Reduced Methyl Viologen." *Journal of Bacteriology* **98**(1): 51-&.
- Zeikus JG (1980) Chemical and fuel production by anaerobic bacteria. *Annu Rev Microbiol* 34:423-464
- Zhang, Y. H. P. and L. R. Lynd (2003). "Cellodextrin Preparation by Mixed-acid Hydrolysis and Chromatographic Separation." *Analytical Biochemistry* **322**(2): 225-232.
- Zhang, Y. H. P. and L. R. Lynd (2004). "Toward an Aggregated Understanding of Enzymatic Hydrolysis of Cellulose: Noncomplexed Cellulase Systems." *Biotechnol. Bioeng.* **88**(7): 797-824.
- Zhang, Y. H. P., M. E. Himmel and J. R. Mielenz (2006). "Outlook for Cellulase Improvement: Screening and Selection Strategies." *Biotechnol. Adv.* **24**(5): 452-481.
- Zhang, Y.-H. P. and L. R. Lynd (2004). "Toward an Aggregated Understanding of Enzymatic Hydrolysis of Cellulose: Noncomplexed Cellulase Systems." *Biotechnology and Bioengineering* **88**(7): 797-824.
- Zhao, H., J. H. Kwak, Y. Wang, J. A. Franz, J. M. White and J. E. Holladay (2007). "Interactions Between Cellulose and N-methylmorpholine-N-oxide." *Carbohydrate Polymers* **67**(1): 97-103.

Vita

Date of Birth: 6th April, 1984

Place of Birth: Taipei, Taiwan

Educational Background:

Bachelor of Science in Chemical and Biological Engineering, May 2007
University of British Columbia
Vancouver, British Columbia, Canada

Work Experience

- **Teaching assistant**, Chemical and Materials Engineering, University of Kentucky (2007-2008)
- **International researcher**, Science and Technology Policy Research and Information Center, National Applied Research Laboratories. Taipei, Taiwan (Summer 2006)
- **Undergraduate lab assistant**, Chemical and Biological Engineering, University of British Columbia (2005-2007)
- **Laboratory Assistant**, Michael Smith Biotechnology Laboratory. Vancouver, British Columbia, Canada (Summer 2005)

Research Mentoring

- **Undergraduate research mentor**, Chemical and Materials Engineering, University of Kentucky (Kaitlyn Clark (Summer 2011), Craig Needham (Summer 2010))
- **Undergraduate student mentor**, Engineering Tri-mentoring Program. University of British Columbia (2006-2007)

Publications

H.-F. Li, B. L., Knutson, S. E. Nokes, B. C., Lynn, and M. D. Flythe (2012). "*Metabolic control of Clostridium thermocellum via inhibition of hydrogenase activity and the glucose transport rate.*" Appl. Microbiol. Biotechnol. 93(4): 1777-1784.

H.-F. Li, M. D. Flythe, S. E. Nokes, S. E. Rankin, and B. L. Knutson, "*Modeling of enzymatic hydrolysis and cellulase inhibition by cellobiose on cellulose thin films monitored by Quartz Crystal Microbalance*" (Submitted)

H.-F. Li, S. E. Nokes, S. E. Rankin, and B. L. Knutson, "*Modeling the effect of enzyme concentration dependence of hydrolysis of cellulose thin film using Quartz Crystal Microbalance*" (in progress)

H.-F. Li, S. E. Nokes, S. E. Rankin, and B. L. Knutson, "*Direct monitoring of the temperature dependence of cellulose hydrolysis by Clostridium thermocellum using Quartz Crystal Microbalance and liquid Atomic Force Microscopy*" (in progress)

Presentations

- R. Garlapalli, **H.-F. Li**, S. E. Rankin, B. L. Knutson and S. E. Nokes. “*Quartz Crystal Microbalance Investigation of Cellulase Binding, Activity and Inhibition on Model Cellulose Films*”, 2012 Chemical & Materials Engineering Dept Poster Session, Lexington, KY, Sep, 2012.
- S. E. Rankin, R. Garlapalli, **H.-F. Li**, B. L. Knutson, and S. E. Nokes, “*Quartz Crystal Microbalance Investigation of Trichoderma Reesei Cellulase Interactions with Model Biomass Component Films*”, Kentucky Innovation & Entrepreneurship Conference, Louisville, KY. Jun, 2012.
- H.-F. Li**, B. L. Knutson, S. E. Nokes, B. C., Lynn, and M. D. Flythe, “*Hydrogenase Inhibition as the Mechanism of Product Selectivity by Clostridium Thermocellum in High-Pressure Cultures*”, American Institute of Chemical Engineers Annual Conferences, Minneapolis, MN. Oct, 2011.
- H.-F. Li**, R. Garlapalli, M. D. Flythe, S. E. Nokes, S. E. Rankin, B. L. Knutson, “*Inhibition of Enzymatic Hydrolysis by Soluble Sugars on Model Cellulose Thin Film using Quartz Crystal Microbalance*”, American Institute of Chemical Engineers Annual Conferences, Minneapolis, MN. Oct, 2011.
- M. K. Clark, S. E. Rankin, B. L. Knutson, **H.-F. Li**, “*Synthesis of Thin Film Silica Membranes for the Recovery of Proteins*”, American Institute of Chemical Engineers Annual Conferences, Minneapolis, MN. Oct, 2011.
- S. E. Rankin, **H.-F. Li**, R. Garlapalli, B. L. Knutson, and S. E. Nokes, “*Quartz Crystal Microbalance Investigation of Cellulase Binding, Activity and Inhibition on Model Cellulose Films*”, Kentucky Innovation & Entrepreneurship Conference, Louisville, KY. May, 2011.
- H.-F. Li**, M. D. Flythe, S. E. Nokes, S. E. Rankin, and B. L. Knutson, “*Inhibition of Enzymatic Hydrolysis by Soluble Sugars on Model Cellulose Thin Film Using Quartz Crystal Microbalance*”, Naff Symposium: Biochemistry at Interfaces, Lexington, KY. Apr, 2011.
- H.-F. Li**, B. L., Knutson, S. E. Nokes, B. C., Lynn, and M. D. Flythe, “*Hydrogenase Inhibition as the Mechanism of Enhanced Ethanol Production by Clostridium Thermocellum in Biphase Continuous Culture*”, American Institute of Chemical Engineers Annual Conferences, Salt Lake City, UT. Nov, 2010.
- C. Needham, S. E. Rankin, B. L. Knutson, **H.-F. Li**, “*The Effect of Molecular Imprinting on the Adsorption of Simple Sugars on the Adsorption of Simple Sugars onto Silica Films*”, Research Experiences for Undergraduates (REU) Student Presentation, Jul, 2010.
-
-